

# The Structure of Random Particle Packings

## Die Struktur ungeordneter Packungen

Der Naturwissenschaftlichen Fakultät

der Friedrich-Alexander-Universität  
Erlangen-Nürnberg

zur

Erlangung des Doktorgrades Dr. rer. nat.

vorgelegt von

Fabian Schaller  
aus Nürnberg



Als Dissertation genehmigt von der  
Naturwissenschaftlichen Fakultät  
der Friedrich-Alexander-Universität  
Erlangen-Nürnberg

Tag der mündlichen Prüfung: 8. Juni 2017

Vorsitzende/r des Promotionsorgans: Prof. Dr. Georg Kreimer

Gutachter/in: PD Dr. Gerd Schröder-Turk  
Prof. Dr. Eric Lutz  
Prof. Dr. Karen Daniels





## Abstract

In particulate systems with short-range interactions, such as granular matter or simple fluids, the local structure has crucial influence on the macroscopic physical properties. This thesis advances our understanding of granular matter by a comprehensive study of Voronoi-based local structure metrics applied to amorphous ellipsoid configurations. In particular, a methodology for a local, density-resolved analysis of structural properties is developed. These methods are then applied to address the question of when the global packing fraction alone is a sufficient descriptor of the structure, and situations for which this is not the case.

Packings of monodisperse spherical particles are a common simple model for granular matter and packing problems. This work focuses on packings of ellipsoidal particles, a system which offers the possibility to study the influence of particle shape on packing properties, in particular particle anisotropy.

A large scale experimental study of jammed packings of oblate mm-sized ellipsoids with various aspect ratios  $\alpha$  is performed. Packings are prepared with different preparation protocols to achieve different global packing fractions  $\phi_g$  and imaged by X-ray tomography. Additional datasets of packings are created by Discrete Element Method simulations of frictional and frictionless particles with and without gravity. Furthermore, packings of Ottawa sand samples are analyzed, in an attempt to investigate the relevance of the ellipsoid model system for real world granulates.

The structure of the packings is analyzed by Set Voronoi diagrams, an extension of the conventional Voronoi diagram to aspherical particles. We find some surprising structural properties, specifically related to the local packing fraction  $\phi_l$ , defined as particle volume divided by its Voronoi cell volume. A universality is found in the probability density function to find a particle with  $\phi_l$  in a given packing. The width of the density function is independent of the aspect ratio  $\alpha$ . For spheres, Aste *et al.* [EPL 79:24003, 2007] proposed an analytic model for the distribution of Voronoi cell volumina. Their model strongly depends on the locally densest configuration, a quantity that was, prior to this work, not known for ellipsoids. We numerically investigate the locally densest structures and analyze their occurrence as local building blocks of granular packings. Knowledge of the densest structures allows to rescale the Voronoi volume distributions onto the single-parameter family of  $k$ -Gamma distributions. Remaining deviations are explained by an excessive formation of distorted icosahedral clusters.

A robust tool to characterize spatial structures is provided by Minkowski tensors, which generalize the concepts of interface and moment tensors. Here, we investigate the shape properties of the Voronoi cells by anisotropy indices  $\beta_v^{r,s}$  derived from these tensors. These local anisotropy indices point towards a significant difference in the local structure of random packings of spheres and ellipsoids. While the average cell shape  $\beta_v^{r,s}$  of all cells with a given value of  $\phi_l$  is very similar in dense and loose jammed sphere packings, the structure of dense and loose ellipsoid packings differs substantially such that this does not hold true.

The average number of contacts  $Z$  of a particle with its neighbors is an important predictor of the mechanical properties of a packing as forces in granular matter are transmitted through contacts. This conceptually straightforward parameter is, however, difficult to analyze, since contact detection is hindered by experimental noise and is often connected to a numerical cut-off. It is less reliable than the continuously defined analysis by Minkowski tensors. In our jammed packings of ellipsoids, we find, that  $Z$  is a monotonously increasing function of the global packing fraction  $\phi_g$  for all aspect ratios  $\alpha$ . This dependence can be explained by a local analysis where each particle is described by its local packing fraction  $\phi_l$  and the average number of neighbors.

Our results clearly demonstrate the need for a local analysis when ellipsoid packings are analyzed. Local analyses of this type reveal differences in the structure, which are not captured by global averages. This points to an important structural difference to the sphere pack case where the global  $\phi_g$  seems to suffice to rationalize most observed properties, at least to a good approximation. While our study specifically addressed “granular matter” models of hard particles subject to gravity, these findings are likely to also rationalize observations of other soft matter particulate systems, including colloidal particles or other micron- or nanometer-sized particles.

## Zusammenfassung

In Teilchensystemen mit kurzreichweitigen Wechselwirkungen, wie z.B. in Granulaten oder einfachen Gasen, ist die lokale Struktur für die makroskopischen physikalischen Eigenschaften wichtig. Diese Arbeit trägt mit einer umfangreichen Studie von amorphen Konfigurationen von Ellipsoiden zum Verständnis der granularen Materie bei. Die Teilchen-Konfigurationen werden mit lokalen Strukturparametern analysiert, welche auf Voronoi-Diagrammen basieren. Insbesondere wird eine Methode für eine lokale Analyse entwickelt, die Strukturparameter nach der Packungsdichte auflöst. Mit dieser Methode wird die Frage untersucht, wann die Struktur der Packung effektiv durch einen einzelnen Parameter, die globale Dichte, charakterisiert wird und wann das nicht der Fall ist.

Ein einfaches Modell für granulare Materie und Packungsprobleme sind Systeme von Kugeln. Reale Granulate bestehen aus Teilchen, die in Größe und Form variieren. Diese Arbeit konzentriert sich auf Packungen von Ellipsoiden, welche es ermöglichen, den Einfluss von der Teilchenform auf die Packungseigenschaften zu untersuchen.

Diese Arbeit beinhaltet eine groß angelegte experimentelle Studie von oblaten millimetergroßen Ellipsoiden mit verschiedenen Aspektverhältnissen. Um verschiedene globale Packungsdichten  $\phi_g$  zu erhalten, werden die Packungen mit verschiedenen Methoden präpariert. Anschließend werden die Packungen per Röntgentomographie untersucht. Zusätzlich werden Packungen von reibungsbehafteten und reibungsfreien Teilchen, mit und ohne Einfluss von Gravitation, mit der Diskrete-Elemente-Simulationsmethode erstellt. Um die Relevanz des Ellipsoid-Modells für reale Granulate zu testen, werden Packungen von sogenanntem Ottawa Sand untersucht.

Die Struktur der Packungen wird mit Mengen-Voronoi-Diagrammen (Set Voronoi diagrams) untersucht, eine Erweiterung des konventionellen Voronoi-Diagramms für nicht-kugelförmige Teilchen. Wir finden einige überraschende Eigenschaften, besonders bezüglich der lokalen Packungsdichte  $\phi_l$ , welche das Verhältnis zwischen Teilchenvolumen und dem Volumen seiner Voronoi-Zelle ist. Die Wahrscheinlichkeitsdichteverteilung gibt die Wahrscheinlichkeit an, ein Teilchen mit  $\phi_l$  in einer Packung zu finden. Überraschenderweise hängt die Breite der Wahrscheinlichkeitsdichteverteilung nur von  $\phi_g$  ab und ist unabhängig vom Aspektverhältnis  $\alpha$  der Teilchen. Ein analytisches Modell für die Verteilung der Volumen der Voronoi-Zellen in Kugelpackungen wurde von Aste *et al.* [EPL 79:24003, 2007] vorgeschlagen. Das Modell hängt von der lokal dichtestmöglichen Konfiguration ab, welche vor dieser Arbeit für Ellipsoide nicht bekannt war. Wir untersuchen numerisch die dichtesten lokalen Strukturen und analysieren deren Auftreten als Bausteine von granularen Packungen. Mit Hilfe unserer berechneten dichtesten Strukturen können wir die Verteilung der Voronoi-Zellvolumen auf die einparametrische Familie von  $k$ -Gamma Funktionen reskalieren. Die verbleibenden Unterschiede können mit einer übermäßigen Bildung von deformierten ikosaeder-förmigen Clustern erklärt werden.

Ein robustes Werkzeug zur Charakterisierung von räumlichen Strukturen sind Minkowski-Tensoren, welche das Konzept von Oberflächen- und Momententensoren verallgemeinern. Wir erforschen die Formeigenschaften von Voronoi-Zellen mit

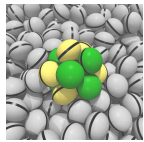
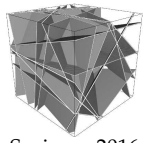
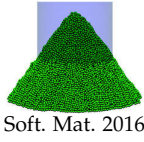
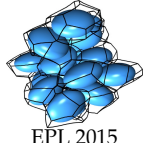


Anisotropiemaßen  $\beta_v^{r,s}$ , die von diesen Tensoren abgeleitet sind. Diese lokalen Anisotropiemaße deuten auf einen signifikanten Unterschied in der lokalen Struktur zufälliger Packungen von Kugeln und Ellipsoiden hin: In dichten und losen Kugelpackungen ist die durchschnittliche Zellform  $\beta_v^{r,s}$  aller Zellen mit gegebener lokaler Packungsdichte  $\phi_l$  sehr ähnlich. Im Gegensatz dazu ist die Struktur in dichten und losen Ellipsoidpackungen unterschiedlich.

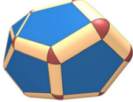
Die durchschnittliche Anzahl an Kontakten  $Z$  von einem Teilchen mit seinen Nachbarn ist eine wichtige Größe, um die mechanischen Eigenschaften von Packungen vorherzusagen, da Kräfte durch Kontakte übertragen werden. Diese konzeptionell einfache Größe ist schwer zu berechnen, da die Kontaktpunktbestimmung durch experimentelles Rauschen erschwert wird und oft stark von numerischen Schwellwerten abhängt. Kontaktzahlen sind daher weniger verlässlich, als eine Analyse mit den kontinuierlich definierten Minkowski-Tensoren. Unsere Analyse ergibt, dass in gejamten Ellipsoidpackungen  $Z$  eine mit  $\phi_g$  monoton steigende Funktion für alle Aspektverhältnisse  $\alpha$  ist. Diese Abhängigkeit kann mit einer lokalen Analyse erklärt werden, in der jedes Teilchen durch seine lokale Packungsdichte  $\phi_l$  und seine durchschnittliche Anzahl an Nachbarn beschrieben ist.

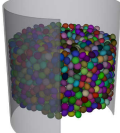
Unsere Resultate zeigen deutlich die Notwendigkeit einer lokalen Analyse für Packungen von Ellipsoiden. Derartige lokale Analysen enthüllen Unterschiede, welche durch eine globale Analyse nicht aufgedeckt werden. Dies zeigt einen wichtigen strukturellen Unterschied zu Kugelpackungen auf, bei denen die globale Packungsdichte  $\phi_g$  die meisten beobachteten Parameter beschreibt, zumindest in einer guten Näherung. In dieser Studie wurden speziell granulare Materie Modelle von harten Teilchen unter dem Einfluss von Gravitation untersucht. Diese Forschungsergebnisse finden aber auch Anwendung in anderen Bereichen der weichen Materie, wie zum Beispiel bei Kolloiden oder bei Teilchen auf der Nanometerskala.

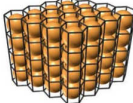
# Publications

This cumulative thesis comprises the following nine peer-reviewed research articles:


- [P1]  **F. M. Schaller**, R. F. B. Weigel, and S. C. Kapfer. Densest local structures of uniaxial ellipsoids. *Phys. Rev. X*, 6:041032, 2016.  
PRX 2016
- [P2]  M. A. Klatt, G. Last, K. Mecke, C. Redenbach, **F. M. Schaller**, and G. E. Schröder-Turk. Cell shape analysis of random tessellations based on minkowski tensors. *Springer Lecture Notes in Mathematics, Tensor Valuations and their applications in stochastic geometry and imaging*, vol 2177, 2017. *arXiv:1606.07653*.  
Springer 2016
- [P3]  N. Topic, **F. M. Schaller**, G. E. Schröder-Turk, and T. Pöschel. The microscopic structure of mono-disperse granular heaps and sediments of particles on inclined surfaces. *Soft Matter*, 12:3184–3188, 2016.  
Soft. Mat. 2016
- [P4]  **F. M. Schaller**, S. C. Kapfer, J. E. Hilton, P. W. Cleary, C. De Michele K. Mecke, T. Schilling, M. Saadatfar, M. Schröter, G. W. Delaney, and G. E. Schröder-Turk. Non-universal Voronoi cell shapes in amorphous ellipsoid packs. *EPL (Europhysics Letters)*, 111(2):24002, 2015.  
EPL 2015
- [P5]  **F. M. Schaller**, M. Neudecker, M. Saadatfar, G. W. Delaney, G. E. Schröder-Turk, and M. Schröter. Local origin of global contact numbers in frictional ellipsoid packings. *Phys. Rev. Lett.*, 114:158001, 2015.  
PRL 2015
- [P6]  **F. M. Schaller**, S. C. Kapfer, M. E. Evans, M. J. F. Hoffmann, T. Aste, M. Saadatfar, K. Mecke, G. W. Delaney, and G. E. Schröder-Turk. Set Voronoi diagrams of 3D assemblies of aspherical particles. *Philosophical Magazine*, 93(31-11):3993–4017, 2013.  
Phil. Mag. 2013


- [P7]   
NJP 2013 G. E. Schröder-Turk, W. Mickel, S. C. Kapfer, **F. M. Schaller**, B. Breidenbach, D. Hug, and K. Mecke. Minkowski tensors of anisotropic spatial structure. *New Journal of Physics*, 15:083028, 2013.

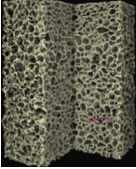
- [P8]   
AIP 2013 **F. M. Schaller**, M. Neudecker, M. Saadatfar, G. Delaney, K. Mecke, G. E. Schröder-Turk, and M. Schröter. Tomographic analysis of jammed ellipsoid packings. *AIP Conference Proceedings*, 1542:377–380, 2013.

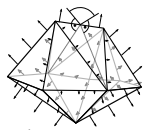
- [P9]   
AIP 2013 G. E. Schröder-Turk, R. Schielein, S. C. Kapfer, **F. M. Schaller**, G. W. Delaney, T. Senden, M. Saadatfar, T. Aste, and K. Mecke. Minkowski tensors and local structure metrics: Amorphous and crystalline sphere packings. *AIP Conference Proceedings*, 1542:349–352, 2013.

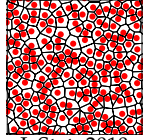
The following five publications are articles that I have co-authored and that are related to the same research project, but are not formally part of this cumulative dissertation since they were either completed prior to my PhD thesis work or are not yet published.

- [P10]   
accepted 2017 **F. M. Schaller**, H. Punzmann, G. E. Schröder-Turk, and M. Saadatfar. Towards minimal models for realistic granular materials: Tomographic analysis of bidispersed assemblies of ellipsoids. *accepted for publication in Proceedings of Powders and Grains 2017: 8th International Conference on Micromechanics of Granular Media, EDP Sciences, 2017.*

- [P11]   
accepted 2017 S. Weis, P. Schönhöfer, **F. M. Schaller**, M. Schröter, and G. E. Schröder-Turk. Pomelo, a tool for computing Generic Set Voronoi Diagrams of Aspherical Particles of Arbitrary Shape. *accepted for publication in Proceedings of Powders and Grains 2017: 8th International Conference on Micromechanics of Granular Media, EDP Sciences, 2017.*

- [P12]   
Acta. Mat. 2012 M. Saadatfar, M. Mukherjee, M. Madadi, G. E. Schröder-Turk, F. Garcia-Moreno, **F. M. Schaller**, S. Hutzler, A. P. Sheppard, J. Banhart, and U. Ramamurty. Structure and deformation correlation of closed-cell aluminium foam subject to uniaxial compression. *Acta Materialia*, 60:3604 – 3615, 2012.

- [P13]  G. E. Schröder-Turk, W. Mickel, S. C. Kapfer, M. A. Klatt, **F. M. Schaller**, M. J. F. Hoffmann, N. Kleppmann, P. Armstrong, A. Inayat, D. Hug, M. Reichelsdorfer, W. Peukert, W. Schwieger, and K. Mecke. Minkowski tensor shape analysis of cellular, granular and porous structures. *Advanced Materials*, 23:2535–2553, 2011.

- [P14]  S. C. Kapfer, W. Mickel, **F. M. Schaller**, M. Spanner, C. Goll, T. Nogawa, N. Ito, K. Mecke, and G. E. Schröder-Turk. Local anisotropy of fluids using Minkowski tensors. *Journal of Statistical Mechanics*, P11010:1–20, 2010.

Throughout the introductory section (chapters 1-6), citations starting with a **P** refer to publications listed here. All other references can be found in the Bibliography chapter.

The icons placed on the document margins next to the captions throughout this thesis indicate contributions of this work to the respective sections. Verbatim quotes from my articles in these sections are not necessarily labeled as such.

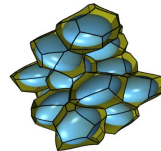
# Contents

<b>1 Granular matter – from spherical to aspherical particle models</b>	<b>1</b>
<b>2 Tomographic experiments and simulations of ellipsoid packings</b>	<b>13</b>
2.1 Preparation and tomographic imaging of packings . . . . .	13
2.1.1 Frictional monodisperse ellipsoids . . . . .	13
2.1.2 Frictional bidisperse ellipsoids . . . . .	15
2.1.3 Ottawa sand . . . . .	17
2.2 Simulations . . . . .	19
2.2.1 Dense packings – Lubachevsky-Stillinger-Donev protocol . . .	19
2.2.2 Discrete Element Simulations (DEM) of frictional particles . . .	19
2.2.3 Equilibrium fluids – Molecular dynamics & Monte Carlo . . . .	20
<b>3 Quantitative morphology of spatial tessellations and granular assemblies</b>	<b>21</b>
3.1 Set Voronoi diagrams as tessellations for non-spherical particles . . . .	21
3.1.1 Algorithm for parametrizable particles . . . . .	23
3.1.2 Set Voronoi diagram for tomographic (voxelized) images . . . .	23
3.2 Shape analysis by Minkowski tensors . . . . .	25
3.2.1 Minkowski functionals and tensors . . . . .	25
3.2.2 Anisotropy indices based on Minkowski tensors . . . . .	27
3.3 Local (density-resolved) analysis - Looking at the particle scale . . . .	28
<b>4 What can we learn from the Voronoi diagram of hard particle systems?</b>	<b>31</b>
4.1 <i>Cuddling ellipsoids</i> - locally densest structures . . . . .	32
4.2 Voronoi Volume distributions . . . . .	34
4.2.1 Extending the k-Gamma model to non-spherical particles . . .	34
4.2.2 Distributions of local packing fraction . . . . .	35
4.3 Shape and anisotropy . . . . .	37
4.3.1 Global averages . . . . .	37
4.3.1.1 Packings of spheres . . . . .	37
4.3.1.2 Packings of ellipsoids . . . . .	38
4.3.2 Local analysis reveals differences in dense and loose packings .	40
<b>5 Contact numbers and mechanical stability</b>	<b>43</b>
5.1 Global averages . . . . .	43
5.2 Local contact analysis . . . . .	46
<b>6 Outlook</b>	<b>49</b>
<b>7 Bibliography</b>	<b>53</b>
<b>Publications</b>	<b>69</b>
[P1] Densest local structures of uniaxial ellipsoids . . . . .	69
[P2] Cell shape analysis of random tessellations based on Minkowski tensors	81



[P3] The microscopic structure of mono-disperse granular heaps and sediments of particles on inclined surfaces . . . . .	121
[P4] Non-universal Voronoi cell shapes in amorphous ellipsoid packs . . . . .	129
[P5] Local origin of global contact numbers in frictional ellipsoid packings . . . . .	137
[P6] Set Voronoi diagrams of 3D assemblies of aspherical particles . . . . .	153
[P7] Minkowski tensors of anisotropic spatial structure . . . . .	181
[P8] Tomographic analysis of jammed ellipsoid packings . . . . .	221
[P9] Minkowski tensors and local structure metrics: Amorphous and crystalline sphere packings . . . . .	227





# 1 Granular matter – from spherical to aspherical models



*Reynold's Dilatancy*

Granular packings play an important role in everyday life. The interaction between the constituent particles is very simple, but fascinating physics can result from packing properties or collective effects of the assembly of grains. An early example of the intriguing physics in granulates is Reynold's dilatancy, described by Osborne Reynolds in 1886 [166, 167]. Sand on the beach is, when undisturbed, densely packed. If

the sand is covered with a thin film of water and you step on it, the sand appears to be drying out. The explanation for this phenomena is that sand on the beach is densely packed and, locally, in a minimal volume configuration. In order to accommodate any deformation, such as the one resulting from stepping on it, the packing needs to expand. The water moves into newly created or expanded void space which leads to the impression of the drying sand [75, 105]. This example illustrates the typical property of granular matter physics that structure, shape, geometry and topology are the key ingredients of an explanation of a physical effect.

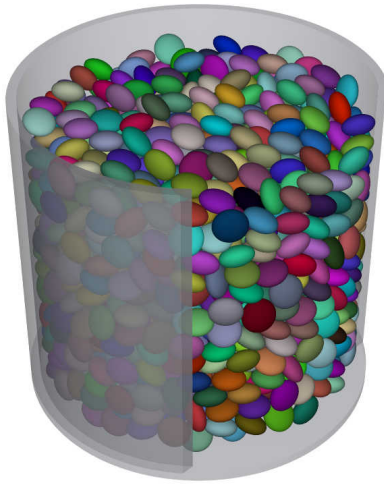
Another important physical question relates to the stability of packings of granulates. In the desert, sand dunes are sufficiently strong to support people walking on them, see Fig. 1.1 (left). But, by contrast, earth quakes can cause large sections of sand and rock to start to slide, see Fig. 1.1 (right). In geology, the rigidity of such granular



Figure 1.1: (left) People walking up a sand dune in Namib desert. (right) Landslide triggered by an earthquake in Haiti in 2010. Picture by Randy Jibson, USGS [1].

matter and the understanding of what triggers geological processes like avalanches or landslides is of great importance [95, 97]. The structure and grain arrangement are essential determinants of the stability of the granular assembly.

A wealth of other physical properties result in granular systems, from the collective effects and despite the simplicity of the interactions, including segregation phenomena [51, 123, 141, 148, 158], pattern formation [10, 70, 135, 168], shear-thinning or -thickening [37, 88], localization of stresses and arch formation [72, 136, 156, 193], development of characteristic features such as characteristic angles of repose [39, 98, 116], and many others. The various facets of the physics of granular media and packing problems are the subject of review articles [10, 69, 123, 197, 200] and text books [6, 15, 48, 62, 87, 90, 145, 168].



*Granular Matter*, as opposed to granular gases or *particulate fluids*, specifically deals with *jammed* configurations. Jammed configurations are stable packings of particles where every particle is trapped by its neighbor particles and cannot move<sup>1</sup> [156, 200]. The picture on the left shows a jammed packing of ellipsoidal particles in a cylindrical container. The properties of jammed particle packings are intriguingly non-trivial and depend on the particle properties, such as shape or friction, which is the main topic of this thesis. Given that the microscopic physics is governed by simple hard-core interactions<sup>2</sup>, the geometric structure of these packings is of great importance.

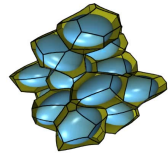
### Structural analysis of particle packings

Tomographic methods have revolutionized our understanding of granular materials, giving unprecedented access to the internal structure of a packing. Specifically, X-ray tomography is a non-destructive technique to obtain 3D real-space data of almost any packing suitable for particle sizes from  $\mu\text{m}$  to cm. In the standard circular tomography, the sample is rotated in total by  $360^\circ$  while projections are taken from all



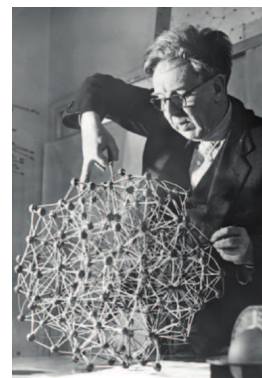
<sup>1</sup>Several different notions of jamming can be distinguished, such as locally, collectively or strictly jammed. For further information see ref. [197].

<sup>2</sup>Frictional particles can share additional tangential forces.



directions.<sup>3</sup> Afterwards, a 3D gray-scale image, representing the density field, is constructed from all the projections. Helical scanning methods, in which the sample is vertically translated while being rotated, increase the signal to noise ratio and offer the opportunity to scan long samples [181, 201]. The huge advantage of the helical scanning is the theoretically exact reconstruction of the 3D gray-scale image in contrast to circular scanning which depends on approximations [113, 201]. From the received 3D gray-scale image, positions and orientations of the single particles can be acquired by methods based on watershed algorithms, see e.g. Refs. [149, 169, 171] and [P8]. With so-called *power watershed* algorithms, the separating planes between the touching particles can be estimated with sub-voxel resolution [100]. This thesis addresses packings of 3D particles, such as spheres, ellipsoids and sand grains. Packings are prepared with different preparation methods to create a large range of packing densities. Tomographic images are recorded and their structure is investigated.

Prior to the availability of tomography methods, structural analysis was performed by manual dissection. Pioneering work in the description of amorphous packings where grains are randomly arranged was done by John Desmond Bernal [31] and David Scott [179, 180] in the 1960s, who experimentally investigated the structure of random sphere packings initially as models for the structure of liquids. They showed that jammed amorphous packings of *frictional* hard spheres can only be prepared in a finite interval of packing fractions. The packing fraction or packing density  $\phi_g$  is defined as the ratio of the particles' volumes and the space they are packed into. The lowest limit, called *Random Loose Packing* (RLP), has a packing fraction of  $\phi_{\text{RLP}} \approx 0.55$ . Below the RLP limit, no mechanically stable random packing exists [101]. The upper bound is named *Random Close Packing* (RCP) with a packing fraction of  $\phi_{\text{RCP}} \approx 0.64$  [179], substantially below the theoretically maximal value of  $\phi_{\text{fcc/hcp}} \approx 0.74$ , see below. By contrast, jammed packings of *frictionless* spheres always reach the RCP limit, in sufficiently large samples [156]. An exact definition of the RCP limit is still missing and details are under debate: It was shown that packings above the RCP limit and a critical packing fraction of 0.649 contain crystalline domains [104, 110]. In the context of crystallization seeds, Alexey Anikeenko showed an appreciable fraction of polytetrahedral aggregates at critical packing fraction of  $\approx 0.646$  [7], which is close to  $\phi_{\text{RCP}}$ . On the more conceptual level, Salvatore Torquato introduced the *Maximally random jammed* (MRJ) state which is defined as the least ordered packing among all jammed packings and results in a packing fraction of  $\phi_{\text{MRJ}} \approx 0.64$  for frictionless spheres [198]. This is in contrast to RCP which asks for the densest of all random packings. Further theories exist, see e.g. Refs. [22, 164], but an exact definition is still missing.

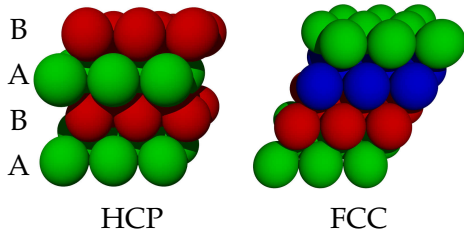


John Desmond Bernal<sup>4</sup>

<sup>3</sup>The resolution of the resulting image is increased by rotating  $360^\circ$  rather than the minimum needed  $180^\circ + \text{fan angle}$  [76].

<sup>4</sup>Picture from Ref. [69]

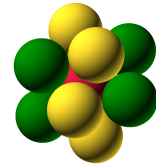
**Globally and locally densest configurations**



A For spheres, the densest possible *crystalline* structures are known and can be identified.  
 C These are the face-centered cubic (FCC) or hexagonal close-packed (HCP) configurations resulting in a packing fraction of  $\phi_{fcc/hcp} \approx 0.74$ . Both packings consist of stacked hexagonal lattice planes of spheres,

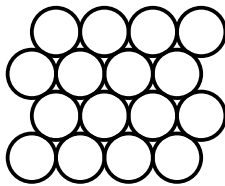
which are shifted against each other. The HCP crystal consists of two (A-B-A), the FCC crystal of three (A-B-C) alternating planes, see figure on the left. Combinations of FCC and HCP are as well densest packings. The conjecture that the FCC structure is the densest crystal packing was proposed by Kepler in the 17th-century [15], but remained unproven for many years. Recently it was proven by Thomas Hales [81, 126]. The question of non-densest crystalline sphere packings has been exhaustively addressed by Werner Fischer, Elke Koch and others, see [118] and references therein.

As described above, the globally densest sphere packings, i.e. the crystalline ones, are known in 3D. However, there is a difference between what is the densest local and what is the densest global configuration. The local density of a particle  $\phi_l$  is defined as the ratio between the particle's volume and the volume of its Voronoi cell, see below. Locally, the question of the densest configuration is related to a classical problem in mathematics dating back to Isaac Newton:



icosahedral cluster

The "Kissing problem" poses the question how many spherical particles can simultaneously touch a central sphere. The answer, in dimension 3, is twelve [48, 177]. The icosahedral cluster, see image on the right, is the most symmetric way to arrange the twelve "kissers" and maximizes the local packing density. With a packing fraction of  $\phi_{ico} = 0.755$ , ideal icosahedra are about 1% denser than the previous mentioned best crystal arrangements (FCC/HCP) of congruent spheres [15]. Icosahedral clusters are, however, not *space-tiling*, i.e. it is not possible to fill a whole container with spheres all arranged in icosahedral configurations to one another. By embedding (distorted) icosahedral clusters, disordered granular packings can locally (but of course not globally) exceed the density limit for the space-tiling sphere packings. Fig. 1.2 (top) shows a summary of possible jammed packings of spherical particles.



The frustration between the local and global features is an inherent feature of sphere packings in 3D Euclidean space. For disc packings in two dimensions, the globally and locally densest structures are the same, namely the hexagonal configuration [48]. Hence, in two dimensions, the locally densest structure is space-tiling in contrast to three dimensions. Disc packings in two dimensions have a strong tendency to crystallize during compaction [131, 132, 139]. One way to avoid crystallization is to introduce polydispersity, a standard "trick" widely used in the glass community [159, 186].



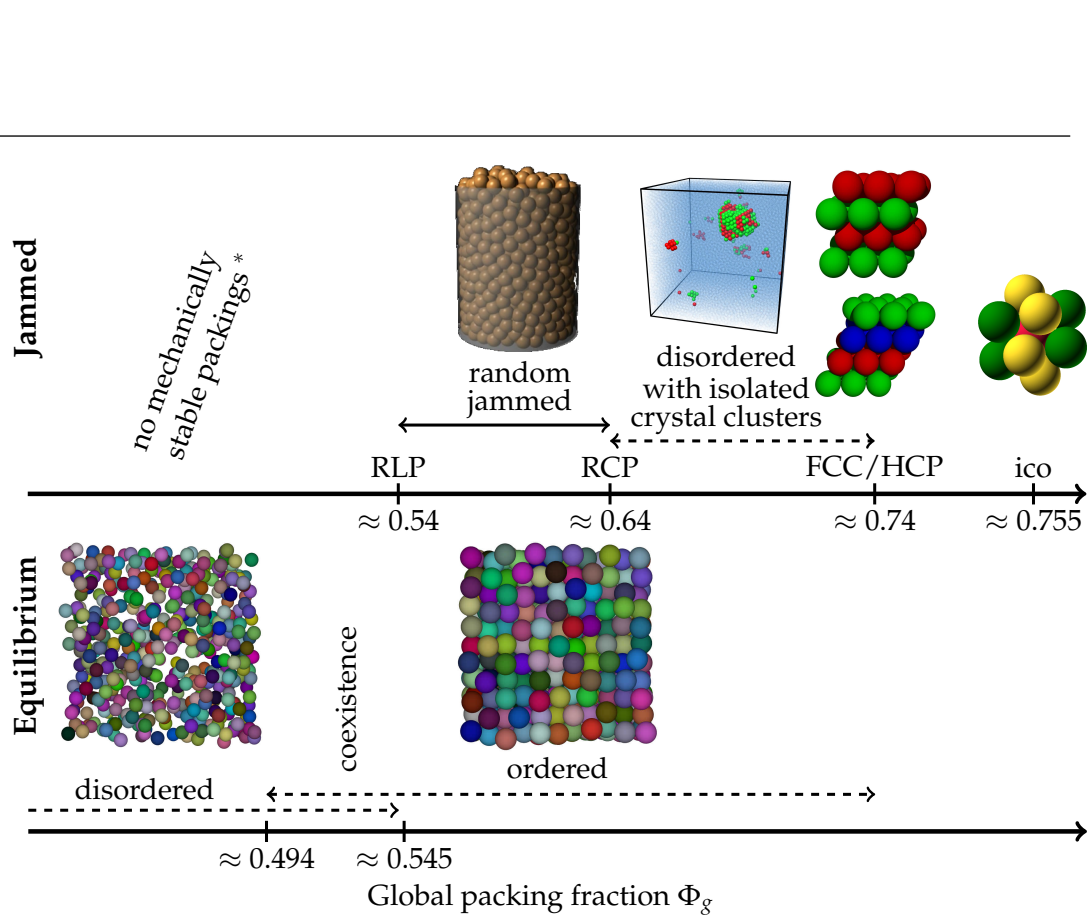
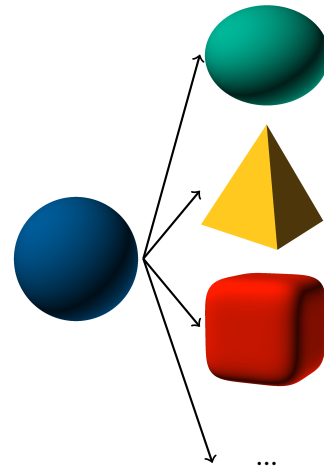
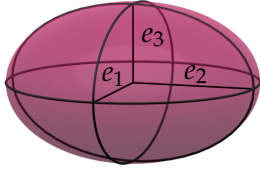


Figure 1.2: Simplified phase diagram of equilibrium and jammed spherical particles, x-axis not to scale.  
 \* An exception is tunneled crystals, i.e. crystal sphere packing with an anomalously low density, which can pack looser than the RCP limit [196].

### Shape matters – packings of aspherical particles

In general, particles in nature and industry, such as sand or pebbles, vary widely in size and shape. In order to understand packing effects of such complex shapes, the packing properties of simple geometric shapes have to be known. Spheres are only the simplest case and are also special in terms of their rotational symmetry in all directions, which affect the degrees of freedom. The study of packings of particles with simple aspherical shape offers the possibility to assess the effect of particle shape on the packing properties. Obvious generalizations of spheres are ellipsoids, packings of which are the main subject of this thesis and which have been extensively studied elsewhere [47, 54, 55, 56, 57, 60, 137, 190, 208, 210]. Other particle shapes studied in the literature are tetrahedra [40, 80, 150], superellipsoids [54, 102, 190], lense-shaped particles [44] and many more [41, 61, 119, 170, 194, 202]. The packing properties of polyhedra are as well under investigation [41, 50]. For all of these shapes, it still remains a challenge to understand how collective properties of packings arise from microscopic mechanisms on the particle level.





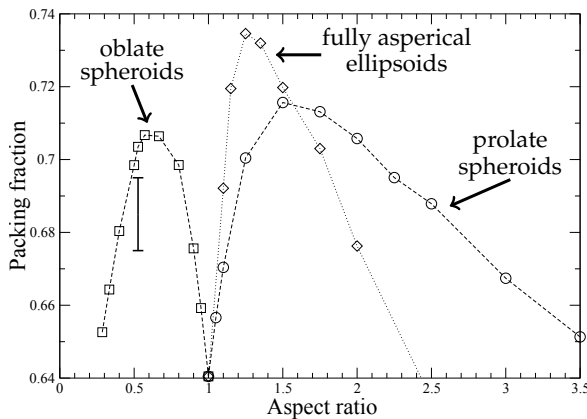
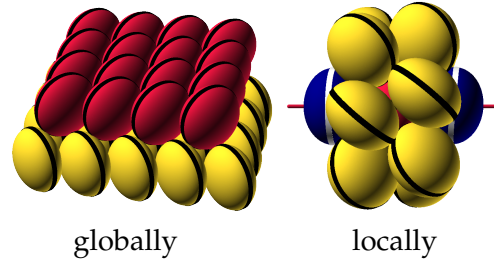
uniaxial ellipsoid:  $e_1 = e_2 \neq e_3$   
aspect ratio:  $\alpha = e_3/e_1$

Ellipsoids offer a systematic pathway to study the influence of shape to the structure of particle packings. The shape can be varied by changing the aspect ratio of the particles. Here, we consider uniaxial ellipsoids with two half-axes of the same length, also known as spheroids, or ellipsoids of rotation. The aspect ratio  $\alpha$  is defined as the fraction of the individual axis and the two with identical lengths. Ellipsoids with  $\alpha < 1$  are called oblate and ellipsoids  $\alpha > 1$  prolate.

A first property of interest for aspherical particles is the maximally dense crystal packing, equivalent to the FCC/HCP packing in spheres. The finding of the densest crystal packings for ellipsoidal particles is more complex than for spheres, due to their additional rotational degrees of freedom. Candidates were proposed by Donev

*et al.* [57], but without proof of optimality. Recently, for self-dual ellipsoids ( $\alpha : \alpha^{1/2} : 1$ ) with  $\alpha \approx 1.4$ , a new densest crystal structure was discovered [103]. While a mathematical proof of optimality is missing, it is clear that the densest crystal packings of ellipsoids are denser than the FCC and HCP packings of spheres, see Fig. 1.3.

The question of the locally densest configurations of ellipsoidal particles is part of this thesis. In a generalization of the kissing problem, we consider a central particle and the  $N$  first-shell neighbor particles and numerically optimize their local structure. The resulting configurations and the optimal number of nearest neighbors depends on the aspect ratio of the particles [P1], see section 4.1.



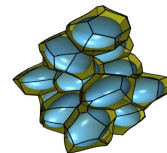
Packing fraction of jammed frictionless ellipsoids<sup>5</sup>.

lattice packings [106, 107] and the densest local configurations [P1], see Fig. 1.3 (top) and section section 4.1. In real granular packings, another important parameter

Random packings of ellipsoids have been mainly studied with simulations. Donev *et al.* [56] generalized the Lubachevsky-Stillinger (LS) sphere packing algorithm [131, 132] to the case of ellipsoids [58, 59]. They showed, that *frictionless* ellipsoids can form denser amorphous jammed packings than spheres, even denser than the densest crystal packings of spheres. In this sense the sphere is worst in building dense amorphous packings, which is observed as well for

<sup>5</sup>Plot reproduced from Ref. [56], with permission from AAAS.





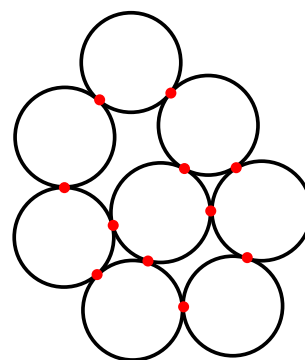
despite from particle shape, which effects packing properties as e.g. stability of the packing, is friction – a second focus point of this thesis. Discrete Element Method (DEM) simulations offer the opportunity to create packings of *frictional* ellipsoids. Packing experiments on ellipsoid packings were performed with two different types of ellipsoidal particle shapes [56, 137]. This thesis represents the first experimental large scale study comprising five different aspect ratios and two different friction coefficients, see Ref. [P5] and chapter 2 and 5.

Performing DEM simulations with highly frictional ellipsoids, the limit of the loosest random packings can be investigated [55]. While various definitions of the loosest packings exist for spheres, more recent work focuses on the definition as the loosest random packing that can be achieved by pouring or sedimenting grains under the influence of gravity and is mechanically stable [43, 101]. Delaney *et al.* [55] called this limit the *Sedimented Loose Packing* (SLP). A crucial point in random packings of ellipsoids is the definition of randomness. Particles with a preferred direction, such as ellipsoids, can show orientational order (align with each other), in the absence of any translational order [54, 154]. Packings of aspherical particles prepared by sedimentation can have a significant degree of orientational ordering, because the particles tend to align with the direction of gravity [55]. A simplified phase diagram for jammed ellipsoidal particles is presented in Fig. 1.3 (top). An explanation for the observed high correspondence of packings of prolate and oblate ellipsoids is still missing.

### Contact numbers and mechanical stability

In granular systems the average number of contacts a particle forms with its neighbors is used commonly as a predictor of the mechanical properties of the system, since forces are transferred through the contacts. The distribution of the contacts throughout the system can give information about how the system responds to external forces [25, 73, 92, 136].

The minimal number of contacts required for a stable packing is called the *isostatic* contact number  $Z_{\text{iso}}$ . For example, *frictionless* spheres have an isostatic contact number  $Z_{\text{iso}} = 6$  [156, 200]. This can be obtained by a simple constraint counting [200]: Frictionless contacts can only fix one normal force, which is shared between the two particles involved. Hence, per particle each contact provides 0.5 constraints and as each particle possesses three translational degrees of freedom, at minimum of six contacts is needed for a particle to be fully constrained by its neighbors. For spheroids this number increases to 10 and for fully aspherical ellipsoids 12 contacts are needed due to their additional rotational degrees of freedom [200]. For *frictional* particles  $Z_{\text{iso}}$  reduces to four. In this case the particles have as well rotational degrees of freedom and each contact can fix three force components, one normal and two tangential. Details about contact numbers of granular packings are given in chapter 5 and Ref. [P5].



contacts are marked in red

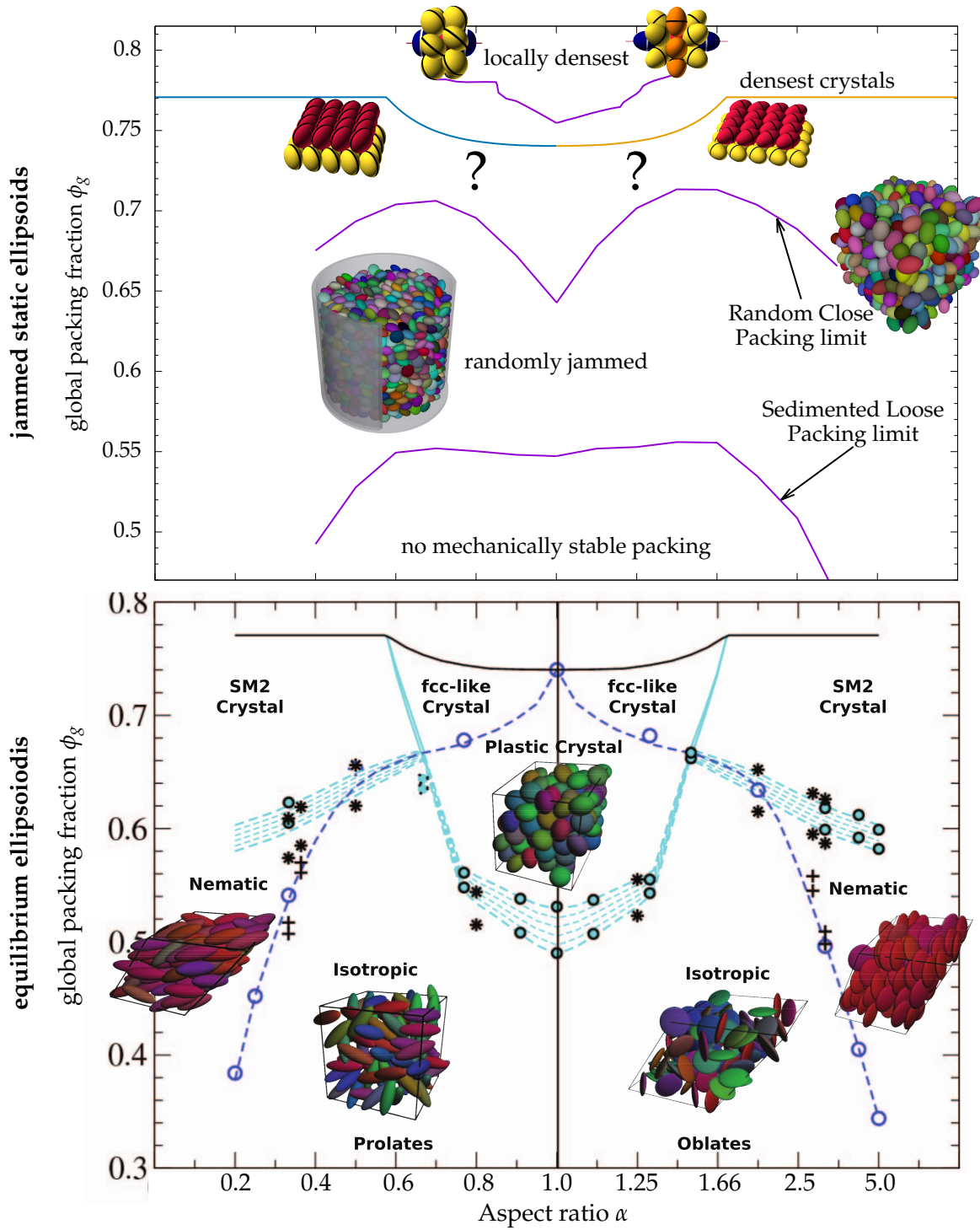
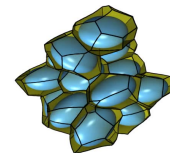


Figure 1.3: Simplified phase diagram of jammed (top) and equilibrium (bottom) uniaxial ellipsoids. Image of equilibrium phase diagram is reprinted from Ref. [154], with the permission of AIP Publishing.

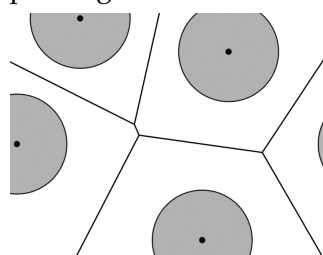


While conceptually important and simple, contact numbers are nearly impossible to extract robustly from 3D images. In experimental packings of particles, e.g. imaged by X-ray tomography, contacts between particles are very hard to detect due to noise in the imaging and in the particle detection [P8]. Even in simulations, the contact detection is hard and often connected to a numerical cut-off. A slight change of the position of one particle can change the whole contact network around that particle. Furthermore, there are particle systems where the particles are not in contact, see below. This deficiency calls for alternative structure metrics, methods to gain quantitative information about the spatial arrangement.

## Structure metrics and Voronoi diagrams

Commonly used structure metrics to describe global (averaged) properties are the *mean intercept length tensor MIL* characterizing anisotropy by a directional analysis of the segments of random lines within the two different phases of a binary image [84, 206], *hyperuniformity* which characterizes spatial density fluctuations [195], or *Fourier transforms*, see e.g. Refs. [38, 199].

A widely used locally defined order metric is the bond-orientational order parameter  $Q_l$  defined by Steinhard et. al [189].  $Q_6$  depends crucially on the neighborhood definition which can change the numerical values as well as the qualitative functional trend [147]. Furthermore it is not a continuous function of the particle coordinates. Given all these shortcomings,  $Q_6$  is not a very robust measure to describe disordered packings.



Voronoi tessellation

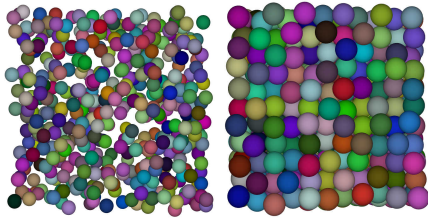
More robust metrics to describe the local structure of particle packings can be derived from Voronoi tessellations [157]. The Voronoi tessellation associates with each particle a region of space, called the Voronoi cell, that is closer to this particle than to any other. The Voronoi cells capture the local geometrical arrangement of a particle relative to its neighbors. The statistical distribution of the volumes of the Voronoi cells of sphere packs has been studied in the context of granular materials [18]

[P4] [P5] and liquid and super-cooled fluids [187]. In particular, distributions of Voronoi cell volumes are sensitive to structural transitions in granular assemblies [68, 70, 115, 129, 176, 187, 205] [P4]. For spheres, an analytic model exists, which predicts the full distribution of Voronoi cell volumes [14, 18]. An extension to ellipsoidal particles is described in chapter 4. In the so-called Edwards ensemble (a statistical mechanics approach to describing granular material through an analogy with equilibrium ensembles), Voronoi cells relate to the equivalent of temperature, the so-called compactivity [8, 23, 32, 64].

Different measures have been invented to quantitatively describe the geometric shape of the Voronoi tessellations. Simple descriptors are the volume or the surface area of the cell. Tensorial measures are sensitive to anisotropic and orientational aspects of the cells. Examples are the tensor of inertia  $\mathbf{I}$  [77], the quadrupole ten-

sor  $\mathbf{Q}$  [96, 151] or Minkowski Tensors  $\mathbf{W}_V^{r,s}$ , the approach used in our work, see Refs. [P4], [P7] and [P13]. An overview is presented in chapter 3 as well as an extension for the Voronoi tessellation for non-spherical particles.

### Equilibrium hard particle systems



*Equilibrium hard sphere system - below and above the phase transition*

In contrast to the above discussed athermal systems, where thermal fluctuations are neglectable, are thermal equilibrium systems. A common reference system is the hard sphere equilibrium fluid (also known as Gibbs ensemble [42]), where the only interaction between the particles is hard-core repulsion. No external force, like gravity, is applied to the system. Hard sphere fluids show a first-order phase transition between a disordered and ordered state which is of purely entropic nature. In between, from  $0.494 \lesssim \phi_g \lesssim 0.545$ , a coexistence region exists, see Fig. 1.2 (bottom). This is different to the hard disc fluid in two dimensions, which show a two step transition which was the subject of much debate around the famous KTNHY conjecture [109]. A morphometric analysis of the Voronoi diagram can reveal these phase transitions, see e.g. Ref. [P14]. For non-spherical particles the behavior is more complex. Frenkel *et al.* provided the first basic picture of the phase diagram of hard spheroids [71]. They showed that ellipsoids can form additional phases which are nematic phases or plastic solids, that appear for different aspect ratios at different packing fractions. Nematic phases show orientational order but no order in the position of the particles, plastic solids show order in position but no orientational order [53, 154]. An overview is shown in Fig. 1.3 (bottom).

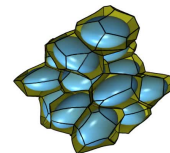
### Beyond granular materials – nano- and micron-scale packings in soft matter

Questions related to particulate assemblies are, however, by no means restricted to granular materials. The question how particles pack exists on various length scales, and is very important in many different fields from biology to industry. On the nano scale, physicists discovered that the crossribs and ridges of the wing scales of the butterflies of the *Pieridae* family are decorated with small ellipsoidal beads, see figure on the left. A high pigment concentration in these beads and light scattered at the irregular arrangement are responsible for the different colors of the butterflies [188, 207].

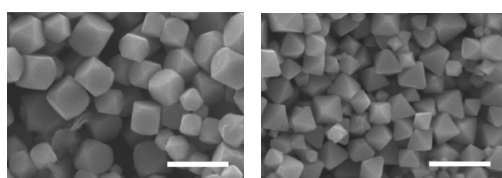


*Scanning electron micrograph of wing scale. Image from [207]*

A further particularly striking example of the relevance of shape is provided by a recent study of 'pear-shaped' particles [65, 178]. These particles are tapered ellipsoids, that is, rotationally symmetric particles with one wide and one narrow



end. As a thermodynamic hard-core fluid these assemblies adopt –apart from the conventional liquid crystalline nematic, smectic and disordered phases– a highly-symmetry network-like bicontinuous ‘Gyroid’ phase. This phase with one of the highest spatial symmetries possible in 3D space is generated in this purely entropy-driven system, without attractive or repulsive interactions except for the hard core collisions. It is an interesting open question if granular systems, rather than thermal systems, can also be coaxed into adopting such high-symmetry meso-scale spatial order.



truncated cubes

octahedra

(scale bar: 1  $\mu\text{m}$ )

Images reprinted with permission from [91].  
Copyright 2009 American Chemical Society.

In chemistry, the influence of shape to the formation of self-assembled packing structures of nanocrystals or the synthesis of colloidal particles of varying shape is of great interest [74]. The Figure on the right shows SEM images of  $\text{Cu}_2\text{O}$  nanocrystals. Examination of their facet-dependent physical and chemical properties may enhance properties and functionality of nanomaterials [91, 93].

### Polydisperse packings and shape variations

The properties of particle packings have broad relevance in nature, industrial applications and physics, where particles have usually different sizes and are often irregular and randomly shaped. To assess the effect of grain size, we perform experiments with bidisperse ellipsoids, i.e. ellipsoids with the same shape (aspect ratio) but two different sizes, see section 2.1.2. Varying the mixing ratio of the two particle sizes will help to understand packings of real polydisperse packings, where all particles have different sizes. Experiments on Ottawa sand are performed to investigate the effect of grain irregularity to particle packings, see section 2.1.2 and Ref. [P10].

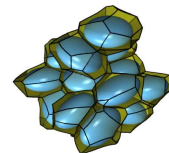
Packings of particles with complex shapes show complicated behavior with various effects. The paradigmatic approach of physics is the reduction of a system of such complexity to the quintessential toy model that has minimal ingredients to still show the effect in question. The simplest approximation of a granulate are spheres, which already show a complex behavior where details are still under investigation. Ellipsoids offer the possibility to investigate the effect of particle shape to the packing properties. By varying the aspect ratio, the particle shape can be changed continuously from spherical to very elongated. The effect of grain size variations can be assessed with packings of bidisperse ellipsoids, and the effect of



Packing experiment with  
Ottawa sand

shape irregularity by Ottawa sand grains with the same volume. The analysis of these toy models helps to generate and improve particle models and to understand the collective behavior of particle systems with complex grain shapes.





## 2 Tomographic experiments and simulations of ellipsoid packings

This chapter provides an overview over the different particle types, experimental setups, tomographic imaging methods as well as the numerical simulation methods used for creating packings of ellipsoids. With more than 100 tomographic datasets and more than 1000 numerically generated datasets, this work represents one of the most comprehensive study of packings of ellipsoidal particles.

### 2.1 Preparation and tomographic imaging of packings

#### 2.1.1 Frictional monodisperse ellipsoids



3D printer



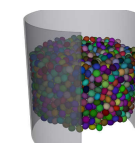
pharmaceutical placebo pills

Our experimental study comprises two different types of oblate ellipsoids with various aspect ratios, the properties of which are summarized in Tab. 2.1. The pharmaceutical placebo pills (PPP) have an aspect ratio of  $\alpha = 0.59$ . Due to

their sugar coating, their surface is rather smooth and their static coefficient of friction  $\mu_s$  is rather low. The second particle type are gypsum ellipsoids cured with resin, produced with a 3D printer (Zprinter 650, Z corporation). The aspect ratio of these 3DP particles ranges from 0.4 to 1 (i.e. spherical). Their rougher surface results in a



PRL 2015



AIP 2013

aspect ratio $\alpha$	half axis		type	friction coefficient $\mu_s$	particles in core region	number of analyzed packings
	short [mm]	long [mm]				
spheres	3.1		3DP	$0.75 \pm 0.07$	660-850	15
0.80	2.65	3.30	3DP	$0.75 \pm 0.05$	750-850	17
0.60	2.20	3.75	3DP	$0.67 \pm 0.03$	620-710	16
0.59	2.15	3.55	PPP	$0.38 \pm 0.05$	850-910	15
0.40	1.60	4.00	3DP	$0.67 \pm 0.05$	620-730	10

Table 2.1: Material properties of the particles used in the experiments.  
3DP = 3D printer particles, PPP = Pharmaceutical placebo pill.

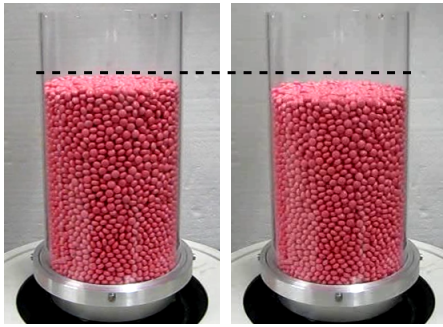
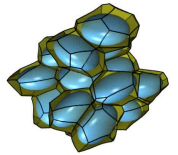
higher friction coefficient  $\mu_s$ , which leads to looser packings compared to the PPP particles.

Packings of frictional particles can result in a range of global packing fractions. To cover a large part of possible packings, we prepare initial loose packings of ellipsoids inside a perspex cylinder with an inner diameter of 104 mm. The global packing fraction can be increased by tapping the packing using a shaker. The final density depends on the initial preparation method and on the number of applied taps. We use three different methods to prepare the initial packings:

- *tube*: A tube with an inner diameter of 90 mm is placed into the container and then slowly filled with ellipsoids poured through a funnel. Then the tube is manually pulled out very slowly. Particles close to the cylinder wall can move into the freed space and create a loose packing. This method is very easy to apply but creates a radial inhomogeneity of the packing fraction, because particles in the center cannot use the freed space and are more densely packed than particles close to the cylinder wall. Most of the packings created with this method are discarded because of these radial inhomogeneities.
- *horizontal grid*: A tube with an inner diameter of 90 mm is placed into the container. Inside the tube are several meshes of metal rods. By pulling out the tube very slowly, the particles are slightly lifted and rotated by the rods which gives all particles the ability to rotate and arrange in a loose packing. The orientations are distributed fairly randomly. This method creates the most homogeneous packings and is therefore used most.
- *fluidized*: The ellipsoids are fluidized by an upward air flow through the cylinder, which is then slowly reduced to let the ellipsoids settle in a very loose configuration. By using this method, the particles can align with the air flow, which can result in a packing with orientationally ordered domains. The airflow needs to be very homogeneous to create disordered packings. Applying an inhomogeneous airflow to the packing, only parts of it will be lifted and convection occurs. This method is used to create the loosest packings.

Except for the loosest samples, the packings are then compactified by applying sinusoidally shaped pulses on an electromagnetic shaker (LDS V555).





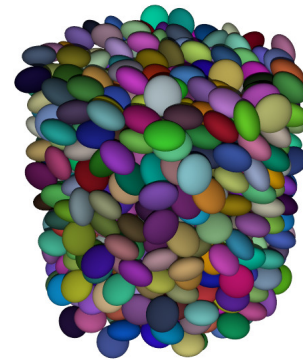
*Compaction by tapping*

We apply three taps per second with a peak acceleration  $2g$  (where  $g = 9.81\text{m/s}^2$ ). The chosen peak acceleration is higher than the gravitational acceleration on earth which allows the particles to move and rearrange [161]. The pulse width is 50 ms, resulting in very fast pulses followed by a relaxation time of 270 ms which allows the particles to fully settle before the next pulse is applied. It can be thought of as tapping the container on a table top. By varying the number of taps (up to 1500), packings of different densities are created.

Tomograms of the prepared packings are acquired using circular X-ray computed tomography with a resolution of  $64\ \mu\text{m}$  per voxel. The resulting three-dimensional gray scale image is the starting point for the identification of all particle centers and orientations using the methods described in [P8]. To reduce boundary effects, particles close to the top and bottom of the packing as well as close to the container wall are discarded, details see Ref. [P5]. The resulting configurations are in addition tested for spatial homogeneity. The particle positions and orientations can be downloaded from the Dryad repository [2].



*Volume rendering of tomographic grayscale image*



*detected particles*

### 2.1.2 Frictional bidisperse ellipsoids



Most published studies analyzed packings of monodisperse particles. Given the obvious relevance of polydisperse packings to model realistic systems we analyze bidisperse ellipsoid packings, i.e. packings which contain ellipsoids of two different sizes but both with the same aspect ratio. The aim of this work is to identify the key mechanisms of granular compaction and to study the Voronoi diagram of such bidisperse packings. The packings analyzed here consist of pharmaceutical placebo pills with aspect ratio  $\alpha \approx 0.57$  and large axis lengths of 8.9 mm and 10.2 mm. The particles mixing ratio is chosen such that the total volume of each particle type in the container is identical. This results in a mixing ratio of 3:2 (small particles : large particles).



Figure 2.1: *Loose packing preparation: (left) During the initial filling the container is rotated on a motorized platform. (middle) The two grids have been pulled out slowly to create a loose packing with random particle orientations. (right) Final loose packing.*

Pictures of the different stages of the preparation of the initial packing are shown in Fig. 2.1. To create an initial random packing, the particles are poured into a container of diameter 144 mm. During the filling stage, the container is rotated slowly on a motorized platform ( $\approx 10$  rotations per minute) to create a homogeneous filling. After the cylinder is completely filled, two grids, which have been placed before at the bottom of the container, are pulled slowly through the packing to create a loose packing. The circular grids have a square mesh size of  $\approx 20$  mm, spatially separated by  $\approx 25$  mm in height and their mesh orientation is rotated by 45 degrees with respect to each other. This technique leads to a reproducible loose packing with a packing fraction of  $0.657 \pm 0.003$ , see Fig. 2.2. To compactify the packing, we follow the same tapping procedure as for the monodisperse packings by performing sinusoidal pulse taps of an accelerations of 2 g with an electromagnetic shaker (TIRA TV51140).

The resulting packings are imaged by helical X-ray tomography in which the sample is vertically translated while being rotated. This offers the opportunity to scan the whole length of the sample. Another advantage of the helical scanning method is that the resulting 3D gray-scale image can be reconstructed without approximations and results in a less image [113, 181, 201]. The resulting gray-scale image has a voxel size of  $56 \mu\text{m}$ . The particle positions and orientations are again detected by the watershed based segmentation method described in Ref. [P8]. Particles close to the boundaries (cylinder walls, top and bottom) are removed from the analysis.

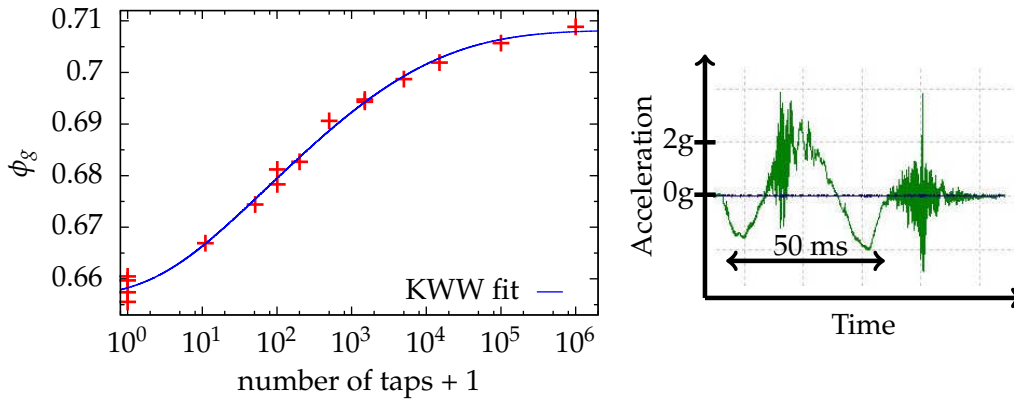
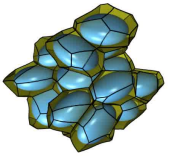


Figure 2.2: (left) Change of the global packing fraction  $\phi_g$  during tapping of packings of bidisperse ellipsoids. In blue the fit of the KKW law to the data. (right) Acceleration during a single tap. The acceleration at the container base is measured using an accelerometer (B&K 4507, 1000mV/g) via the shaker systems motion controller (Vibration Research, VR9500).

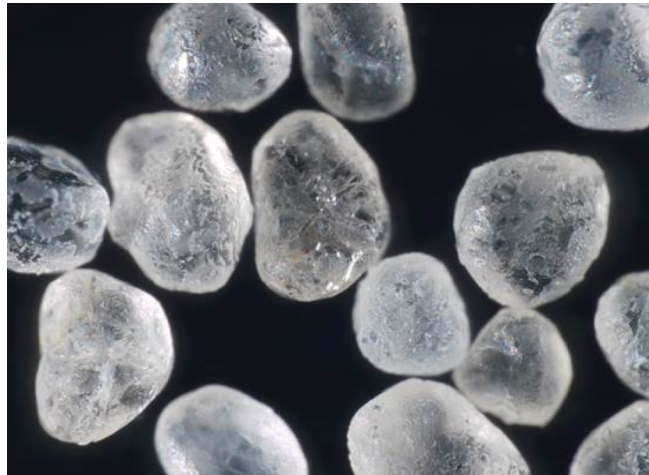
Fig. 2.2 shows the densification of the system during tapping. Up to  $10^6$  taps are applied, which results in the packing with the highest global packing fraction  $\phi_g \approx 0.709$ . The densification is reminiscent to relaxation and compaction dynamics in glassy systems which are commonly fitted by a stretched exponential law, the KKW (Kohlrausch, Williams, Watts) law [117, 161]

$$\phi_g = \phi_{\text{inf}} - (\phi_{\text{inf}} - \phi_0) \cdot \exp \left[ - (\text{\#taps} / \tau)^\beta \right] \quad (2.1)$$

A fit of the KKW law to our data of bidisperse ellipsoids is presented in Fig. 2.2.

### 2.1.3 Ottawa sand

The most complex analyzed samples in this work are packings of Ottawa sand. Ottawa sand is silica sand mined from Ottawa, Illinois. The sand is composed of rounded grains with high crush resistance and is used as a standard by the American Society of Testing Materials [29]. To reduce the polydispersity in grain size, the sand is sieved and only sand grains between  $500 \mu\text{m}$  and  $1 \text{mm}$  in diameter are used in the experiments.





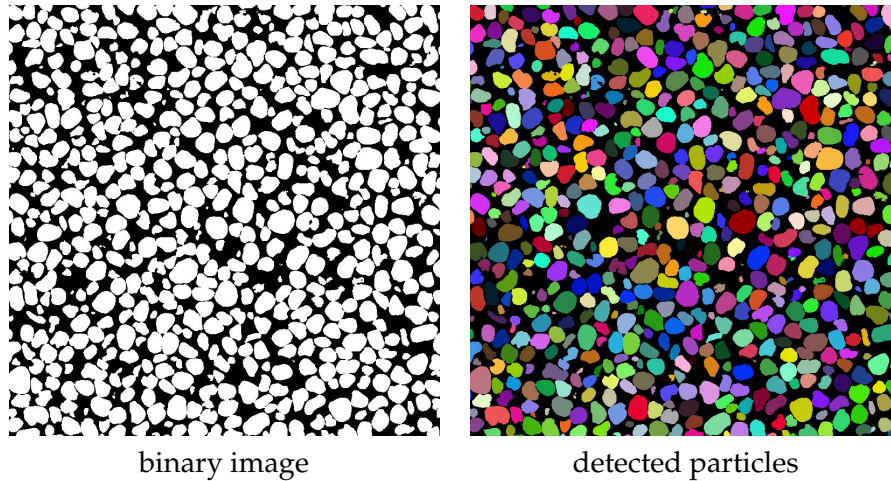
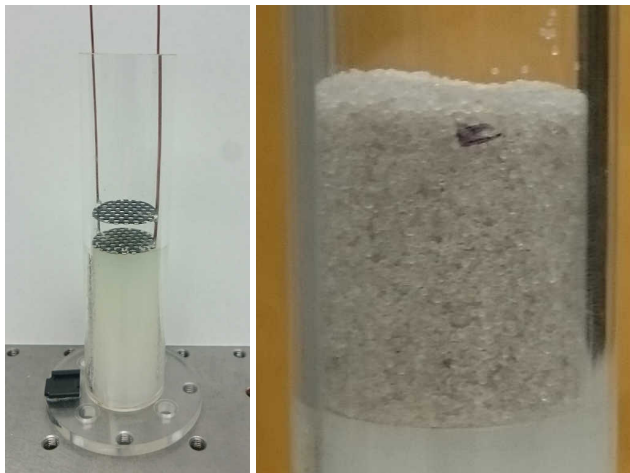


Figure 2.3: (left) Slice of a 3D binarized tomographic image of a packing of Ottawa sand. (right) Detected particles after using the watershed based method in Ref. [P8].

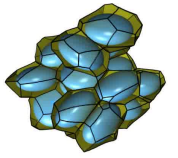


Packing experiment with Ottawa sand  
(left) container with grid, (right) final packing

The preparation method is similar to the preparation of the ellipsoid packings. A loose packing is created by filling the grains inside a cylindrical perspex container with a diameter of 24 mm. By pulling a double grid through the sand, the packing is loosened and the grains are oriented randomly. Afterwards most of the packings are compacted by sinusoidal taps with different accelerations, from 0.5 g to 2 g. After imaging the particles by helical X-ray tomography with a voxel size of 9  $\mu\text{m}$ , the particles are

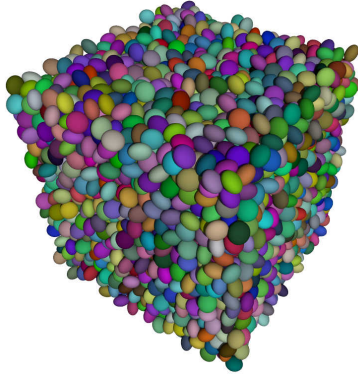
detected by a watershed segmentation method [146, 149, 169, 171] [P8], see Fig. 2.3.

First experiments show a visual onset of convection inside the packing after a few taps with an acceleration of 2g. Particles in the middle of the container move upwards and a sand pile-up in the middle is observed. The resulting packings are radially very inhomogeneous. In the future, more packing experiments with a smaller acceleration are planned to reduce convection effect and generate more homogeneous dense packings.



## 2.2 Simulations

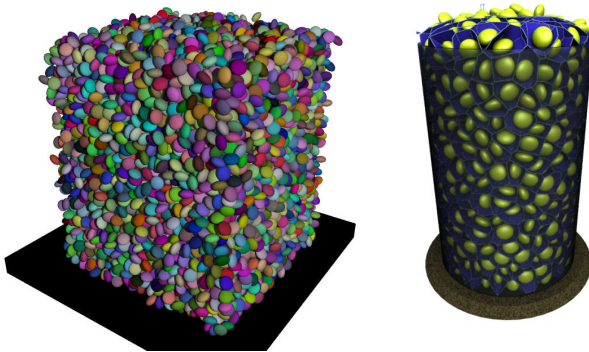
### 2.2.1 Dense packings – Lubachevsky-Stillinger-Donev protocol



Dense jammed random packings of frictionless ellipsoids are created by the Lubachevsky-Stillinger-Donev protocol [58, 59], that corresponds to a slow compression of an initially loose packing to a jammed structure. This packing protocol does not implement gravity. As initial condition, 5000 small particles are randomly placed in a box with periodic boundary conditions. The compression of the system is realized by expanding the particles. The expansion rate has to be chosen rather slow to produce dense jammed packings, but not too slow, to avoid the eventual formation of crystalline domains.

In our simulations an expansion rate of  $3 \times 10^{-6}$  to  $1 \times 10^{-5}$  times the thermal velocity is used. The resulting packings are essentially free of orientational order<sup>6</sup>. Thus, our packings are representative of the random close-packed (or maximally random jammed) state for the respective aspect ratio [54, 56]. Particles with aspect ratios between  $0.7 \leq \alpha \leq 1.4$  are analyzed. For each aspect ratio, at least 100 random packings are created.

### 2.2.2 Discrete Element Simulations (DEM) of frictional particles



*Static packings of frictional sedimented ellipsoids with different boundary conditions.*

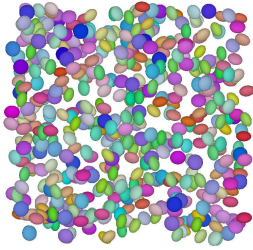
Simulations of jammed static structures are obtained by discrete element simulations (DEM) using the implementation developed at CSIRO [45, 55] in cooperation with Gary Delaney. DEM simulations allow for the simulation of friction and gravity. The particles are virtually sedimented in a viscous fluid. The simulations are performed in a square box with periodic

boundary conditions in x-y direction (gravity in z-direction) as well as for ellipsoid settling in a cylindrical container. In total 120 configurations, of 9323 ellipsoids with aspect ratios between 0.3 and 1.0 (spheres) are generated. By varying the friction coefficient of the particles and viscosity of the fluid different packing fractions are achieved. The loosest packings are obtained for particles with very high friction

<sup>6</sup> The nematic order parameter tensor is close to isotropic, its largest eigenvalue is smaller than 0.04. See Ref. [5] page 130 ff. for details.

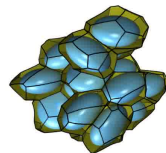
coefficient, see sedimented loose packing (SLP) in Fig. 1.3 and Fig. 4.6. Packings of frictionless particles result in the densest packings [55].

### 2.2.3 Equilibrium fluids – Molecular dynamics & Monte Carlo



*Equilibrium fluid  
of ellipsoids.*

As reference data, equilibrium configurations of hard-core ellipsoids in the fluid phase are generated. No external forces, such as gravity, are applied to the particles and the configurations are in general not jammed. The configurations are obtained by event-driven molecular dynamics simulations [52] (MD, the same data sets as in ref. [53]). For low densities, because of their faster convergence, canonical Monte Carlo simulations are performed (MC, [160]). All datasets contain 1024 particles and are performed with periodic boundary conditions. In the limit of vanishing density  $\phi_g \rightarrow 0$ , where the typical distance between particles is large compared to the particle size, the distributions of center points coincides with the Poisson point process [P4][P14], see Fig. 4.6.



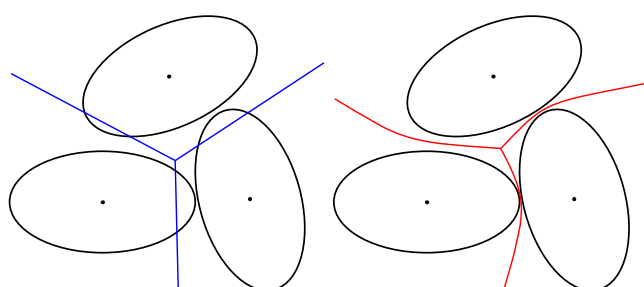
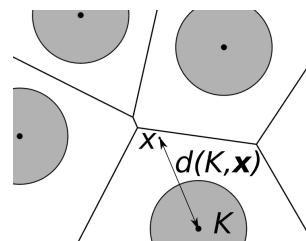
### 3 Quantitative morphology of spatial tessellations and granular assemblies

This chapter presents an overview of the analysis tools used in this work. These tools include Set Voronoi diagrams as an extension to the conventional Voronoi diagram for non-spherical particles, Minkowski Tensors as robust analysis tool to characterize shape, and a local density resolved analysis which can reveal differences in structure which are not captured by global averages.

#### 3.1 Set Voronoi diagrams as tessellations for non-spherical particles

The Voronoi diagram is a fundamental geometric structure that has found applications in numerous fields [157]. Its construction in three-dimensional systems has become a common element of structural analyses of assemblies of spheres, including packing problems of granular matter [18, 30, 68, 110, 115, 133, 155, 176, 184, 185, 209, 211] [P4], glass-forming systems [9, 159, 187], fluid systems [67, 124, 172] [P14], etc. Other applications include random foam structures [121, 122] or ordered systems such as crystal chemistry [21, 33].

For a set of spherical particles, the most common way to tessellate the void space between the particles is the conventional Voronoi tessellation, by which the Voronoi cell of a particle is that of its centre point. Given a set of points, the Voronoi cell of a point is the region of space that is closer to this point than to any other with respect to the Euclidean distance  $d$  [157]. In condensed matter physics, this tessellation is also known as the Wigner–Seitz unit cell.



Conventional and Set Voronoi tessellation for ellipsoids

In most applications, the considered particles are not spherical. Shapes of interest are, for example, ellipsoids [53, 55, 56, 57, 71, 137] [P1][P4][P5], tetrahedra [80, 150], supercubes [54] and pear-shaped particles [65]. For these particles, the conventional construction of the point Voronoi diagram fails, because

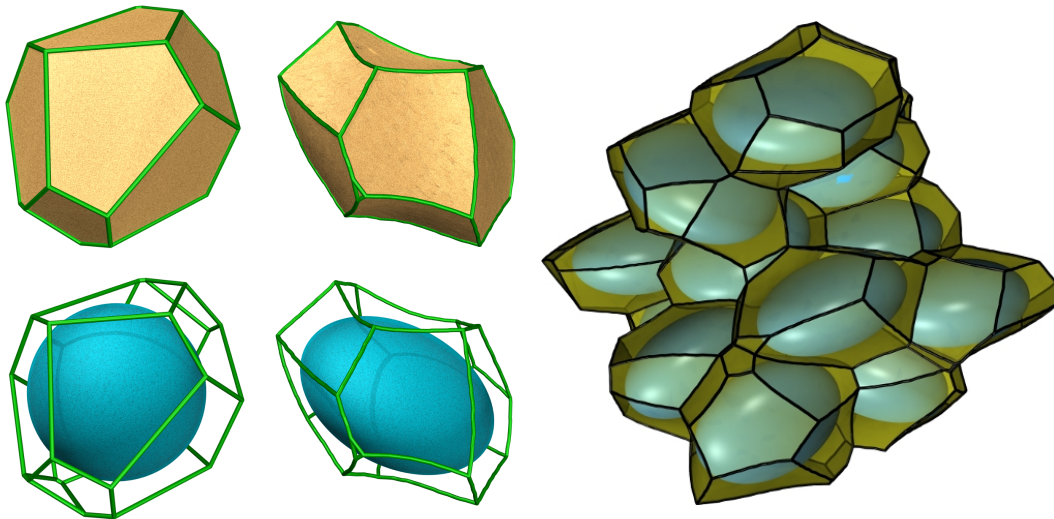


Figure 3.1: *Difference between the conventional Voronoi and the Set Voronoi cells. (left) A Sphere and its Voronoi cell (middle) Set Voronoi cell of an ellipsoid with curved edges and facets. (right) Subset of a packing of ellipsoids with Set Voronoi tessellation. Pictures are taken from Ref. [P7]. A flip-book movie of this rotating packing can be found in the right top corner of this work.*

facets of the cell may intersect with the particles. The same problem exists for the case of polydisperse particle packings. For these cases, we extend the conventional Voronoi construction to the *Set Voronoi* tessellation. The Set Voronoi cell of a given particle is composed of all points in space that are closer to the surface (as opposed to the centre) of the given particle than to the surface of any other. For the case of monodisperse spheres, this definition reduces to the conventional Voronoi diagram. Fig. 3.1 shows the difference between conventional Voronoi cells for monodisperse spheres with flat facets and Set Voronoi cells with curved facets and edges. For the case of poly-disperse spheres (or disks), any facet in between two spheres of different radii is curved. This is different to the Laguerre tessellation (or weighted Voronoi diagram) which has flat facets [13, 20, 127], and which has been used to construct cells around poly-disperse spheres e.g. as initial configurations for fluid foams [122].

In the literature this generalization is also known as *navigational map* or *Voronoi S regions* [133, 134, 144]. In the computational geometry literature, these constructions are often called *generalised Voronoi diagrams* (or curved or non-affine Voronoi diagrams [36]), or *Area Voronoi diagrams* for the planar case [157]. The Set Voronoi construction is a special case of the medial axis representations of non-convex objects [34, 182]. In mathematical morphology, it is referred to as *skeleton by zone of influence* [162].

In the following we describe two algorithms to calculate Set Voronoi tessellations for arbitrary shaped objects. These algorithms are an extension to Voronoi algorithms, which have been proposed for simple objects (such as lines planes, spheres, cylinders, spherocylinders, poly-disperse spheres etc.) [83, 85, 133], and, as approximations, for sets that include polyhedra using octrees [35].



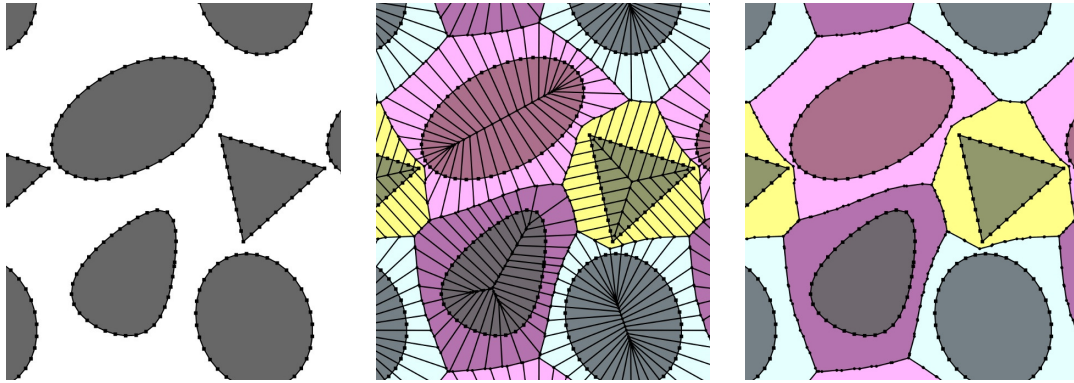
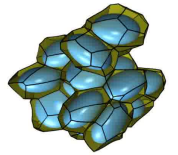


Figure 3.2: Construction of the Set Voronoi Diagram by discretizing the surface of the particles. The Set Voronoi cell is approximated by the union of the point Voronoi cells of all triangulation vertices for each particle. Pictures are taken from Ref. [P6].

Most recently, Baule *et al* [27] have described an exact construction for the Set Voronoi diagram of particles that can be represented by unions or intersections of spheres, as dimers or trimers. For ellipsoids, spherocylinders and tetrahedra approximations are presented. This work is of particular interest as it lends itself to analytical treatment of some aspects of the Voronoi diagram.

### 3.1.1 Algorithm for parametrizable particles

If the surface of the particles is known, for example from numerical simulation data, we can use the following triangulation approach. At first, we discretize the particles' bounding surfaces by a sufficiently dense set of vertices. Second, we compute the conventional point Voronoi diagram for all those vertices. Finally, the Set Voronoi cell of a given particle is approximated by the union of the Point Voronoi cells of all triangulation vertices of that particle. An illustration is shown in Fig. 3.2. This method allows us to calculate the Set Voronoi diagram for all kinds of particles; for example, tetrahedra, supercubes, cuboids, pear-shaped particles, which are currently under investigation.

Note, that this algorithm is closely related to Voronoi-based medial axis algorithms, developed for 3D space in [182]. The exterior medial axis of a given body  $K$  is the locus of all points in the complement (i.e. the outside) of  $K$  that are equidistant to two distinct points on the bounding surface  $\partial K$ . The facets of the Set Voronoi diagram of a set of disjoint objects represents precisely the medial axis (or surface) if the particles are convex. In this sense, our algorithm is a special case of the medial axis algorithm.

### 3.1.2 Set Voronoi diagram for tomographic (voxelized) images

Experimental data mostly consists of voxelized 3D images, for example from confocal microscopy or tomography. The computation of Voronoi domains directly in voxelized space is an alternative to the triangulation approach discussed above. No

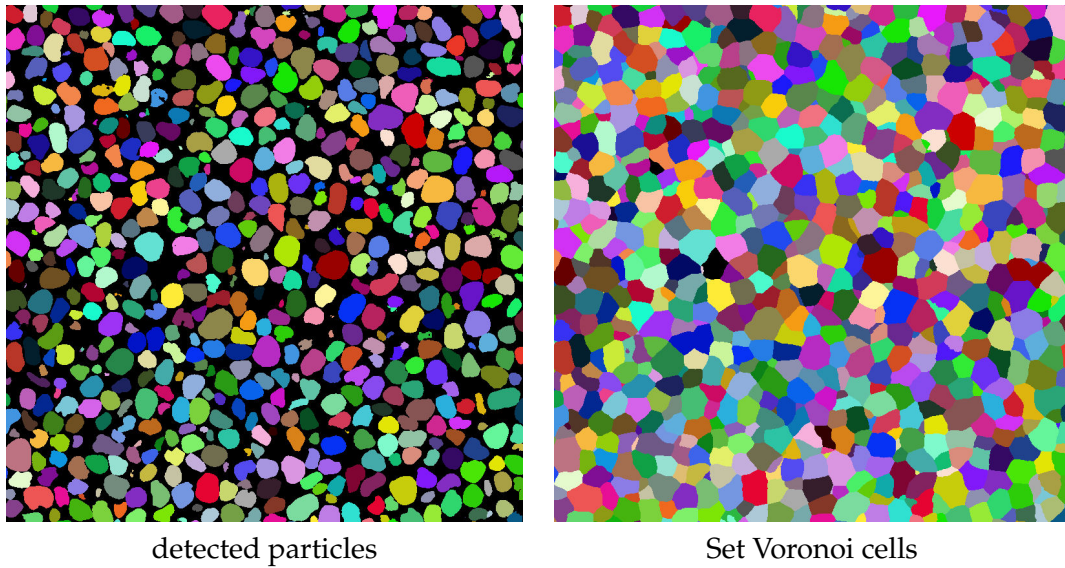


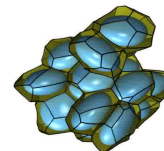
Figure 3.3: *Slice of a 3D image of a packing of Ottawa sand.*

parametrizations of the particle shapes in the sample are required. The resolution of the resulting 3D Voronoi image is limited to the resolution of the input data.

Here, we describe an algorithm, based on a Watershed transform [146, 149, 169], which is used to identify the space around each particle that correspond to the Set Voronoi cells. Such algorithms have already been used for related problems in granular materials [171, 192].

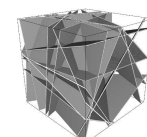
We start with a voxelized 3D image where all the grains are detected and labeled individually. An example is presented in Fig. 3.3 (left), which shows the detected grains of a packing of Ottawa sand. The voxel-based approach uses the Euclidean distance map  $D(\mathbf{x})$  of the void space in between the set of the particles<sup>7</sup>. We exploit the fact that the facets (in 3D) or edges (in 2D) of the Set Voronoi cells represent ridge lines of the Euclidean distance map  $D(\mathbf{x})$ .  $D(\mathbf{x})$  is a continuous function that increases in the direction away from the nearest particle. The gradient  $|\nabla D(\mathbf{x})| = 1$  is differentiable for all points  $\mathbf{x}$  except along the Voronoi cell facets (in 3D) or edges (in 2D) where the gradient direction is discontinuous; these are the ridge lines. For any given particle, its basin is composed of all points in space from which descent along the gradient directions  $\nabla D$  leads to points on the boundary of that given particle, hence the name watershed algorithm. The basin of each particle is its Set Voronoi cell. As an example, Fig. 3.3 (right) shows the result of a voxel-based Set Voronoi tessellation of a packing of Ottawa sand grains.

<sup>7</sup>The Euclidean distance map  $D(\mathbf{x})$  assigns to each space point (voxel) the Euclidean distance to the nearest (boundary) point of the set of particles.

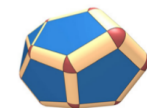


## 3.2 Shape analysis by Minkowski tensors<sup>8</sup>

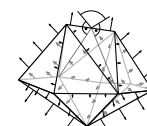
Minkowski Tensors have been developed as robust and anisotropy-sensitive structure metrics, with a particular strong point being their foundation in comprehensive rigorous mathematical theory, from integral geometry. The general framework has been developed in [P7] and earlier works [4, 94, 175]. Publications [P4], [P7], [P13] and [176] have specifically developed and established their use for granular materials and the characterization of structural properties, and publication [P7] establishes the link to the integral geometry literature.



Springer 2016



NJP 2013



Adv. Mat. 2011

### 3.2.1 Minkowski functionals and tensors

Minkowski functionals, also known as *intrinsic volumes*, and Minkowski tensors, their tensorial generalization, are emerging as commonly used quantities to describe spatial structures. They have been applied to various applications in physics [11, 12, 122, 138, 142, 143, 173, 174, 176] and biology [24, 28].

For a three-dimensional body  $K$  representing the spatial structure, the scalar Minkowski functionals are, up to pre-factors, the volume  $W_0(K)$ , the area of the bounding surface  $W_1(K)$ , the integral of the mean curvature over the bounding surface  $W_2(K)$  and the topological Euler-Poincaré index  $W_3(K)$ . The use of the encompassing term Minkowski functionals for these fundamental shape indices makes sense in the light of a theorem due to Hadwiger that states (in essence and omitting mathematical detail) that any motion-invariant conditionally-continuous additive functional  $f(K)$  of a body  $K$  is a linear combination of the Minkowski functionals [79]. In this sense, mathematical theory imposes that scalar Minkowski functionals are the relevant shape indices w.r.t. to physical properties represented by such additive functionals.

By definition, the scalar Minkowski functionals are rotation-invariant, which makes them not explicitly sensitive to directional and anisotropic features of morphology. This fact motivates their generalization to tensorial shape indices which are called Minkowski tensors, capable of quantifying anisotropic and orientational aspects of morphology and geometry.

Here, we focus on the generalization to Minkowski tensors of rank two, while in principal, Minkowski tensors can be defined for arbitrary rank. An intuitive generalization of the scalar functionals  $W_0 \propto \int_K dV$  and  $W_\nu(K) \propto \int_{\partial K} g_\nu dA$  (for  $\nu = 1, \dots, 3$ ) is achieved by introducing tensor products of position vectors  $\mathbf{r}$  and surface normal vectors  $\mathbf{n}$  into the integrals ( $g_1 = 1$ .  $g_2$  and  $g_3$  are the point-wise mean and Gaussian curvature of the bounding surface  $\partial K$ , possibly their discrete equivalents applicable to polyhedra). For spatial geometries there are six relevant linearly-independent tensors.

<sup>8</sup>This section contains verbatim extracts of ref. [P13] of which I am co-author.

**motion covariant**

$$\mathbf{W}_0^{2,0}(K) := \int_K \mathbf{r} \otimes \mathbf{r} \, d\mathbf{V}, \quad (3.1)$$

$$\mathbf{W}_1^{2,0}(K) := \frac{1}{3} \int_{\partial K} \mathbf{r} \otimes \mathbf{r} \, d\mathbf{A}, \quad (3.2)$$

$$\mathbf{W}_2^{2,0}(K) := \frac{1}{3} \int_{\partial K} H(\mathbf{r}) \mathbf{r} \otimes \mathbf{r} \, d\mathbf{A}, \quad (3.3)$$

$$\mathbf{W}_3^{2,0}(K) := \frac{1}{3} \int_{\partial K} G(\mathbf{r}) \mathbf{r} \otimes \mathbf{r} \, d\mathbf{A}, \quad (3.4)$$

**motion invariant**

$$\mathbf{W}_1^{0,2}(K) := \frac{1}{3} \int_{\partial K} \mathbf{n} \otimes \mathbf{n} \, d\mathbf{A}, \quad (3.5)$$

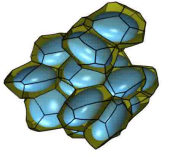
$$\mathbf{W}_2^{0,2}(K) := \frac{1}{3} \int_{\partial K} H(\mathbf{r}) \mathbf{n} \otimes \mathbf{n} \, d\mathbf{A}. \quad (3.6)$$

Here,  $H(\mathbf{r}) = (\kappa_1 + \kappa_2)/2$  and  $G(\mathbf{r}) = (\kappa_1 \kappa_2)$  are the mean and Gaussian curvature of  $\partial K$  and  $\otimes$  the tensor product defined as  $(\mathbf{a} \otimes \mathbf{a})_{ij} = a_i a_j$  for any vector  $\mathbf{a}$ . Note that the labels  $\nu, r, s$  define different tensors and are not the indices of its components; the components are indexed by  $i, j$  and denoted  $(\mathbf{W}_\nu^{r,s})_{ij}$ . The label  $\nu$  represents the same integral types as for the scalar Minkowski functionals ( $\nu = 0$  the volume integral,  $\nu = 1$  the surface integral,  $\nu = 2$  the mean-curvature weighted surface integral, etc) and  $r$  and  $s$  the tensorial powers of the position and surface normal vectors, respectively. Generalizing Hadwiger's statement, Alesker's theorem [4] states, that all motion-covariant, conditionally continuous, and additive tensorial functionals  $\mathbf{F}(K)$  can be expressed as a linear combination of the Minkowski tensors listed above and the scalar functionals multiplied by the rank-two unit tensor. This list of tensors has also been shown to be linearly independent [94].

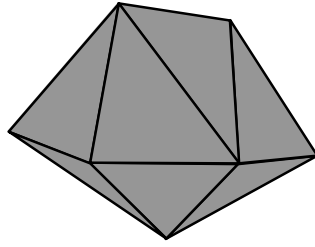
In the following we focus on the interpretation of the two mostly used tensors in this work,  $\mathbf{W}_0^{2,0}$  and  $\mathbf{W}_1^{0,2}$ . The tensor  $\mathbf{W}_0^{2,0}$  can be interpreted as a so-called *moment tensor* of a solid body  $K$  that quantifies the distribution of mass within the body. It bears resemblance to the tensor of inertia  $\mathbf{I}(K) = \int_K (-\mathbf{r} \otimes \mathbf{r} + |\mathbf{r}|^2 \mathbf{E}_3) \, d\mathbf{V} = -\mathbf{W}_0^{2,0} + \text{tr}(\mathbf{W}_0^{2,0}) \mathbf{E}_3$  with the three-dimensional unit matrix  $\mathbf{E}_3$  and  $\text{tr}$  denoting the trace of a matrix and depends on the chosen origin  $\mathbf{0}$ . In contrast, the tensors  $\mathbf{W}_1^{0,2}$  is translation-invariant and the morphological interpretation is the orientational distribution of surface patches  $\partial K$ . For example, given a rectangular prism of size  $L_x \times L_y \times L_z$  aligned with the coordinate axes; the tensor  $\mathbf{W}_1^{0,2}$  is diagonal with components  $(\mathbf{W}_1^{0,2})_{xx} \propto L_y$ ,  $(\mathbf{W}_1^{0,2})_{yy} \propto L_x$  and  $(\mathbf{W}_1^{0,2})_{zz} \propto L_z$ , reflecting the portions of interface oriented along the three orthogonal directions. An illustration for a more general body is shown in Fig. 3.4.

Minkowski functionals are based on integral geometry and fundamental measure theory in mathematics. They are very robust and versatile and can be used in many applications. Further details can be found in Refs. [175], [P7] and [P13].

As part of this thesis and other work, a computer programm called *Karambola* was developed. *Karambola* is able to calculate Minkowski Tensors of three-dimensional bodies and surfaces. It is developed at the Institute of Theoretical Physics in Erlangen, with particular contribution by Sebastian Kapfer and Gerd Schröder-Turk, and is available as free software (<http://theorie1.physik.uni-erlangen.de/karambola>).

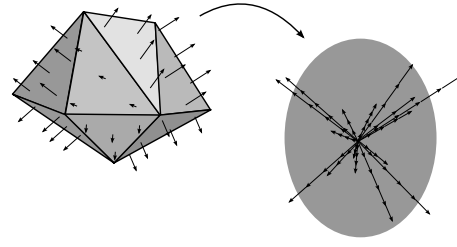


$$\mathbf{W}_0^{2,0}(K) := \int_K \mathbf{r} \otimes \mathbf{r} \, dV$$



moment tensor solid

$$\mathbf{W}_1^{0,2}(K) := \frac{1}{3} \int_{\partial K} \mathbf{n} \otimes \mathbf{n} \, dA$$



normal distribution

Figure 3.4: Geometric interpretation the Minkowski tensors for 3D polyhedral bodies.  $\mathbf{W}_0^{2,0}$  can be interpreted as the moment tensor of a solid body  $K$ , quantifying the distribution of mass.  $\mathbf{W}_1^{0,2}$  represents the distribution of normals of the surface  $\partial K$ . Pictures are taken from Ref. [P13].

### 3.2.2 Anisotropy indices based on Minkowski tensors

The measurement of the order and crystallinity of a sphere packing is a longstanding problem. Different methods have been devised, i.e. the widely used bond-orientational order parameter  $Q_l$  defined by Steinhard et. al [189] or methods based on Minkowski tensors [110, 176] [P7][P13] which are used in this work. These order metrics are all defined with reference to the known densest crystal phases of spheres. The advantage of using Minkowski tensors is that they vary continuously in position of the particles in contrast to other order parameters like  $Q_l$ , where slight changes in particle positions can lead to a large change of the structure metric [147].

While the natural format of Minkowski tensors is, as the name implies, tensorial, it is more convenient to reduce them to scalar indices. The degree of anisotropy of a given body  $K$  (in our case a Voronoi cell) is conveniently expressed as the ratio  $\beta_v^{r,s}$  of minimal to maximal eigenvalue of the Minkowski tensor  $\mathbf{W}_v^{r,s}$ .

$$\beta_v^{r,s} := \frac{|\mu_{\min}|}{|\mu_{\max}|} \in [0,1] \quad (3.7)$$

$\beta_v^{r,s}$  is 1 (and  $K$  said to be isotropic) for any shape that has statistically identical mass distribution in any set of three orthogonal directions; this includes the sphere, but also regular polyhedra and the FCC, BCC and HCP Voronoi cells [110]. Small values of  $\beta_v^{r,s}$  indicate elongated (anisotropic) cells. The eigenvectors to the eigenvalues, referred to as  $\mathbf{e}_i$  are indicators of the orientation of the Voronoi cell  $K$ . Fig. 3.5 shows a Set Voronoi cell of an ellipsoid and the eigensystem of the volume tensor  $\mathbf{W}_0^{2,0}$ . Note however the difference of  $\beta_v^{r,s}$  to measures of asphericity [187] that quantify deviations from a spherical shape.

Structural information of a packing can be gained from the average anisotropy index  $\langle \beta_1^{0,2} \rangle = \sum_{i=1}^N \beta_1^{0,2}(K_i) / N$ , which is the arithmetic mean over all Voronoi cells  $K_i$  of the packing. For spheres, the average anisotropy index of the densest ordered



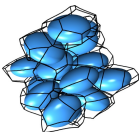


Figure 3.5: (left) Particle in its Set Voronoi cell. (right) Eigensystem of the cell.

structures, which are the crystalline FCC and HCP packing, is  $\langle \beta_V^{r,s} \rangle = 1$ . Disorder is quantified by a deviation from ordered reference structures. Hence, the more disordered a packing of spheres, the smaller is the anisotropy index  $\langle \beta_V^{r,s} \rangle$ . For most non-spherical particles, the densest ordered structures are unknown and are missing as reference structures. Nevertheless, changes of the anisotropy index of a packing can reveal interesting properties, see section 4.3.

Alternative methods for the characterization of anisotropy exist. Anisotropy indices  $q_r$  derived from spherical Minkowski tensors of arbitrary rank  $r$  can be used to characterize spatial structures [108, 147]. Kraynik *et al.* [121] and others [66] described 3D foam cells by anisotropy indices derived from the normal vector distribution of the cells, similar in spirit to the Minkowski tensors. For porous media, anisotropy indices derived from the *mean intercept length tensor MIL* are used for the investigation of the micro-structure of bone, see e.g. Refs. [84, 152, 204, 206]. Deformations of cellular or granular material have been quantified by means of the so-called *texture tensor* [19, 78], which has been used to characterize anisotropy, e.g. for Antarctic ice crystals [63] and liquid foam cells [99]. Further anisotropy indices are based on wavelet analysis [191], the orientation of volumes [153], or star-volumes [111, 152]. Ref. [114] compares of anisotropy indices based on mean-intercept length, star-volume and star-length distributions.

### 3.3 Local (density-resolved) analysis - Looking at the particle scale



EPL 2015

To get a deeper insight and understanding of packings of particles it is useful to not only look at global averages but to also look on the particle scale. Here, we use a local density-resolved analysis based on the idea that the physical mechanisms underlying granular matter occur at the particle scale. A similar approach has been used for the analysis of sphere packings [17, 176]. This analysis provides information how local structure changes depending on local packing fraction.

Figure 3.6 illustrates the concept of the local (or density-resolved) analysis. Particles are grouped by their local packing fraction  $\phi_i$ , i.e. into sets  $\mathcal{S}(\phi_i)$  composed of all

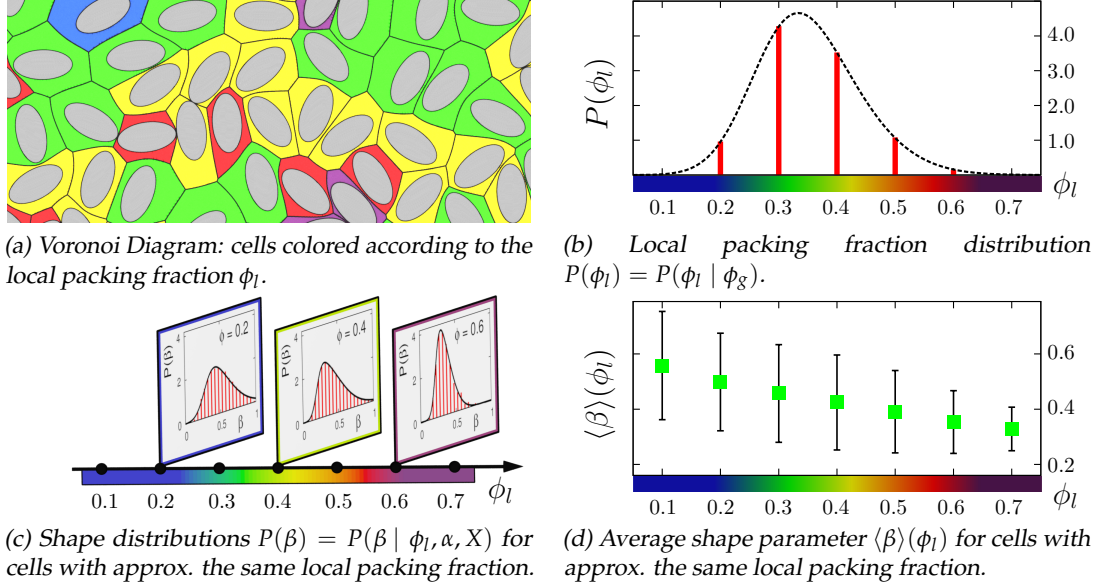
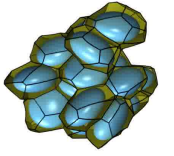
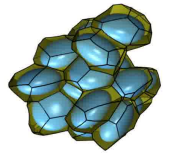


Figure 3.6: Illustration of the density resolved analysis. Pictures are taken from Ref. [P4].

particles  $i$  with  $\phi_l - \frac{\Delta}{2} \leq \phi_i < \phi_l + \frac{\Delta}{2}$  for  $\phi_l = \Delta, 2\Delta, 3\Delta, \dots$  with a small interval  $\Delta$  ( $\Delta = 0.1$  in Fig. 3.6). The function  $P(\beta | \phi_l, \alpha, X)$  is the probability distribution of the shape measures  $\beta$ , restricted to the cells in  $\mathcal{S}(\phi_l)$ , i.e. to those with local packing fraction  $\phi_l$ . The average  $\langle \beta \rangle(\phi_l, \alpha, X) = \int \beta P(\beta | \phi_l, \alpha, X) d\beta$  over all cells in  $\mathcal{S}(\phi_l)$  provides information on how local structure changes depending on local packing fraction  $\phi_l$ . In general, both  $P$  and  $\langle \beta \rangle$  depend on further parameters including the aspect ratio  $\alpha$  and other variables  $X$ , which can be for example the packing protocol or the friction between the particles.







## 4 What can we learn from the Voronoi diagram of hard particle systems?

In packings of particles, the microscopic interactions are encoded in the local structure comprising a particle and its immediate neighbors. Voronoi diagrams are a convenient means to capture, geometrically, the local structure of the particles and their neighborhood. In this chapter, an established model for the Voronoi volume distribution in sphere packings is extended towards ellipsoids [P1]. Furthermore, the Voronoi cell shapes of jammed packings of ellipsoids are quantified by Minkowski tensors. We show that a local analysis reveals non-universalities, which are not captured by global averages [P4].

Voronoi tessellations are widely used to describe the structure of granular assemblies, such as jammed granular packings [18, 30, 61, 68, 70, 110, 115, 133, 155, 176, 184, 185, 209, 211] [P4], glass-forming systems [9, 159, 187] or fluid systems [67, 124, 172] [P14]. Commonly investigated parameters are the Voronoi cell volume and surface area, the number of Voronoi facets or the shape of the Voronoi cells, and correlations thereof.

Short-range spatial anticorrelations between Voronoi volumes are observed in dense 2D disc packings [211] and maximally random jammed packings [115], which do not occur in the Voronoi tessellation of the Poisson point process. This indicates that in dense jammed packings, large Voronoi cells are accompanied by small cells, and vice versa.

In jammed packings of spheres [18] and in dense and glass-forming liquids [187] distributions of Voronoi volumes were found to be universal, but the theoretical modeling of such distributions remains an open problem. For non-interacting particles (ideal gas, Poisson point process), the distribution of Voronoi volumes is almost perfectly fit by a three-parameter Gamma distribution [89, 115, 128, 157]. No fitting curve of comparable accuracy exists for interacting particles, let alone jammed packings of particles considered in this work.

A simple statistical mechanics model for the Voronoi cell volume distribution of packings of spherical particles was proposed by Aste *et al.* [14, 18]. In their model, the probability density  $f(V)$  is given by a so-called  $k$ -Gamma distribution

$$f(V) = \frac{k^k}{(k-1)!} \frac{(V - V_{\min})^{k-1}}{(\langle V \rangle - V_{\min})^k} \exp\left(-k \cdot \frac{V - V_{\min}}{\langle V \rangle - V_{\min}}\right). \quad (4.1)$$

This analytic model yields the full distribution of the Voronoi cell volumina, but crucially depends on the minimal cell volume  $V_{\min}$ . Note that  $V_{\min}$  is the smallest

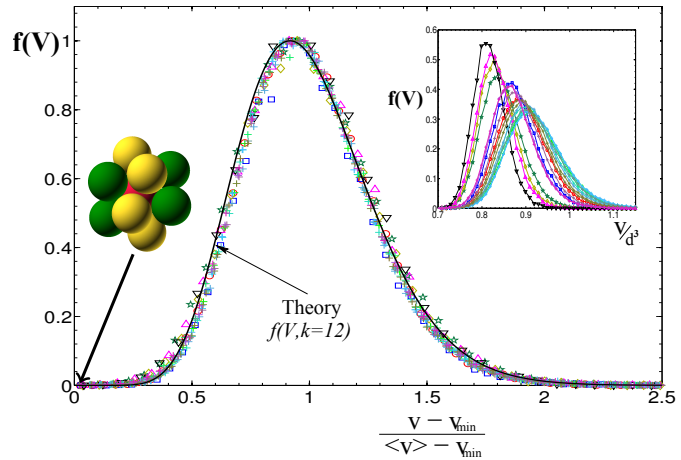
possible local arrangement, which is in general different from the densest crystal configuration. For spheres,  $V_{\min}$  is known, which is the icosahedral cluster.

The parameter  $k$  has been linked to a granular temperature. It was found that  $k$  varies between 11 and 15, which agrees with the typical number of Voronoi neighbors in sphere packings [14].

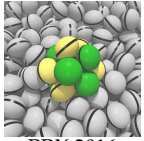
To extend this model for packings of other particle shapes,  $V_{\min}$  for these particle shapes is needed. In the following section we determine  $V_{\min}(\alpha)$  for ellipsoids, which was unknown prior to our work [P1]. With the knowl-

edge of the densest structures we can rescale the Voronoi volume distributions onto the single-parameter family of  $k$ -Gamma distributions, see section 4.2.1.

A similar universality is observed for the rescaled probability density of the quadron volume in 2D disc packings [140]. A  $k$ -Gamma distribution with  $k$  between three and four is a good representation as well.



Plot adapted from Ref. [18] with permission from EPL.

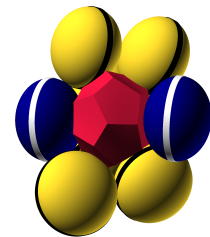


PRX 2016

## 4.1 Cuddling ellipsoids - locally densest structures

Here, we investigate the locally densest structures of uniaxial ellipsoids  $1 : 1 : \alpha$ , as a generalization of the classical *kissing problem* and motivated by their relevance for understanding Voronoi volume distributions. The classical kissing problem in mathematics asks how many equal sized spheres can simultaneously touch a central sphere [48, 177]. This question dates back to Isaac Newton, but it took more than 250 years till it was proven that 12 is the correct answer [177]. The most symmetric arrangement of the spheres is the icosahedral cluster.

In order to generalize this problem to prolate and oblate ellipsoids, we search for the configuration of a central ellipsoid and its  $N$  nearest neighbors, that minimizes the volume of the central particle's Set Voronoi cell  $V_{\text{cell}}$ . This is equivalent to maximizing the local packing density  $\phi_l = V_\alpha / V_{\text{cell}}$ , where  $V_\alpha = 4\pi\alpha/3$  is the particle volume. In the solution of this modified problem, the particles do not necessarily have to touch (kiss) the central particle. Therefore we will refer to it as the *cuddling problem*.



We define  $V_{\min}(\alpha)$  as the minimal Voronoi cell volume for each aspect ratio, and  $\phi_{\max}(\alpha)$  as the corresponding local packing fraction. The central particle is surrounded by  $N$  neighbor particles, which have 3 translational and 2 rotational (uniaxial

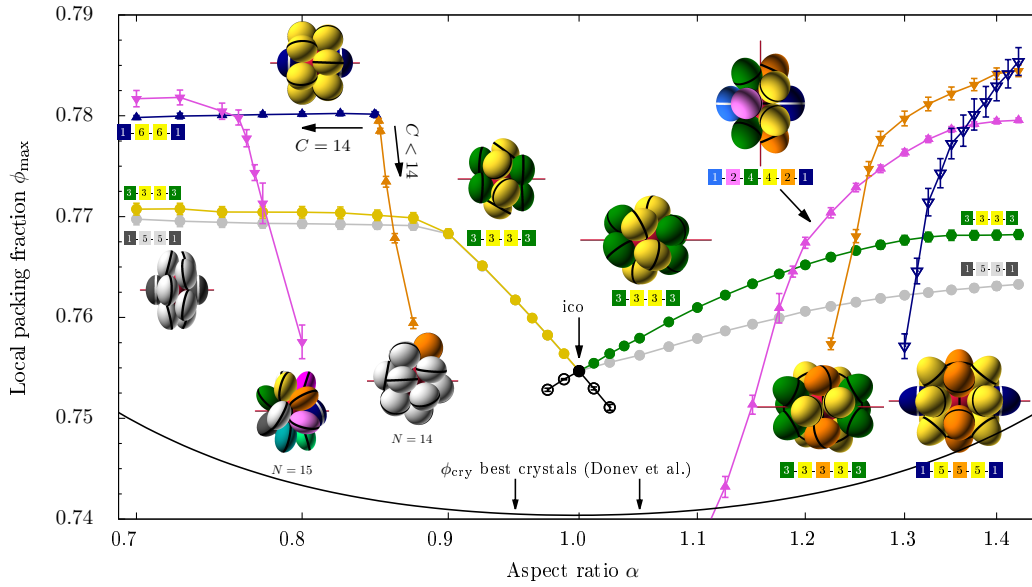
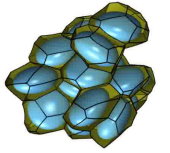


Figure 4.1: Dense local structures of ellipsoids: Local packing fraction of the central Set Voronoi cell vs. the aspect ratio  $\alpha$  of the particles. We identify several branches of candidate structures which are distinguished by the number and symmetry of Voronoi neighbors. The plot symbols mark the number of neighbors ( $N = 12$ :  $\bullet$ ,  $N = 14$ :  $\blacktriangle$ ,  $N = 15$ :  $\blacktriangledown$ ,  $N = 17$ :  $\nabla$ ), while different line colors mark a change in symmetry. The solid line at the bottom of the graph represents the densest-known crystal structure, and “ico” is the icosahedral cluster. Usually, in the optimal structures, the contact number  $C$  is equal to the number of Voronoi neighbors  $N$ . One exception is the oblate  $N = 14$  structure which loses contacts around  $\alpha \approx 0.85$  (see kink). Picture is taken from [P1].

ellipsoids) degrees of freedom. The resulting optimization problem in  $5N$  variables is solved by a simulated annealing scheme, to explore candidate structures, followed by a downhill algorithm. We identify the presumed optimal structure for each aspect ratio  $\alpha$  and Voronoi coordination number  $N$ , see Fig. 4.1.

For spherical particles, the densest local structure is the symmetric icosahedral cluster. We observe that spherical particles are the worst case of the local packing problem, which is already known for lattice packings [106, 107]. As the particles become more aspherical, a general trend towards denser structures exists and the number of neighbors  $N$  to form the optimal structures increases. Most of the densest motifs we discover exhibit a high degree of symmetry, inducing a natural classification by crystallographic point groups, see Ref. [P1]. For very oblate ellipsoids,  $\alpha \lesssim 0.76$ , fifteen neighbors without any obvious symmetry pack densest around the central particle (labeled  $N = 15$  in Fig. 4.1). We conjecture that for even larger asphericities than considered here, the densest structures are typically disordered without any symmetries.

This work offers the opportunity to extend the analytic model for the Voronoi volume distribution of packings of spherical particles proposed by Aste *et al.* [14, 18] towards ellipsoids, see next section.

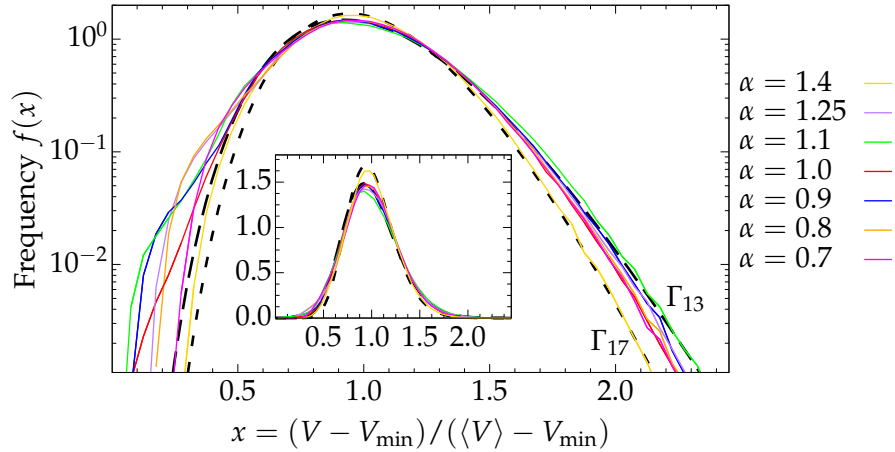
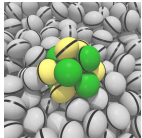
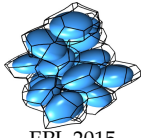


Figure 4.2: Distribution of rescaled Set Voronoi cell volumina in random ellipsoid packings. Data for different aspect ratios  $\alpha$ , compared with two  $k$ -Gamma distributions with  $k = 13$  and  $k = 17$ . The inset shows the same data on a linear scale.



PRX 2016



EPL 2015



PRL 2015

## 4.2 Voronoi Volume distributions

### 4.2.1 Extending the $k$ -Gamma model to non-spherical particles

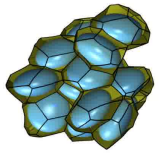
While Voronoi diagrams are a powerful tool for characterizing granular packings, there is currently no established theory for aspherical particles. Aste *et al.* proposed the so called  $k$ -Gamma model, an analytic model for spherical particles [14, 18] which predicts, under simplifying assumptions<sup>9</sup> the full distribution of Voronoi volumina, see Eq. (4.1). The shape of the  $k$ -Gamma distributions strongly depend on  $V_{\min}$ , the locally densest arrangement, which was previously unknown for ellipsoids [P1].

Combining the results for  $V_{\min}(\alpha)$  presented in section 4.1 and the  $k$ -Gamma model, we can now predict the full distribution of Voronoi volumina, with only a single parameter  $k$ . We test the model by analyzing dense disordered packings of monodisperse ellipsoids generated with the Lubachevsky-Stillinger-Donev protocol [58, 59]<sup>10</sup>.

Fig. 4.2a contrasts our data for dense random packings with the predictions from the  $k$ -Gamma model. Both for spheres and ellipsoids, the model curves satisfactorily reproduce the skewed distributions of the data. Upon closer inspection, however, the data exhibit a shoulder at small volumes which deviates from the  $k$ -Gamma curve. The position of the shoulder is lowest for spheres, and shifts into the main peak (larger  $x$ ) for aspherical particles. A similar feature is also present in packings of bidisperse disks (see Fig. 2 and 3 in Ref. [129]) and random-close-packed colloidal

<sup>9</sup>Aste *et al.* assume each Voronoi cell being composed of  $k$  elements which contribute independently to the Voronoi cell volume  $V_{\text{cell}}$ . The volumes of the elements sum up to the total cell volume  $V_{\text{cell}}$ . An assumed minimal elementary cell volume results in the minimal Voronoi cell volume  $V_{\min}$ .

<sup>10</sup>These packings are representative of the random close-packed (or maximally random jammed) state for the respective aspect ratio [54, 56] and are in agreement with published tomography experiments and numerical sedimentation data for oblate ellipsoids [P4].



particles (see Fig. 4 in Ref. [125]).

The origin of the shoulder contribution can be identified by fitting an unnormalized  $k$ -Gamma probability density to the upper portion of the data. We find an excess of Voronoi cells at low volumes, indicating that there are ‘attractor’ motifs at these packing fractions which are preferentially formed. Resolving the local packing fraction distribution for each Voronoi coordination number  $N$  shows that this excess mainly stems from  $N = 12$  cells which show a bimodal  $\phi_l$  distribution (Fig. 4.4, bottom row), see next section. Evidently, the attractors which cause our packing to deviate from the  $k$ -Gamma model are the  $N = 12$  motifs for the relevant aspect ratio. Excluding such specific packing motifs, the  $k$ -Gamma model provides useful and accurate parametrization of dense frictionless ellipsoid packings.

The accordance between  $k$  and the average number of neighbors which was found in packings of spheres, does not exist in packings of ellipsoids. We find that  $k$  increases with asphericity up to 17.4 for our most aspherical particles ( $\alpha = 1.4$ ) while the average number of Voronoi neighbors stays almost constant,  $\langle N \rangle \approx 14$ . A table with values for all aspect ratios can be found in Ref. [P1].

### 4.2.2 Distributions of local packing fraction

A surprising universality is discovered by looking at the local packing fraction  $\phi_l = V_{\text{particle}}/V_{\text{cell}}$  in jammed granular packings of spheres and ellipsoids.  $f(\phi_l)$  is the probability density function to find a particle with  $\phi_l$  in a given packing. An integration over  $f(\phi_l)$  will result in the average local packing fraction  $\langle \phi_l \rangle = \int_0^1 \phi_l f(\phi_l) d\phi_l$ .<sup>11</sup>

Fig. 4.3 (top plot) shows the probability distributions of the local packing fraction  $f(\phi_l)$  for packings of ellipsoids with different aspect ratios  $\alpha$ . When plotting the standard deviation  $\sigma$  of each distribution against the local packing fraction a collapse is observed, see

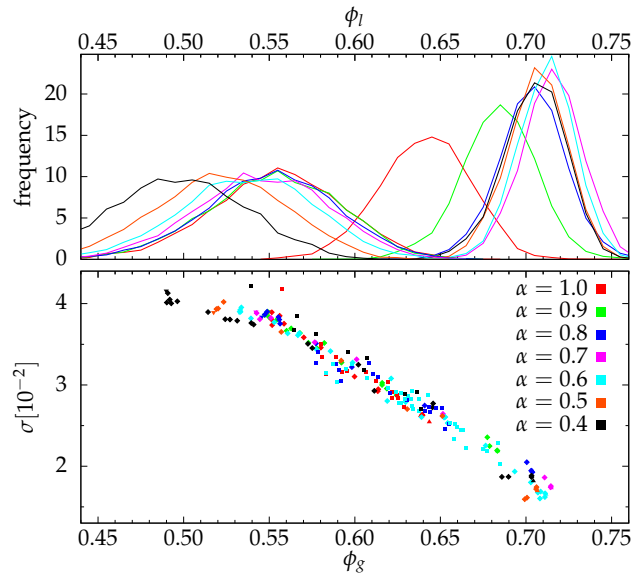
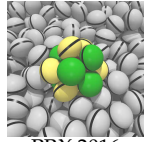
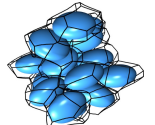


Figure 4.3: (top) Probability distribution of local packing fractions  $\phi_l$  of dense and loose jammed static ellipsoid packings. The aspect ratios of the particles are between  $0.4 \leq \alpha \leq 1.0$ . (bottom) Collapse of the standard deviations  $\sigma$ .



PRX 2016



EPL 2015



PRL 2015

<sup>11</sup>Note the difference between the average local packing fraction  $\langle \phi_l \rangle$  and the global packing fraction, which is defined as  $\phi_g = \frac{\sum V_{\text{particle}}}{\sum V_{\text{cell}}}$  with  $\sum$  being the sum over all particles in the packing. For monodisperse packings,  $\phi_g$  is the harmonic mean of the local packing fraction  $\phi_l$ . The difference between  $\phi_l$  and  $\langle \phi_l \rangle$  is very small in the jammed particle packings considered in this work.

Fig. 4.3 (bottom plot). Data in this plot represents jammed static structures across the range of accessible packing fractions for oblate ellipsoids  $0.4 \leq \alpha \leq 1$  from different experimental packing protocols and simulations of sedimenting ellipsoids [P4]. A similar universality is observed in two dimensional dense configurations of bidisperse discs [163].

With high statistics data generated using the Lubachevsky-Stillinger-Donev protocol [58, 59], we can resolve the tails of the distribution which are not yet accessible in experiment. Fig. 4.4 displays the frequency of Voronoi cells in our dense disordered packings with a given coordination number  $N$  and local packing fraction  $\phi_l$ . It can be observed that the densest clusters in a random packing readily exceed the densest known crystals packings of packing fraction  $\phi_{\text{cry}}$ , indicated by the dashed line. The maximal local packing fractions for each Voronoi coordination number found in Fig. 4.1 are indicated by vertical bars. At small asphericity, the densest local structure is the icosahedral cluster. It is known that random packings of spheres contain distorted variations of icosahedral clusters [7], while the probability for perfect ico clusters vanishes [176]. We can confirm these results for packings of moderate asphericity.

More aspherical ellipsoids ( $\alpha \leq 0.8$  and  $\geq 1.25$ ) could pack denser with fourteen or more neighbors [P1], see Fig. 4.1. As Fig. 4.4 demonstrates, such structures are not formed in significant amounts. Instead, the densest clusters are again  $N = 12$  cells, which turn out to be distorted variations of the  $N = 12$  optimal structures.

By looking looking at the individual packing fraction distributions of each coordination number  $N$ , a bimodal distributions for the  $N = 12$  cells is observed, see Fig. 4.4 (bottom row) This bimodality is linked to the shoulders in the Voronoi volume distributions, see section 4.2.1, and stems from an excess formation of distorted icosahedral clusters.

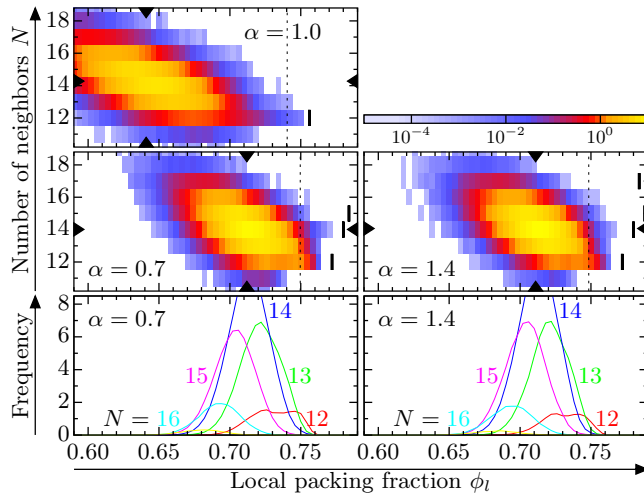
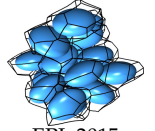
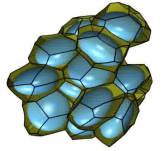
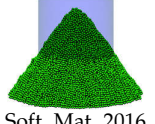


Figure 4.4: Distribution of Voronoi neighbor count  $N$  and local packing fraction  $\phi_l$ . The bold vertical bars indicate the densest local structures for each  $N$  (see Fig. 4.1). The vertical dashed line marks the densest known crystalline packing  $\phi_{\text{cry}}$  [57], and the triangular ticks on the axes mark the global packing fraction and mean Voronoi neighbor count of the dense disordered packings. Bottom row: Marginal distributions of the above for different  $N$ . Image adapted from [P1].

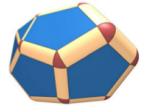




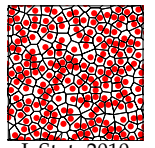
EPL 2015



Soft. Mat. 2016



NJP 2013



J. Stat. 2010

## 4.3 Shape and anisotropy

Characterizing cell shapes, in our case Voronoi cells, is a commonly used way to describe spatial structures. Scalar quantities, such as the cell volume, surface area, integrated curvatures or the isoperimetric ratio, have widely been used for characterizing spatial structure. Example are the structure of maximally random jammed sphere packings [115], foam cells [122] or random tessellations [128] [P2].

Treating the scalar quantities as the leading term of a shape description of the Voronoi cells, we now proceed to higher-order terms. Here, we use the tensorial shape measures  $\mathbf{W}_0^{2,0}$  and  $\mathbf{W}_1^{0,2}$ , introduced in section 3.2, to characterize cell shape. The scalar indices  $\beta_0^{2,0}$  and  $\beta_1^{0,2}$ , derived from these tensors, are used to quantify the anisotropy of the cells.

We analyze the structure of jammed packings of spheres and ellipsoids and compare them to reference data of equilibrium fluid configurations. A density-resolved analysis of these packings gives further insight to the local structure and reveals non-universalities which are not captured by the global averages.

### 4.3.1 Global averages

#### 4.3.1.1 Packings of spheres

Here, we analyze the structure of different assemblies of spherical particles, from fluid configurations without gravity to jammed static packings generated under sedimentation. The structure is quantified by the average Voronoi cell shape anisotropy  $\langle \beta_1^{0,2} \rangle$ , see section 3.2.2 for details.

Fig. 4.6 presents a "phase diagram" where  $\langle \beta_1^{0,2} \rangle$  is displayed as function of global packing fraction  $\phi_g$ . Jammed configurations generated by DEM simulations (see section 2.2.2) of sedimenting ellipsoids are represented in red. Our results are in quantitative agreement with previously published data [176] for simulations and experiments of jammed sphere packings (gray stars), where packings below and above the RCP limit have been created. All configurations become more isotropic upon compaction, i.e.  $\beta_1^{0,2}$  increases with increasing  $\phi_g$  and the cells becoming in average less elongated, approaching the isotropic FCC and HCP structures with  $\beta_1^{0,2} = 1$  for  $\phi_g \rightarrow \phi_{fcc/hcp} \approx 0.74$ .

As a reference system, we analyze data of equilibrium fluid configurations which have been generated by two different methods, a Monte Carlo (MC, [120]) and an event-driven molecular dynamics simulation (MD, [165]). In general, at a given global packing fraction  $\phi_g$ , the equilibrium configurations are more isotropic than the jammed packings. These configurations show a discontinuity in  $\langle \beta_1^{0,2} \rangle$  at the hard spheres phase transition, from a disordered to a ordered state, with the ordered state being more isotropic. From  $0.494 \lesssim \phi_g \lesssim 0.545$ , a coexistence region exists. For vanishing density  $\phi_g \rightarrow 0$  the shape anisotropy corresponds to the value  $\langle \beta_1^{0,2} \rangle \approx 0.46$  of the Poisson point process [P14]. More information about the simulation method and the detailed analysis can be found in Ref. [P14].



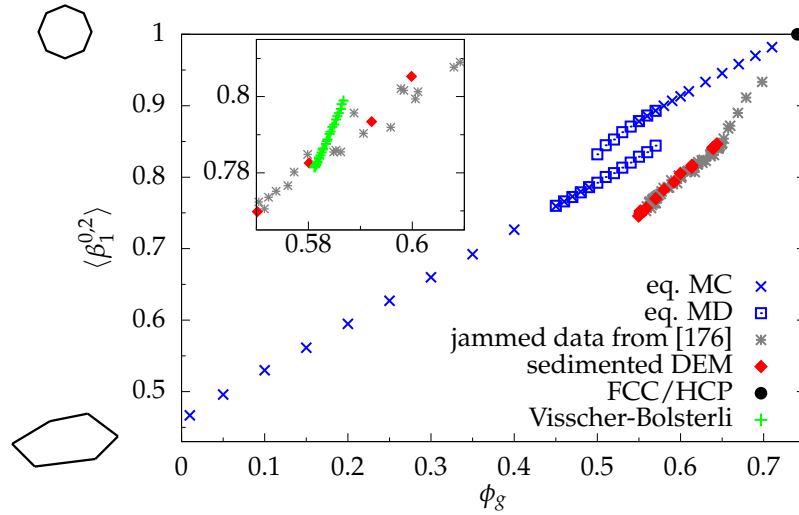


Figure 4.5: Average anisotropy index  $\langle \beta_1^{0,2} \rangle$  as function of the global packing fraction  $\phi_g$  for equilibrium configurations of spheres [P14], static jammed sphere packings [176] and the FCC/HCP crystal. The inset shows data generated with the Visscher-Bolsterli algorithm for spheres on an inclined plane [P3]. The two sketches on the left-hand side illustrate the anisotropy parameter.

The inset in Fig. 4.5 shows a system where particles are sedimented on an inclined surface simulated with the Visscher-Bolsterli algorithm [203], see Ref. [P2] for details. In this algorithm, particles are sedimented sequentially and stick to their position once they reached their potential minima or the inclined surface. By changing the slope of the surface from  $0^\circ$  up to  $\approx 52^\circ$  degree, the packing density is varied. For angles above  $52^\circ$  degrees, no stable packing can be achieved. Interestingly, these configurations show a higher increase of  $\langle \beta_1^{0,2} \rangle$  when varying  $\phi_g$  than the corresponding jammed packings. The detailed analysis of packings generated with this simulation method can be found in Ref. [P3].

#### 4.3.1.2 Packings of ellipsoids

We investigate the influence of particle shape to the packing structure by using ellipsoids. By varying the aspect ratio  $\alpha$  of the particles, the shape can be changed continuously from spherical to very elongated. In this section, the Voronoi cell shape analysis is applied to equilibrium configurations and jammed packings of oblate ellipsoidal particles. We use the Set Voronoi construction because we are analyzing non-spherical particles. For characterizing shape, we use the average anisotropy measure  $\langle \beta_0^{2,0} \rangle$  based on the volume moment tensor, because the volume tensor is more robust against discretization errors of the surface of the Set Voronoi cell surface.

We analyze data of equilibrium ellipsoid fluids obtained by MC and MD simulations (for  $\phi_g$  below the transition point to the nematic phase), and data of experiments and simulations of jammed random ellipsoid structures. Details about the simulation

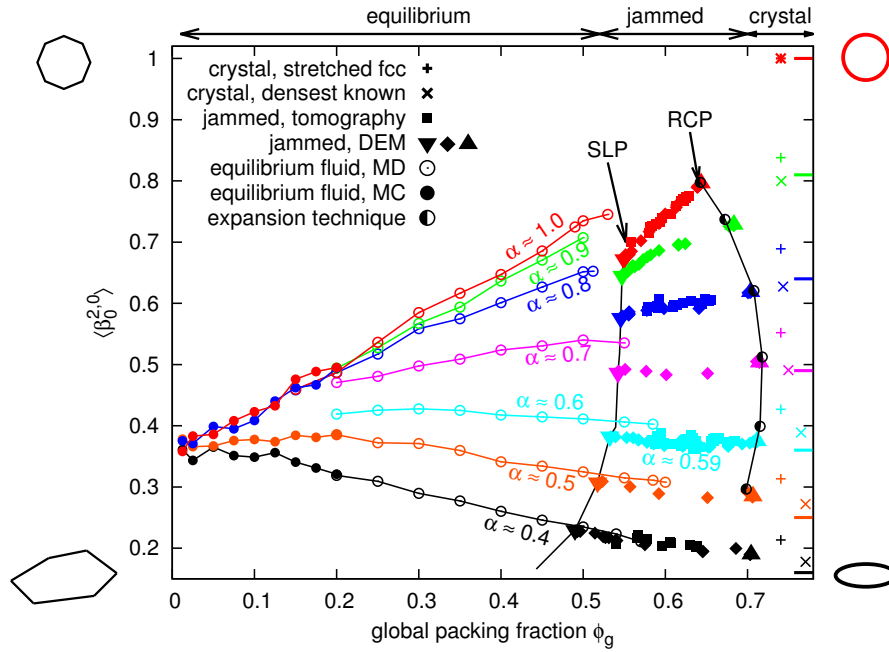
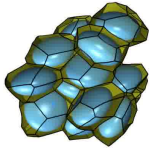


Figure 4.6: Average anisotropy index  $\langle \beta_0^{2,0} \rangle$  of the Set Voronoi cells of packings of ellipsoids as function of  $\phi_g$  for equilibrium ellipsoid configurations, static jammed ellipsoid and crystal packings. The two sketches on the left-hand side illustrate the anisotropy parameter. Dashes on the right-hand vertical axis and ellipsoid sketches aside mark the anisotropies of the particles themselves, i.e.  $\beta_0^{2,0}$  evaluated for a particle rather than its Voronoi cell.

methods and experimental setups are given in chapter 2. As reference two dense crystalline configurations, the *stretched FCC* obtained by scaling the  $x$  coordinate of the FCC sphere packing  $\alpha$ , and the structure discussed by Donev *et al.* [57]) are shown. Fig. 4.6 shows the average Voronoi cell shape anisotropy, quantified by  $\langle \beta_0^{2,0} \rangle$  plotted as function of the global packing fraction  $\phi_g$ .

For equilibrium fluids in the limit of vanishing density  $\phi_g \rightarrow 0$ , where the typical distance between particles is large compared to the particle size, the Voronoi cell shape does not depend on the shape of the particles. In this case, the shape anisotropy corresponds, as shown before for spheres, to the value of the Poisson point process, for the case of  $\beta_0^{2,0} \approx 0.37$  [P14]. For denser equilibrium fluids [53, 160] the trend of the Voronoi shape anisotropy measure  $\langle \beta_0^{2,0} \rangle$  is well understood by realising that the shape of the Voronoi cells becomes more similar to the shape of the particle itself when  $\phi_g$  increases. The dashes on the right hand vertical axis in Fig. 4.6 show the anisotropy for an ellipsoidal particle itself, rather than its Voronoi cell. When  $\alpha$  is small, the curve  $\langle \beta_0^{2,0} \rangle(\phi_g)$  hence decreases, while for larger  $\alpha$ ,  $\langle \beta_0^{2,0} \rangle(\phi_g)$  increases with  $\phi_g$ .

For jammed packings of ellipsoids between the SLP and RCP limit, an excellent agreement between the tomographic experiments (■, with different preparation protocols) and the numerical data points from DEM simulations (▼, ◆, ▲) is observed.

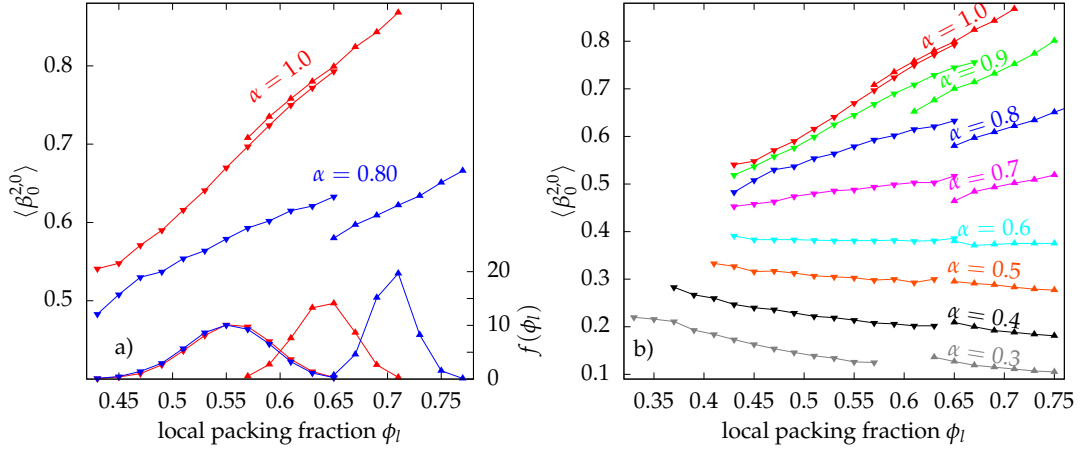


Figure 4.7: Relationship between local packing fraction  $\phi_l$  and the Voronoi cell anisotropy  $\beta_0^{2,0}$ . Each curve represents DEM data for a fixed value of  $\phi_g$ , and is averaged over three independent realisations. a) Local analysis for spheres ( $\alpha = 1$ ) and slightly oblate ellipsoids ( $\alpha = 0.8$ ). Curves on the bottom (using the right hand abscissa) show  $P(\phi_l)$ . b) Local Voronoi cell anisotropy  $\langle \beta_0^{2,0} \rangle(\phi_l)$  for the DEM estimates for SLP and RCP packings.

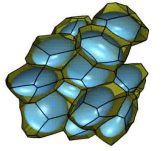
As we know from the previous section, packings of jammed spheres get more isotropic as the packing fraction  $\phi_g$  increases. The same trend is observed for ellipsoids with aspect ratios close to 1. For ellipsoids with smaller value of  $\alpha$ , the slope of  $\langle \beta_0^{2,0} \rangle(\phi_g)$  becomes smaller and eventually even adopts slightly negative values for small  $\alpha$ , such as  $\alpha = 0.4$ , supported further by the local analysis in Fig. 4.7 (right plot).

### 4.3.2 Local analysis reveals differences in dense and loose packings

To get a deeper insight into the structure of packings, we use the density-resolved structure analysis, introduced in section 3.3. We apply this local structure analysis of  $\beta_0^{2,0}$  to the data of jammed spheres and ellipsoids, the result is shown in Fig. 4.7. For the sake of clarity, only results for packings created by DEM simulations are shown. The following results are in agreement with experimental data, see Ref. [P4].

The local structure analysis reveals a difference in the structure of packings of spheres and packings of ellipsoids: in sphere packings, the average shape of the Voronoi cells of a given local packing fraction  $\phi_l$  is, as far as it is captured by the anisotropy index  $\beta_0^{2,0}$ , almost identical in dense and loose packings. This is evidenced by the near-collapse of the curves  $\langle \beta_0^{2,0} \rangle(\phi_l, \alpha = 1, X)$  for packings of different global packing fraction.  $X$  represents unknown parameters, which can be the packing protocol or the particle friction. For spheres,  $\langle \beta_0^{2,0} \rangle$  is a function of  $\phi_l$  only and is largely independent of the unknown parameters  $X$ .

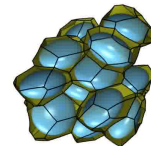
In ellipsoid packings, illustrated for  $\alpha = 0.8$  in Fig. 4.7a, the curves for different  $\phi_g$  do not collapse. The average  $\langle \beta_0^{2,0} \rangle(\phi_l, \alpha, X)$  depends on both  $\alpha$  and  $X$ . This indicates that packings with low and high  $\phi_g$  exhibit differences in their local structures controlled by  $\alpha$  and  $X$ . Fig. 4.7b demonstrates the validity of this result for other



aspect ratios. It is evident that the densest and loosest simulated packings have different structures, except around  $\alpha = 1.0$  (spheres) and  $\alpha = 0.6$  (close to the densest random ellipsoid packing). A similar behavior is observed in the local contact number analysis. The curves of the local contact number analysis collapse while the curves for ellipsoids start to scatter, see Fig. 3a in Ref. [P1].

These universalities and non-universalities imply the following interpretation (at least with respect to averages of the volume tensor shape measure and contact number): Consider a pool of structure motifs, which are the local building blocks of a packing. For jammed packings of spheres, regardless of the global packing fraction  $\phi_l$ , all local building blocks of a packing stem from the same pool. On the contrary, for ellipsoids the pool on local building blocks of a packing depends on further parameters  $X$ . Candidates are friction, local order or other measures of anisotropy. See the detailed explanation of the interpretation in Ref. [P4].





## 5 Contact numbers and mechanical stability

A simple topological and well studied parameter in jammed packings is the average number of contacts between the particles. Because contacts transmit forces they are important for the stability of the packing. Here, we analyze the contact numbers of jammed ellipsoid packings, first as global averages and second in a local density-resolved analysis. We find that the global contact number can be described by an ansatz that solely depends on parameters defined on the particles scale, including the local packing fraction and the aspect ratio of the particles.

While conceptually important and simple, contacts are difficult to detect in experimental data, as experimental images, for example obtained by X-ray tomography, contain noise [P8]. In simulations, the contact number depends on details of the contact model, often connected to a numerical cut-off. The contact network highly depends on the chosen parameters and details of the contact analysis.

Because of their conceptual importance and despite these difficulties in measuring them, contact numbers are widely studied and investigated in granular packings.

### 5.1 Global averages

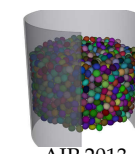
Most studies on contact numbers characterize packings by the average (global) contact number  $Z_g$  a particle forms with its neighbors. Here,  $Z_g$  represents the average number of touching particles which are in geometrical contact. In this sense,  $Z_g$  is also known as the geometrical contact number [185]. This is in contrast to the mechanical contact number which only counts contacts which carry forces. We define the average contact number  $Z_g$  as the average over all local contact numbers  $Z_{1,i}$  of each particle  $i$ :

$$Z_g = \langle Z_{1,i} \rangle = \frac{\sum Z_{1,i}}{\#\text{particles}}.$$

Frictionless ellipsoids have been studied numerically with various simulations [54, 56, 60, 190, 210]. First simulations of the contact numbers of frictionless ellipsoids were performed by Donev *et al.* [56, 60], using the Lubachevsky-Stillinger-Donev protocol, see section 2.2.1. They showed that in amorphous packings of frictionless ellipsoids the average number of contacts  $Z_g$  is higher than in packings of spheres. The rapid increase of  $Z_g$  when deviating from spheres is due to the additional need to block the rotational degrees of freedom of the ellipsoids to form jammed packings. Furthermore, the average contact number of their packings of frictionless ellipsoids is



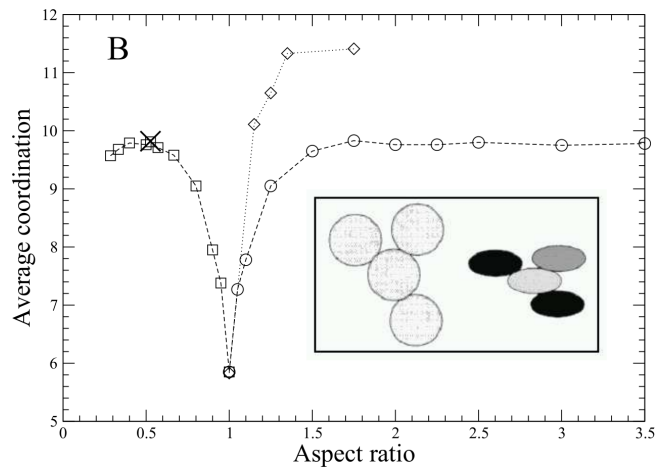
PRL 2015



AIP 2013

less than the number of contacts required for isostaticity<sup>12</sup>, which is  $Z_{\text{iso}} = 10$  (for fully aspherical:  $Z_{\text{iso}} = 12$ ) [56]. As these packings do not have enough contacts to block all degrees of freedom, they should not be mechanically stable. This apparent paradox has been resolved by Donev *et al.* [60], who showed that in this analysis the contacts cannot be treated as the contacts between frictionless spheres: contacts with low curvature, that is "flat" contact, can block rotational degrees of freedom even in the absence of friction. Discrete Element Simulations (DEM) allow us to simulate packings of frictional ellipsoids, which can form looser packings with less contacts [55].

Experimental studies of contact numbers have been mostly performed on spheres. The first studies on contact numbers in jammed packings of spheres were done by Bernal *et al.* [31] in 1960, where a packing of frictional spheres and the distribution of contacts was analyzed with very basic methods. They soaked packings of ball bearings in japan paint to mark the contacts and counted them afterwards by a manual dissection of the packing. Newer experimental studies have been performed by Aste *et al.* [16, 17] using X-ray tomography imaging of spherical beads. Sphere packings between a packing fraction of  $\phi_g = 0.59$  and  $\phi_g = 0.64$  have been analyzed and an increase of the average contact number with the packing fraction was found. All analyzed packings are *hyperstatic* e.g. have an average contact number above 4, which is in agreement with the isostaticity argument. Hanifpour *et al.* [82] analyzed the structure of partly crystalline packings obtained in experiments and a following numerical relaxation by a DEM simulation. They found that the mechanical contact number (only counts contact which carry force) shows a sharp transition at the crystallization onset and stays constant, while the geometrical contact number increases. This suggests the formation of contacts which do not carry forces, to reach a denser and more crystalline configuration. The distribution of forces inside granular packings can be experimentally measured in 2D by using photoelastic particles and placing them between crossed polarizers [25]. Questions of interest to investigate with this method are for example the distribution of stress inside the packing [92] or the response to shearing [136].



Contact number of jammed frictionless ellipsoids<sup>13</sup>  
 □ oblate spheroids, ○ prolate spheroids,  
 ◇ fully aspherical ellipsoids.

<sup>12</sup>A packing is isostatic, when the contacts between the particles form enough constraints to block all degrees of freedom of the particles.

<sup>13</sup>Plot reproduced from Donev *et al.* Ref. [56], with permission from AAAS.



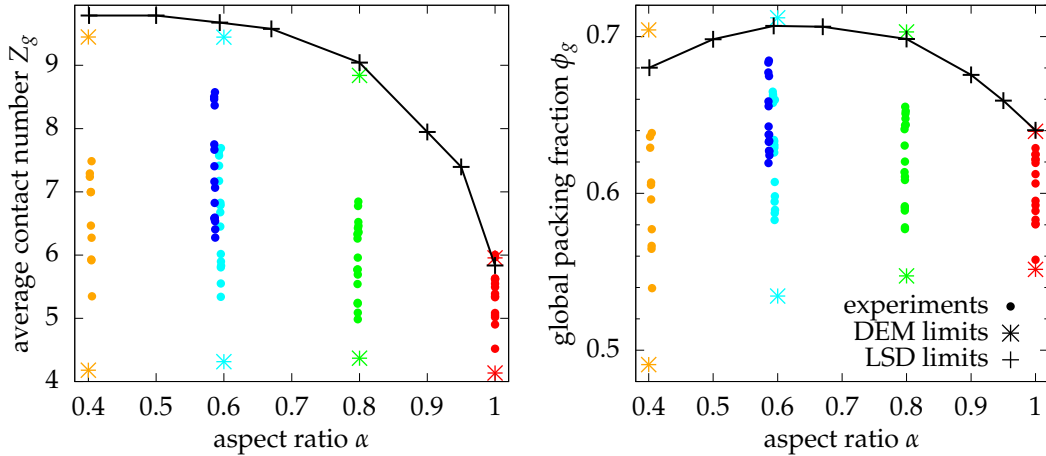
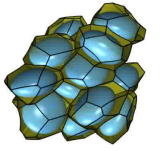


Figure 5.1: Average contact number  $Z_g$  (left) and global packing fraction  $\phi_g$  (right) as a function of the aspect ratio  $\alpha$ . Experimental data is from packing experiments, see Ref. [P5] and section 2.1.1 for details. The DEM limits are obtained by sedimented DEM simulations of frictionless and highly frictional particles, see section 2.2.2 for details. The LSD limits are obtained by simulations using the Lubachevsky-Stillinger-Donev protocol; data is extracted from Donev *et al.* [56].

Packing experiments on packings of ellipsoidal particles were previously only performed with two different types of ellipsoidal particle shapes, uniaxial oblate M&M candies with  $\alpha \approx 0.51$  [56, 137, 208] and fully aspherical particles with aspect ratios 1.25:1:0.8 produced by stereolithography [137]. The packings were characterized by packing fractions and contact numbers.

In this work, we perform a large experimental study on the contact number of frictional ellipsoid packings. Four different aspect ratios and two different friction coefficients are analyzed. Details about the experimental setup are described in section 2.1.1.

Fig. 5.1 displays the average contact number  $Z_g$  and the global packing fraction  $\phi_g$  as a function of the aspect ratio  $\alpha$ . As expected for frictional particles [86, 150, 183], we find that our ellipsoid packings are all hyperstatic over the whole range of packing fraction studied. The contact number of all samples is significantly above the isostatic value of four<sup>14</sup>. Furthermore, we find that the global contact number  $Z_g$  depends on both the global packing fraction  $\phi_g$  and the aspect ratio  $\alpha$  of the ellipsoids.

The data of our experiments is compared to the densest random packings obtained by the Lubachevsky-Stillinger-Donev protocol, see section section 2.2.1 and to the densest and loosest packings obtained by DEM simulations of frictionless and highly frictional particles sedimenting in a viscous fluid, see section 2.2.2 for details. Fig. 5.1 shows that our data lies within these limits.

<sup>14</sup>Frictional contacts can fix three constraints, by blocking one normal and two tangential motions. A contact is shared between the two particles involved, so per particle each contact provides 1.5 constraints. As each particle possesses six degrees of freedom (3 translational and 3 rotational), at minimum four contacts are needed to block all of them [200]



PRL 2015

## 5.2 Local contact analysis

In the theory of particulate systems known as the jamming paradigm [130, 200], the basic control parameter is the global contact number  $Z_g$ , which is a function of the difference between the global packing fraction  $\phi_g$  and some critical value  $\phi_c$ . For soft, frictionless spheres (a practical example would be an emulsion) this is indeed a good description [112] because additional contacts are formed by the globally isotropic compression of the particles which also increases  $\phi_g$ .

In frictional hard granular media, such as sand, salt or pebbles, a change in the global packing fraction  $\phi_g$  is not achieved by a compression of the particles but by changing the geometric arrangement of the grains. As we observed in our experiments, if we want to compress a packing of granulates we do not compress them with a piston but instead tap or vibrate it which changes the geometric structure of the packing. This suggests that the global parameter, such as the global contact number  $Z_g$  and the global packing fraction  $\phi_g$ , are a result of the local geometric structure on the particle scale.

There are some theoretical approaches that have studied contact numbers from a local perspective: Song *et al.* [185] used a mean-field ansatz to derive a functional dependence between  $Z_g$  and the Voronoi volume of a sphere. This ansatz has recently been expanded to arbitrary shapes composed of the unions and intersections of frictionless spheres [26, 27]. For spheres, a comparison between this ansatz and our theory (see below) is shown in the inset of Fig. 5.2. No data is provided for oblate ellipsoids considered here in this work.

Secondly, Clusel *et al.* [46, 49] developed the granocentric model which predicts the probability distribution of contacts in jammed, polydisperse emulsions and for frictionless spheres. The key parameters in this model are the available space around a particle and the ratio of contacts to neighbours. This model is only for frictionless spheres and hence not applicable for our frictional particles.

Recently, Xia *et al.* [208] applied the granocentric model to a dense packing of M&M candies, imaged by X-ray tomography. Their model suggest that particle asphericity can be treated as a polydispersity effect induced by the particle orientations. Their model was only applied to a single particle packing and needs further confirmation.

As discussed, the formation of contacts between particles needs to be explained on the particle level. Thus, we start with an ansatz:

$$Z(\phi_g, \alpha, X) = \int Z_l(\phi_l, \alpha, X) f(\phi_l | \phi_g, \alpha, X) d\phi_l \quad (5.1)$$

The contact function  $Z_l(\phi_l, \alpha, X)$  represents the local physics i.e. the number of contacts formed by a particle of shape  $\alpha$ , inside a Voronoi cell of size  $\phi_l$  and potentially characterized by further locally defined variables  $X$  such as friction, fabric anisotropy, or measures of local order.  $f(\phi_l | \phi_g, \alpha, X)$  is the probability distribution to find a particle with  $\phi_l$  in a given packing, see section 4.2.2. As we have shown for ellipsoids, the standard deviation  $\sigma$  of  $f(\phi_l | \phi_g, \alpha, X)$  only depends on  $\phi_g$ .

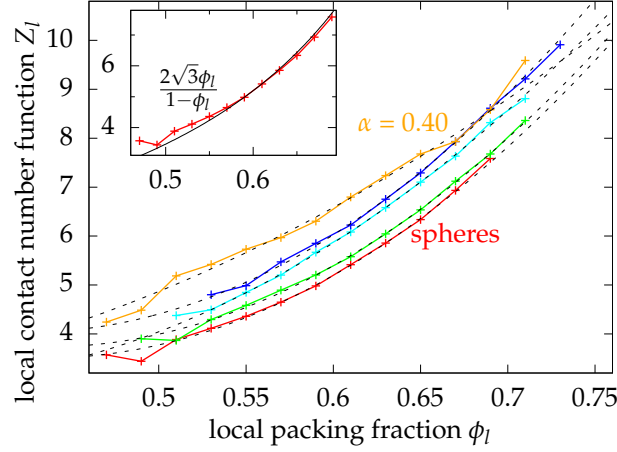
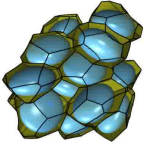


Figure 5.2: Average local contact number function  $Z_l$  describing the average number of contact a particle with local packing fraction  $\phi_l$  will form. Averages over all data sets (i.e. different values of  $\phi_g$ ) for each aspect ratio. The black dashed lines are parabolic fits according to Eq. (5.3). The inset shows the theoretical result from Song et al. [185] for spheres compared with our sphere data. A bin size of 0.02 is used. Figure reproduced from Ref. [P5].

To get an expression for  $Z_l$  we apply the local analysis, described in section 3.3, to contact numbers. As the  $Z_l(\phi_l)$  curves are to first order independent on the global packing fraction  $\phi_g$  and only depend in the aspect ratio<sup>15</sup>, we average for each aspect ratio over all experiments with different  $\phi_g$ . Fig. 5.2 displays the resulting  $Z_l(\phi_l, \alpha)$  curves. Here we have ignored not only  $\phi_g$  but also all higher order terms  $X$  because within the resolution of our experiments we were not able to discern between different possible candidates. In order to obtain an phenomenological description for  $Z_l$  we perform for each aspect ratio a parabola fit using:

$$Z_l(\phi_l, \alpha) = a \phi_l^2 + b \phi_l + c \quad (5.2)$$

Fitting Eq. (5.2) is a purely phenomenological approach, it is justified only by the absence of any theoretical predictions for frictional ellipsoids. The only analytical result available is the mean-field ansatz of Song et al. [185] for spheres and is in good agreement with our data (without any fit parameters) as shown in the inset of Fig. 5.2.

Following our ansatz and using Eq. (5.2), we can write<sup>16</sup>

$$\begin{aligned} Z(\phi_g, \alpha, X) &= \int Z_l(\phi_l, \alpha, X) f(\phi_l | \phi_g, \alpha, X) d\phi_l \\ &= a \sigma^2(\phi_g) + a \phi_g^2 + b \phi_g + c \end{aligned} \quad (5.3)$$

<sup>15</sup>This independence of the global packing fraction has been previously only shown for spheres [17].

<sup>16</sup>With  $E$  being the expectation value, and VAR the variance it follows:

$$\begin{aligned} E[Z_l(\phi_l)] &= E[a \phi_l^2 + b \phi_l + c] = a E[\phi_l^2] + b E[\phi_l] + c = a (\text{VAR}[\phi_l] + (E[\phi_l])^2) + b E[\phi_l] + c \\ &= a \sigma^2(\phi_g) + a \phi_g^2 + b \phi_g + c \end{aligned}$$

We neglect the small difference between  $\phi_g$  and  $\langle \phi_l \rangle$ .

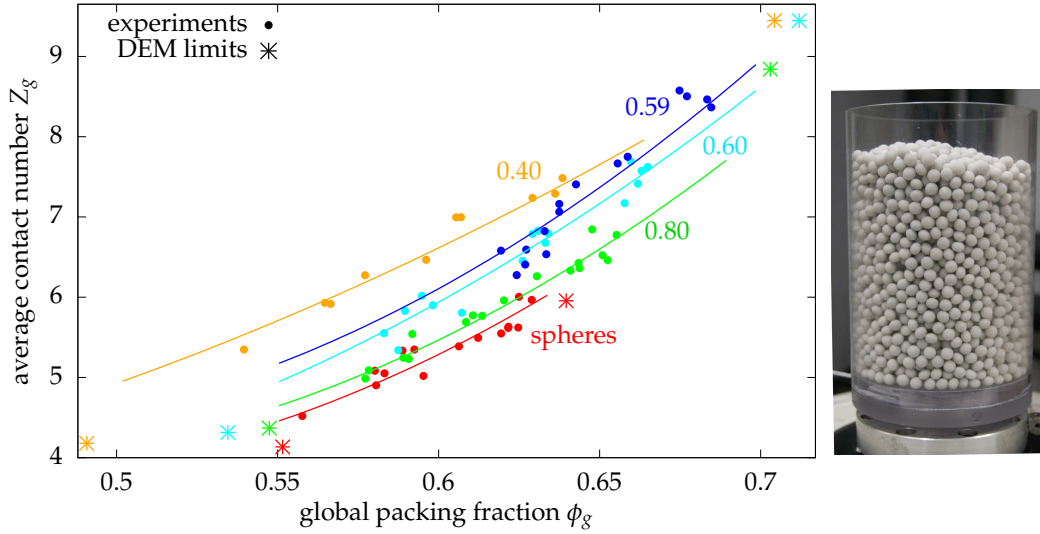
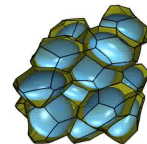


Figure 5.3: (left) Average contact number  $Z_g$  as a function of the global packing fraction  $\phi_g$ . Lines correspond to equation 5.3, which represents the local theory presented here. Experimental data is from packing experiments, see section 2.1.1 for details. Data is from Ref. [P5]. The simulation limits are obtained by sedimented DEM simulations of frictionless and highly frictional particles, see section 2.2.2 for details. (right) Jammed ellipsoids with  $\alpha = 0.8$  in a cylindrical container.

This ansatz only uses the mean value  $\langle \phi_l \rangle$  and the standard deviation  $\sigma$  of the probability distribution function  $f(\phi_l | \phi_g, \alpha, X)$ . No assumptions about shape and other parameters are made.

Fig. 5.3 compares the experimental data with Eq. (5.3). The good agreement demonstrates the validity of our ansatz. Larger deviations are obtained for the particles with  $\alpha = 0.59$ , which have a different friction coefficient. Furthermore, the limits obtained by DEM simulations for the densest and loosest amorphous packings do not match our local theory. These facts show the need for further parameters  $X$  defined on the particle scale (e.g. friction, measures of local order, ...) to refine the theory and to describe jammed packings.

A reason for the need of further parameters  $X$  can be the history-dependent behavior of frictional particles. It has recently been shown for spheres [3] and tetrahedra [150] that for identical  $\phi_g$  the contact number can depend on the preparation history. A modeling of such a behavior will require the addition of further locally defined parameters. However, our data does not allow us to assess the type of higher order corrections required. Further systematic experiments are needed to test possible candidates for the parameters  $X$  and to further refine the model towards a more detailed description of packings of frictional ellipsoids.



## 6 Outlook

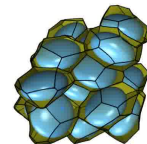
This thesis has addressed the systematic differences between amorphous monodisperse sphere packings –as the simplest model– and amorphous ellipsoid packings – as a simple model to address the effect of shape. Most importantly, this work has clearly demonstrated that for the case of the ellipsoid packing model a local density-resolved analysis, which may in principal directly relate to local physical processes, is needed to fully describe the structural properties, and hence the physics, of this system.

While this work has systematically addressed a particular case, that of uniaxial ellipsoids, it has also shown up many open questions and future directions. The methodology and concepts developed here for the density-resolved analyses of particulate packings form a solid bases to address the following questions that relate to the insight gained from the ellipsoid system:

- The phase diagram of jammed ellipsoids shows similarities between prolate particles with aspect ratio  $\alpha$  and oblate particles of inverse aspect ratio, see Fig. 1.3 (top). The packing fraction of the densest local configurations [P1], the densest crystal configurations [57] and the densest and loosest jammed packing limits [54, 55] show similar trends. Similar correspondences are found in the equilibrium phase diagram of hard ellipsoids [154], see Fig. 1.3 (bottom). Furthermore, these similarities are also present in other parameters, such as the global contact number [56]. An explanation for these correspondences is still missing and needs further investigations.
- A surprising result is the obtained universality in the distribution of the local packing fractions of jammed packings of ellipsoids. The width of the distribution is independent on the aspect ratio for all aspect ratios  $\alpha$ , see Fig. 4.3. Until now, we do not understand the reason for this universality. An interesting question is when this universality breaks down. First results show that jammed packings of tetrahedra do not show this universality. Further investigations in this directions will help to understand the origin of this universality.
- The presented local structure analysis of Voronoi cell shapes and of contact numbers reveals differences between spheres and ellipsoids. Both, cell shapes and contact numbers, show the need for additional parameters  $X$  defined on the particle scale, to describe the structure of packings of ellipsoids. A possible candidate is the friction coefficient between the particles. Experiments and simulations of packings with the same global packing fraction  $\phi_g$  and aspect ratio  $\alpha$ , but of particles with different friction coefficients can confirm or rule

out friction as a possible candidate. Furthermore, other structural parameters need to be tested, as for example measures of local order.

- Analyzing bidisperse ellipsoid packings offers the possibility to assess the effect of variations in particle size to packing properties. Currently, we are working on comparing the structure of bidisperse to the structure of monodisperse ellipsoid packings created by exactly the same preparation protocol. Obtained differences and similarities will help to extract the effect of polydispersity to the structure of particle packings.  
An additional phenomena which can occur in bidisperse packings is size segregation [123]. By tapping or vibrating the packing, particles of the same size can agglomerate. Varying the tapping intensity can lead to packings with and without size segregation. An interesting question is if and when size segregation occurs during tapping and if it hinders the compaction process.
- Understanding compaction processes in granular material is important to understand geological processes. Slotterback *et al.* [184] performed compaction experiments of immersed soda-lime glass spheres by thermal cycling. The packings were imaged by a laser sheet scanning method. They found a preferred particle movement towards the center of the Voronoi cell. By using X-ray imaging techniques where the X-ray source and the detector rotate (similar to medical CT) instead of the sample, the whole compactification process can be analyzed. Taking a tomographic image every few taps allows to follow the particle movements during compaction. It would be interesting to see if compaction by tapping follows the same movements as compaction by thermal cycling. Furthermore, the movements of ellipsoids during compaction can be analyzed and compared to the spherical case. This will help to understand the effect of particle shape to particle movement.
- In industry and geology the mechanical properties of packings of granulates, such as the response to applied external forces, are important to prevent landslides or understand the stability of granular materials. Linking the mechanical properties to structural parameters can shed light into the understanding of structure formation and the stability of granular packings. A possible setup are shear experiments of granulates in a rheometer or shear cell with combined force measurement and 3D imaging of the packing. The goal is to understand changes in the mechanical response and their possible link to structural changes inside the packing.
- Finally, experiments with real world granulates, such as sand or rock, are important to test the relevance of the ellipsoid model for packings of such particles. Observed differences and similarities between packings of real world granulates and toy model systems allow us to analyze the contributions of the different particle parameters, such as friction or shape, to the packing properties. This helps to refine and adjust theories for complex shaped particles.

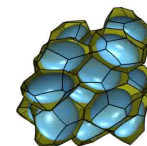


---

We see the ellipsoid toy model described here as an important step towards a complete understanding of granular matter and packing problems. Local structural properties that relate to microscopic mechanisms on the particle level are not necessarily captured by global variables. The local density-resolved analysis developed here is a useful tool to understand how mechanisms on the particle level impact the collective behavior. While technical details may require changes when analyzing real world granulates with variations in size and shape, the conceptual method developed here should be applicable. This local point of view on the particle scale will enable not only progress in our understanding of granular systems, but will be of relevance in the broader context of particulate matter and soft matter.





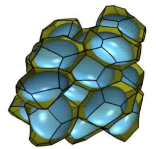


## 7 Bibliography

Publications P1 - P14 are found on page ix.

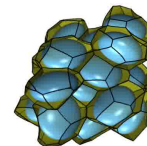
- [1] Credit: U.S. Geological Survey, Department of the Interior/USGS, Photo by Randy Jibson, <<https://www.usgs.gov/media/images/coastal-landslide-caused-2010-haiti-earthquake-0>>.
- [2] Dryad, DOI: 10.5061/dryad.rf623 .
- [3] I. Agnolin and J.-N. Roux. Internal states of model isotropic granular packings. I. Assembling process, geometry, and contact networks. *Phys. Rev. E*, 76:061302, 2007.
- [4] S. Alesker. Description of continuous isometry covariant valuations on convex sets. *Geom. Dedicata*, 74:241–248, 1999.
- [5] M. P. Allen, G. T. Evans, D. Frenkel, and B. M. Mulder. Hard convex body fluids. *Advances in chemical physics*, 86(1):1452–1455, 1993.
- [6] B. Andreotti, Y. Forterre, and O. Pouliquen. *Granular media: between fluid and solid*. Cambridge University Press, 2013.
- [7] A. V. Anikeenko and N. N. Medvedev. Polytetrahedral nature of the dense disordered packings of hard spheres. *Phys. Rev. Lett.*, 98:235504, 2007.
- [8] A. V. Anikeenko, N. N. Medvedev, and T. Aste. Structural and entropic insights into the nature of the random-close-packing limit. *Phys. Rev. E*, 77:031101, 2008.
- [9] M. I. Aoki and K. Tsumuraya. Ab initio molecular dynamics studies on volume stability of Voronoi polyhedra under pressures in a metal glass. *The Journal of Chemical Physics*, 104(17):6719–6723, 1996.
- [10] I. S. Aranson and L. S. Tsimring. Patterns and collective behavior in granular media: Theoretical concepts. *Reviews of Modern Physics*, 78(2):641, 2006.
- [11] C. H. Arns, M. A. Knackstedt, and K. R. Mecke. Characterisation of irregular spatial structures by parallel sets and integral geometric measures. *Colloids and Surfaces A: Physicochemical and Engineering Aspects*, 241(1):351–372, 2004.
- [12] C. H. Arns, M. A. Knackstedt, and K. Mecke. 3D structural analysis: sensitivity of minkowski functionals. *Journal of microscopy*, 240(3):181–196, 2010.

- [13] P. F. Ash and E. D. Bolker. Generalized Dirichlet tessellations. *Geometriae Dedicata*, 20(2):209–243, 1986. ISSN 0046-5755.
- [14] T. Aste and T. Di Matteo. Emergence of gamma distributions in granular materials and packing models. *Phys. Rev. E*, 77:021309, 2008.
- [15] T. Aste and D. L. Weaire. *The Pursuit of Perfect Packing*. Taylor & Francis Group, 2008.
- [16] T. Aste, M. Saadatfar, and T. J. Senden. Geometrical structure of disordered sphere packings. *Phys. Rev. E*, 71:061302, 2005.
- [17] T. Aste, M. Saadatfar, and T. J. Senden. Local and global relations between the number of contacts and density in monodisperse sphere packs. *Journal of Statistical Mechanics: Theory and Experiment*, 2006(07):P07010, 2006.
- [18] T. Aste, T. Di Matteo, M. Saadatfar, T. J. Senden, M. Schröter, and H. L. Swinney. An invariant distribution in static granular media. *EPL*, 79(2):24003, 2007.
- [19] M. Aubouy, Y. Jiang, J. A. Glazier, and F. Graner. A texture tensor to quantify deformations. *Granul. Matter*, 5:67–70, 2003.
- [20] F. Aurenhammer. Power diagrams: properties, algorithms and applications. *SIAM J. Comput.*, 16(1):78–96, 1987. ISSN 0097-5397.
- [21] I. A. Baburin, V. A. Blatov, L. Carlucci, G. Ciani, and D. M. Proserpio. Interpenetrating metal-organic and inorganic 3d networks: a computer-aided systematic investigation. part ii [1]. analysis of the inorganic crystal structure database (icsd). *Journal of Solid State Chemistry*, 178(8):2452–2474, 2005.
- [22] V. Baranau and U. Tallarek. Random-close packing limits for monodisperse and polydisperse hard spheres. *Soft Matter*, 10(21):3826–3841, 2014.
- [23] V. Baranau, S.-C. Zhao, M. Scheel, U. Tallarek, and M. Schröter. Upper bound on the Edwards entropy in frictional monodisperse hard-sphere packings. *Soft matter*, 12(17):3991–4006, 2016.
- [24] M. Barbosa, R. Natoli, K. Valter, J. Provis, and T. Maddess. Integral-geometry characterization of photobiomodulation effects on retinal vessel morphology. *Biomed. Opt. Express*, 5(7):2317–2332, 2014.
- [25] D. S. Bassett, E. T. Owens, M. A. Porter, M. L. Manning, and K. E. Daniels. Extraction of force-chain network architecture in granular materials using community detection. *Soft Matter*, 11(14):2731–2744, 2015.
- [26] A. Baule and H. A. Makse. Fundamental challenges in packing problems: from spherical to non-spherical particles. *Soft Matter*, 10:4423–4429, 2014.



- [27] A. Baule, R. Mari, L. Bo, L. Portal, and H. A. Makse. Mean-field theory of random close packings of axisymmetric particles. *Nature Comm.*, 4:2194, 2013.
- [28] C. Beisbart, M.S. Barbosa, H. Wagner, and L. da F. Costa. Extended morphometric analysis of neuronal cells with Minkowski valuations. *The European Physical Journal B - Condensed Matter and Complex Systems*, 52(4):531–546, 2006.
- [29] M. E. Benson, A. B. Wilson, and D. I. Bleiwas. Frac sand in the united states: a geological and industry overview. Technical report, US Geological Survey, 2015.
- [30] J. D. Bernal and J. L. Finney. Random close-packed hard-sphere model. ii. geometry of random packing of hard spheres. *Discuss. Faraday Soc.*, 43:62–69, 1967.
- [31] J. D. Bernal and J. Mason. Packing of spheres: Co-ordination of randomly packed spheres. *Nature*, 188, 1960.
- [32] D. Bi, S. Henkes, K. E. Daniels, and B. Chakraborty. The statistical physics of athermal materials. *Annual Review of Condensed Matter Physics*, 6:63–83, 2016.
- [33] V. A. Blatov, A. P. Shevchenko, and V. N. Serenzhkin. Crystal space analysis by means of Voronoi–Dirichlet polyhedra. *Acta Crystallographica Section A: Foundations of Crystallography*, 51(6):909–916, 1995.
- [34] H. Blum. Biological shape and visual science (part i). *Journal of Theoretical Biology*, 38(2):205 – 287, 1973. ISSN 0022-5193.
- [35] I. Boada, N. Coll, N. Madern, and J. Antoni Sellares. Approximations of 2d and 3d generalized Voronoi diagrams. *International Journal of Computer Mathematics*, 85(7):1003–1022, 2008.
- [36] J.-D. Boissonnat, C. Wormser, and M. Yvinec. Curved Voronoi diagrams. In *Effective Computational Geometry for Curves and Surfaces*, Mathematics + Visualization, pages 67–116. Springer, 2007.
- [37] E. Brown and H. M. Jaeger. Shear thickening in concentrated suspensions: phenomenology, mechanisms and relations to jamming. *Reports on Progress in Physics*, 77(4):046602, 2014.
- [38] B. Brunet-Imbault, G. Lemineur, C. Chappard, R. Harba, and C.-L. Benhamou. A new anisotropy index on trabecular bone radiographic images using the fast Fourier transform. *BMC Medical Imaging*, 5(1):4, 2005.
- [39] M. A. Carrigy. Experiments on the angles of repose of granular materials. *Sedimentology*, 14(3-4):147–158, 1970.

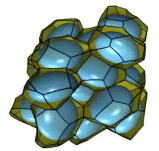
- [40] E. R. Chen, M. Engel, and S. C. Glotzer. Dense crystalline dimer packings of regular tetrahedra. *Discrete & Computational Geometry*, 44(2):253–280, 2010. ISSN 1432-0444.
- [41] E. R. Chen, D. Klotsa, M. Engel, P. F. Damasceno, and S. C. Glotzer. Complexity in surfaces of densest packings for families of polyhedra. *Phys. Rev. X*, 4:011024, 2014.
- [42] S. N. Chiu, D. Stoyan, W. S. Kendall, and J. Mecke. *Stochastic geometry and its applications*. John Wiley & Sons, 2013.
- [43] M. P. Ciamarra and A. Coniglio. Random very loose packings. *Phys. Rev. Lett.*, 101:128001, 2008.
- [44] G. Cinacchi and S. Torquato. Hard convex lens-shaped particles: Densest-known packings and phase behavior. *The Journal of Chemical Physics*, 143(22):224506, 2015.
- [45] P. W. Cleary. Large scale industrial dem modelling. *Engineering Computations*, 21(2/3/4):169–204, 2004.
- [46] M. Clusel, E. I. Corwin, A. O. N. Siemens, and J. Brujić. A ‘granocentric’ model for random packing of jammed emulsions. *Nature*, 460(7255):611–615, 2009.
- [47] A. P. Cohen, S. Dorosz, A. B. Schofield, T. Schilling, and E. Sloutskin. Structural transition in a fluid of spheroids: A low-density vestige of jamming. *Phys. Rev. Lett.*, 116:098001, 2016.
- [48] J. Conway and N. J. A. Sloane. *Sphere Packings, Lattices and Groups*. Springer-Verlag, 1999.
- [49] E. I. Corwin, M. Clusel, A. O. N. Siemens, and J. Brujić. Model for random packing of polydisperse frictionless spheres. *Soft Matter*, 6(13):2949–2959, 2010.
- [50] P. F. Damasceno, M. Engel, and S. C. Glotzer. Predictive self-assembly of polyhedra into complex structures. *Science*, 337(6093):453–457, 2012.
- [51] K. E. Daniels and M. Schröter. Focus on granular segregation. *New Journal of Physics*, 15(3):035017, 2013.
- [52] C. De Michele. Simulating hard rigid bodies. *Journal of Computational Physics*, 229(9):3276–3294, 2010. ISSN 0021-9991.
- [53] C. De Michele, R. Schilling, and F. Sciortino. Dynamics of uniaxial hard ellipsoids. *Phys. Rev. Lett.*, 98:265702, 2007.
- [54] G. W. Delaney and P. W. Cleary. The packing properties of superellipsoids. *EPL (Europhysics Letters)*, 89(3):34002, 2010.



- [55] G. W. Delaney, J. E. Hilton, and P. W. Cleary. Defining random loose packing for nonspherical grains. *Phys. Rev. E*, 83:051305, 2011.
- [56] A. Donev, I. Cisse, D. Sachs, E. A. Variano, F. H. Stillinger, R. Connelly, S. Torquato, and P. M. Chaikin. Improving the density of jammed disordered packings using ellipsoids. *Science*, 303(5660):990–993, 2004.
- [57] A. Donev, F. H. Stillinger, P. M. Chaikin, and S. Torquato. Unusually dense crystal packings of ellipsoids. *Phys. Rev. Lett.*, 92:255506, 2004.
- [58] A. Donev, S. Torquato, and F. H. Stillinger. Neighbor list collision-driven molecular dynamics simulation for nonspherical hard particles. I. Algorithmic details. *Journal of Computational Physics*, 202(2):737 – 764, 2005. ISSN 0021-9991.
- [59] A. Donev, S. Torquato, and F. H. Stillinger. Neighbor list collision-driven molecular dynamics simulation for nonspherical hard particles.: II. Applications to ellipses and ellipsoids. *Journal of Computational Physics*, 202(2):765 – 793, 2005. ISSN 0021-9991.
- [60] A. Donev, R. Connelly, F. H. Stillinger, and S. Torquato. Underconstrained jammed packings of nonspherical hard particles: Ellipses and ellipsoids. *Phys. Rev. E*, 75:051304, 2007.
- [61] K. Dong, C. Wang, and A. Yu. Voronoi analysis of the packings of non-spherical particles. *Chemical Engineering Science*, 153:330 – 343, 2016. ISSN 0009-2509.
- [62] J. Duran. *Sands, powders, and grains: an introduction to the physics of granular materials*. Springer Science & Business Media, 2012.
- [63] G. Durand, F. Graner, and J. Weiss. Deformation of grain boundaries in polar ice. 67:1038–1044, 2004.
- [64] S. F. Edwards and R. B. S. Oakeshott. Theory of powders. *Physica A: Statistical Mechanics and its Applications*, 157(3):1080 – 1090, 1989. ISSN 0378-4371.
- [65] L. J. Ellison, D. J. Michel, F. Barmes, and D. J. Cleaver. Entropy-driven formation of the gyroid cubic phase. *Phys. Rev. Lett.*, 97(23):237801, 2006.
- [66] M. E. Evans, J. Zirkelbach, G. E. Schröder-Turk, A. M. Kraynik, and K. Mecke. Deformation of platonic foam cells: Effect on growth rate. *Phys. Rev. E*, 85: 061401, 2012.
- [67] J. T. Fern, D. J. Keffer, and W. V. Steele. Measuring coexisting densities from a two-phase molecular dynamics simulation by voronoi tessellations. *J. Phys. Chem. B*, 111(13):3469–3475, 2007.
- [68] J. L. Finney. Random Packings and the Structure of Simple Liquids. I. The Geometry of Random Close Packing. *Proceedings of the Royal Society of London A*, 319(1539):479–493, 1970.

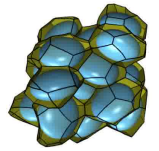


- [69] J. L. Finney. Bernal's road to random packing and the structure of liquids. *Philosophical Magazine*, 93(31-33):3940–3969, 2013.
- [70] N. Francois, M. Saadatfar, R. Cruikshank, and A. Sheppard. Geometrical frustration in amorphous and partially crystallized packings of spheres. *Phys. Rev. Lett.*, 111:148001, 2013.
- [71] D. Frenkel, B. M. Mulder, and J. P. McTague. Phase diagram of a system of hard ellipsoids. *Phys. Rev. Lett.*, 52:287–290, 1984.
- [72] A. Garcimartín, I. Zuriguel, L. A. Pugnaloni, and A. Janda. Shape of jamming arches in two-dimensional deposits of granular materials. *Phys. Rev. E*, 82(3):031306, 2010.
- [73] J. Geng, D. Howell, E. Longhi, R. P. Behringer, G. Reydellet, L. Vanel, E. Clément, and S. Luding. Footprints in sand: The response of a granular material to local perturbations. *Phys. Rev. Lett.*, 87:035506, 2001.
- [74] S. C. Glotzer and M. J. Solomon. Anisotropy of building blocks and their assembly into complex structures. *Nature materials*, 6(8):557–562, 2007.
- [75] J. D. Goddard and A. K. Didwania. Computations of dilatancy and yield surfaces for assemblies of rigid frictional spheres. *The Quarterly Journal of Mechanics and Applied Mathematics*, 51(1):15–44, 1998.
- [76] L. W. Goldman. Principles of ct and ct technology. *Journal of nuclear medicine technology*, 35(3):115–128, 2007.
- [77] H. Goldstein. *Classical Mechanics*. Addison-Wesley, 2nd edition, 1980.
- [78] F. Graner, B. Dollet, P. Marmottant, and C. Raufaste. Discrete rearranging disordered patterns, part I: Robust statistical tools in two or three dimensions. 25:349–369, 2008.
- [79] H. Hadwiger. *Vorlesungen über Inhalt, Oberfläche und Isoperimetrie*. Springer, 1957.
- [80] A. Haji-Akbari, M. Engel, A. S. Keys, X. Zheng, R. G. Petschek, P. Palffy-Muhoray, and S. C. Glotzer. Disordered, quasicrystalline and crystalline phases of densely packed tetrahedra. *Nature*, 462, 2009.
- [81] T. C. Hales. A proof of the Kepler conjecture. *Annals of mathematics*, 162:1065–1185, 2005.
- [82] M. Hanifpour, N. Francois, S. M. Vaez Allaei, T. Senden, and M. Saadatfar. Mechanical characterization of partially crystallized sphere packings. *Phys. Rev. Lett.*, 113:148001, 2014.



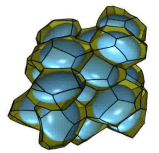
- [83] I. Hanneil and G. Elber. Computing the Voronoi cells of planes, spheres and cylinders in  $\mathbb{R}^3$ . *Comput. Aided. Geom. D.*, 26(6):695 – 710, 2009. ISSN 0167-8396.
- [84] T. P. Harrigan and R. W. Mann. Characterization of microstructural anisotropy in orthotropic materials using a second rank tensor. *J. Mater. Sci.*, 19:761–767, 1984.
- [85] M. Hemmer, O. Setter, and D. Halperin. *Constructing the Exact Voronoi Diagram of Arbitrary Lines in Three-Dimensional Space*, pages 398–409. Springer Berlin Heidelberg, 2010. ISBN 978-3-642-15775-2.
- [86] S. Henkes, M. van Hecke, and W. van Saarloos. Critical jamming of frictional grains in the generalized isostaticity picture. *EPL (Europhysics Letters)*, 90(1): 14003, 2010.
- [87] H. J. Herrmann, J.-P. Hovi, and S. Luding. *Physics of dry granular media*, volume 350. Springer Science & Business Media, 2013.
- [88] C. Heussinger. Shear thickening in granular suspensions: Interparticle friction and dynamically correlated clusters. *Phys. Rev. E*, 88:050201, 2013.
- [89] A. L. Hinde and R. E. Miles. Monte Carlo estimates of the distributions of the random polygons of the Voronoi tessellation with respect to a Poisson process. *Journal of Statistical Computation and Simulation*, 10(3-4):205–223, 1980.
- [90] H. Hinrichsen and D. E. Wolf. *The physics of granular media*. John Wiley & Sons, 2006.
- [91] J.-Y. Ho and M. H. Huang. Synthesis of submicrometer-sized  $\text{Cu}_2\text{O}$  crystals with morphological evolution from cubic to hexapod structures and their comparative photocatalytic activity. *The Journal of Physical Chemistry C*, 113(32): 14159–14164, 2009.
- [92] D. Howell, R. P. Behringer, and C. Veje. Stress fluctuations in a 2d granular couette experiment: A continuous transition. *Phys. Rev. Lett.*, 82:5241–5244, 1999.
- [93] M. H. Huang and P.-H. Lin. Shape-controlled synthesis of polyhedral nanocrystals and their facet-dependent properties. *Advanced Functional Materials*, 22: 14–24, 2012.
- [94] D. Hug, R. Schneider, and R. Schuster. The space of isometry covariant tensor valuations. *St. Petersburg Math. J.*, 19:137–158, 2008.
- [95] K. Hutter. Avalanche dynamics. pages 317–394, 1996.
- [96] J. D. Jackson. *Classical Electrodynamics*. John Wiley & Sons, 1975.

- [97] H. M. Jaeger and S. R. Nagel. Physics of the granular state. *Science*, 255(5051): 1523–1531, 1992.
- [98] H. M. Jaeger, C.-H. Liu, and S. R. Nagel. Relaxation at the angle of repose. *Phys. Rev. Lett.*, 62(1):40, 1989.
- [99] E. Janiaud and F. Graner. Foam in two-dimensional couette shear: a local measurement of bubble deformation. *J. Fluid Mech.*, 532:243–267, 2003.
- [100] C. Jaquet, E. Andó, G. Viggiani, and H. Talbot. Estimation of separating planes between touching 3d objects using power watershed. In *International Symposium on Mathematical Morphology and Its Applications to Signal and Image Processing*, pages 452–463. Springer, 2013.
- [101] M. Jerkins, M. Schröter, H. L. Swinney, T. J. Senden, M. Saadatfar, and T. Aste. Onset of mechanical stability in random packings of frictional spheres. *Phys. Rev. Lett.*, 101:018301, 2008.
- [102] Y. Jiao, F. H. Stillinger, and S. Torquato. Optimal packings of superballs. *Phys. Rev. E*, 79:041309, 2009.
- [103] W. Jin, Y. Jiao, L. Liu, Y. Yuan, and S. Li. Novel dense crystalline packings of ellipsoids. *arXiv preprint arXiv:1608.07697*, 2016.
- [104] Y. Jin and H. A. Makse. A first-order phase transition defines the random close packing of hard spheres. *Physica A: Statistical Mechanics and its Applications*, 389(23):5362 – 5379, 2010. ISSN 0378-4371.
- [105] A. J. Kabla and T. J. Senden. Dilatancy in slow granular flows. *Phys. Rev. Lett.*, 102:228301, 2009.
- [106] Y. Kallus. The 3-ball is a local pessimum for packing. *Advances in Mathematics*, 264:355 – 370, 2014. ISSN 0001-8708.
- [107] Y. Kallus. Pessimal packing shapes. *Geom. Topol.*, 19:343–363, 2015.
- [108] S. Kapfer. *Morphometry and Physics of Particulate and Porous Media*. dissertation, FAU Erlangen-Nuernberg, 2011.
- [109] S. C. Kapfer and W. Krauth. Two-dimensional melting: From liquid-hexatic coexistence to continuous transitions. *Phys. Rev. Lett.*, 114:035702, 2015.
- [110] S. C. Kapfer, W. Mickel, K. Mecke, and G. E. Schröder-Turk. Jammed spheres: Minkowski tensors reveal onset of local crystallinity. *Phys. Rev. E*, 85:030301, 2012.
- [111] L. M. Karlsson and L. M. Cruz-Orive. Stereological characterization of structural anisotropy of rolled steel. *Microsc. Microanal.*, 11(2):1680–1681, 2005.



- [112] G. Katgert and M. van Hecke. Jamming and geometry of two-dimensional foams. *Europhys. Lett.*, 92:34002, 2010.
- [113] A. Katsevich. Theoretically exact filtered backprojection-type inversion algorithm for spiral ct. *SIAM Journal on Applied Mathematics*, 62(6):2012–2026, 2002.
- [114] R. A. Ketcham and T. M. Ryan. Quantification and visualization of anisotropy in trabecular bone. *J. Microsc.*, 213(2):158–171, 2004.
- [115] M. A. Klatt and S. Torquato. Characterization of maximally random jammed sphere packings: Voronoi correlation functions. *Phys. Rev. E*, 90:052120, 2014.
- [116] M. G. Kleinhans, H. Markies, S. J. De Vet, F. N. Postema, et al. Static and dynamic angles of repose in loose granular materials under reduced gravity. *Journal of Geophysical Research: Planets*, 116(E11), 2011.
- [117] J. B. Knight, C. G. Fandrich, C. N. Lau, H. M. Jaeger, and S. R. Nagel. Density relaxation in a vibrated granular material. *Phys. Rev. E*, 51:3957–3963, 1995.
- [118] E. Koch and W. Fischer. Sphere packings and packings of ellipsoids. In *International Tables for Crystallography Volume C: Mathematical, physical and chemical tables*, pages 746–751. Springer, 2006.
- [119] M. Kodam, R. Bharadwaj, J. Curtis, B. Hancock, and C. Wassgren. Cylindrical object contact detection for use in discrete element method simulations, part ii—experimental validation. *Chemical Engineering Science*, 65(22):5863 – 5871, 2010. ISSN 0009-2509.
- [120] W. Krauth. *Statistical mechanics: algorithms and computations*, volume 13. OUP Oxford, 2006.
- [121] A. M. Kraynik, D. A. Reinelt, and F. van Swol. Structure of random monodisperse foam. *Phys. Rev. E*, 67:031403, 2003.
- [122] A. M. Kraynik, D. A. Reinelt, and F. van Swol. Structure of random foam. *Phys. Rev. Lett.*, 93(20):208301, 2004.
- [123] A. Kudrolli. Size separation in vibrated granular matter. *Reports on Progress in Physics*, 67(3):209, 2004.
- [124] V. Senthil Kumar and V. Kumaran. Voronoi neighbor statistics of hard-disks and hard-spheres. *The Journal of Chemical Physics*, 123(7):074502, 2005.
- [125] R. Kurita and E. R. Weeks. Experimental study of random-close-packed colloidal particles. *Phys. Rev. E*, 82:011403, 2010.
- [126] J. C. Lagarias. *The Kepler Conjecture: The Hales-Ferguson Proof*. Springer Science & Business Media, 2011.

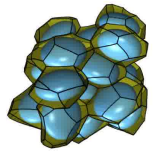
- [127] C. Lautensack and S. Zuyev. Random Laguerre tessellations. *Adv. Appl. Probab.*, 40(3):pp. 630–650, 2008.
- [128] E. A. Lazar, J. K. Mason, R. D. MacPherson, and D. J. Srolovitz. Statistical topology of three-dimensional Poisson-Voronoi cells and cell boundary networks. *Phys. Rev. E*, 88:063309, 2013.
- [129] F. Lechenault, F. da Cruz, O. Dauchot, and E. Bertin. Free volume distributions and compactivity measurement in a bidimensional granular packing. *Journal of Statistical Mechanics: Theory and Experiment*, 2006(07):P07009, 2006.
- [130] A. J. Liu and S. R. Nagel. The jamming transition and the marginally jammed solid. *Ann. Rev. Cond. Matt. Phys.*, 1:347–369, 2010.
- [131] B. D. Lubachevsky and F. H. Stillinger. Geometric properties of random disk packings. *Journal of Statistical Physics*, 60:561–583, 1990. ISSN 0022-4715. 10.1007/BF01025983.
- [132] B. D. Lubachevsky, F. H. Stillinger, and E. N. Pinson. Disks vs. spheres: Contrasting properties of random packings. *Journal of Statistical Physics*, 64:501–524, 1991. ISSN 0022-4715. 10.1007/BF01048304.
- [133] V. Luchnikov, N. N. Medvedev, L. Oger, and J. P. Troadec. Voronoi-Delaunay analysis of voids in systems of nonspherical particles. *Phys. Rev. E*, 59(6): 7205–7212, 1999.
- [134] V. A. Luchnikov, M. L. Gavrilova, N. N. Medvedev, and V. P. Voloshin. The Voronoi–Delaunay approach for the free volume analysis of a packing of balls in a cylindrical container. *Future Generation Computer Systems*, 18(5):673 – 679, 2002. ISSN 0167-739X.
- [135] S. Luding, E. Clément, J. Rajchenbach, and J. Duran. Simulations of pattern formation in vibrated granular media. *EPL (Europhysics Letters)*, 36(4):247, 1996.
- [136] T. S. Majmudar and R. P. Behringer. Contact force measurements and stress-induced anisotropy in granular materials. *Nature*, 435(7045):1079–1082, 2005.
- [137] W. Man, A. Donev, F. H. Stillinger, M. T. Sullivan, W. B. Russel, D. Heeger, S. Inati, S. Torquato, and P. M. Chaikin. Experiments on random packings of ellipsoids. *Phys. Rev. Lett.*, 94(19):198001, 2005.
- [138] H. Mantz, K. Jacobs, and K. Mecke. Utilizing minkowski functionals for image analysis: a marching square algorithm. *Journal of Statistical Mechanics: Theory and Experiment*, 2008(12):P12015, 2008.
- [139] G. Mason. Computer simulation of hard disc packings of varying packing density. *Journal of Colloid and Interface Science*, 56(3):483–491, 1976.



- [140] T. Matsushima and R. Blumenfeld. Universal structural characteristics of planar granular packs. *Phys. Rev. Lett.*, 112:098003, 2014.
- [141] L. B. H. May, L. A. Golick, K. C. Phillips, M. Shearer, and K. E. Daniels. Shear-driven size segregation of granular materials: Modeling and experiment. *Phys. Rev. E*, 81:051301, 2010.
- [142] K. R. Mecke. Morphological characterization of patterns in reaction-diffusion systems. *Phys. Rev. E*, 53(5):4794, 1996.
- [143] K. R. Mecke. *Additivity, Convexity, and Beyond: Applications of Minkowski Functionals in Statistical Physics*, pages 111–184. Springer Berlin Heidelberg, Berlin, Heidelberg, 2000. ISBN 978-3-540-45043-6.
- [144] N. N. Medvedev. Application of the Voronoi-Delaunay method to study structure of empty space in polydisperse systems. *Doklady Academ. Nauk*, 337(6): 767–771, 1994.
- [145] A. Mehta. *Granular Matter: an interdisciplinary approach*. Springer Science & Business Media, 2012.
- [146] F. Meyer. The watershed concept and its use in segmentation : a brief history. *ArXiv e-prints*, 2012.
- [147] W. Mickel, S. C. Kapfer, G. E. Schröder-Turk, and K. Mecke. Shortcomings of the bond orientational order parameters for the analysis of disordered particulate matter. *The Journal of Chemical Physics*, 138(4):044501, 2013.
- [148] M. E. Möbius, B. E. Lauderdale, S. R. Nagel, and H. M. Jaeger. Brazil-nut effect: Size separation of granular particles. *Nature*, 414(6861):270–270, 2001.
- [149] L. Najman and H. Talbot. *Mathematical morphology*. John Wiley & Sons, 2013.
- [150] M. Neudecker, S. Ulrich, S. Herminghaus, and M. Schröter. Jammed frictional tetrahedra are hyperstatic. *Phys. Rev. Lett.*, 111:028001, 2013.
- [151] J. F. Nye. *Physical Properties of Crystals*. Oxford Science Publications, 1985.
- [152] A. Odgaard. Three-dimensional methods for quantification of cancellous bone architecture. *Bone*, 20(4):315–328, 1997.
- [153] A. Odgaard, E. B. Jensen, and H. J. Gundersen. Estimation of structural anisotropy based on volume orientation. A new concept. *J. Microsc.*, 157(2): 149–162, 1990.
- [154] G. Odriozola. Revisiting the phase diagram of hard ellipsoids. *The Journal of chemical physics*, 136(13):134505, 2012.

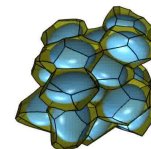
- [155] L. Oger, A. Gervois, J. P. Troadec, and N. Rivier. Voronoi tessellation of packings of spheres: Topological correlation and statistics. *Philosophical Magazine Part B*, 74(2):177–197, 1996.
- [156] C. S. O’Hern, L. E. Silbert, A. J. Liu, and S. R. Nagel. Jamming at zero temperature and zero applied stress: The epitome of disorder. *Phys. Rev. E*, 68:011306, 2003.
- [157] A. Okabe, B. Boots, K. Sugihara, and S. N. Chiu. *Spatial tessellations: Concepts and applications of Voronoi diagrams*. Probability and Statistics. Wiley, NYC, 2nd edition, 2000. 671 pages.
- [158] J. M. Ottino and D. V. Khakhar. Mixing and segregation of granular materials. *Annual Review of Fluid Mechanics*, 32(1):55–91, 2000.
- [159] D. N. Perera and P. Harrowell. Stability and structure of a supercooled liquid mixture in two dimensions. *Phys. Rev. E*, 59:5721–5743, 1999.
- [160] P. Pfliegerer, K. Milinkovic, and T. Schilling. Glassy dynamics in monodisperse hard ellipsoids. *EPL (Europhysics Letters)*, 84(1):16003, 2008.
- [161] P. Philippe and D. Bideau. Compaction dynamics of a granular medium under vertical tapping. *EPL (Europhysics Letters)*, 60(5):677, 2002.
- [162] E. Preteux. Watershed and skeleton by influence zones: A distance-based approach. *Journal of Mathematical Imaging and Vision*, 1(3):239–255, 1992. ISSN 0924-9907.
- [163] J. G. Puckett, F. Lechenault, and K. E. Daniels. Local origins of volume fraction fluctuations in dense granular materials. *Phys. Rev. E*, 83:041301, 2011.
- [164] C. Radin. Random close packing of granular matter. *Journal of Statistical Physics*, 131:567–573, 2008. ISSN 0022-4715. 10.1007/s10955-008-9523-1.
- [165] D. C. Rapaport. *The Art of Molecular Dynamics Simulation*. Cambridge University Press, New York, NY, USA, 2nd edition, 2004. ISBN 0521825687, 9780521825689.
- [166] O. Reynolds. Lvii. on the dilatancy of media composed of rigid particles in contact. with experimental illustrations. *Philosophical Magazine Series 5*, 20(127): 469–481, 1885.
- [167] O. Reynolds. Experiments showing dilatancy, a property of granular material, possibly connected with gravitation. In *Proc. Royal Institution of Great Britain, Read*, volume 12, 1886.
- [168] G. H. Ristow. *Pattern formation in granular materials*. Number 164. Springer Science & Business Media, 2000.





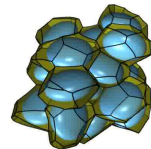
- [169] J. B. T. M. Roerdink and A. Meijster. The watershed transform: Definitions, algorithms and parallelization strategies. *Fundam. Inf.*, 41(1,2):187–228, 2000. ISSN 0169-2968.
- [170] L. K. Roth and H. M. Jaeger. Optimizing packing fraction in granular media composed of overlapping spheres. *Soft matter*, 12(4):1107–1115, 2016.
- [171] M. Saadatfar, A. N. P. Shepard, and M. A. Knackstedt. *Grain Partitioning and its Applications*, pages 269–276. ISTE, 2010. ISBN 9780470612187.
- [172] S. Sastry, T. M. Truskett, P. G. Debenedetti, S. Torquato, and F. H. Stillinger. Free volume in the hard sphere liquid. *Molecular Physics*, 95(2):289–297, 1998.
- [173] C. Scholz, F. Wirner, J. Götz, U. Rude, G.E. Schröder-Turk, K. Mecke, and C. Bechinger. Permeability of porous materials determined from the Euler characteristic. *Phys. Rev. Lett.*, 109:264504, 2012.
- [174] C. Scholz, F. Wirner, M. A. Klatt, D. Hirneise, G. E. Schröder-Turk, K. Mecke, and C. Bechinger. Direct relations between morphology and transport in boolean models. *Phys. Rev. E*, 92:043023, 2015.
- [175] G. E. Schröder, S. Kapfer, B. Breidenbach, C. Beisbart, and K. Mecke. Tensorial minkowski functionals and anisotropy measures for planar patterns. *Journal of microscopy*, 238(1):57–74, 2010.
- [176] G. E. Schröder-Turk, W. Mickel, M. Schröter, G. W. Delaney, M. Saadatfar, T. J. Senden, K. Mecke, and T. Aste. Disordered spherical bead packs are anisotropic. *EPL (Europhysics Letters)*, 90(3):34001, 2010.
- [177] K. Schütte and B. L. van der Waerden. Das Problem der dreizehn Kugeln. *Mathematische Annalen*, 125(1):325–334, 1952.
- [178] P. Schönhöfer, L. J. Ellison, M. Marechal, D. J. Cleaver, and G.E. Schröder-Turk. Purely entropic self-assembly of the bicontinuous ia(-3)d gyroid phase. *submitted for publication in Interface Focus*, 2017.
- [179] G. D. Scott. Packing of spheres: packing of equal spheres. *Nature*, 188(4754): 908–909, 1960.
- [180] G. D. Scott and D. M. Kilgour. The density of random close packing of spheres. *Journal of Physics D: Applied Physics*, 2(6):863, 1969.
- [181] A. Sheppard, S. Latham, J. Middleton, A. Kingston, G. Myers, T. Varslot, A. Fogden, T. Sawkins, R. Cruikshank, M. Saadatfar, et al. Techniques in helical scanning, dynamic imaging and image segmentation for improved quantitative analysis with x-ray micro-ct. *Nuclear Instruments and Methods in Physics Research Section B: Beam Interactions with Materials and Atoms*, 324:49–56, 2014.

- [182] K. Siddiqi and S. Pizer. *Medial representations: mathematics, algorithms and applications*, volume 37. Springer Science & Business Media, 2008.
- [183] L. E. Silbert, D. Ertas, G. S. Grest, T. C. Halsey, and D. Levine. Geometry of frictionless and frictional sphere packings. *Phys. Rev. E*, 65:031304, 2002.
- [184] S. Slotterback, M. Toiya, L. Goff, J. F. Douglas, and W. Losert. Correlation between particle motion and Voronoi-cell-shape fluctuations during the compaction of granular matter. *Phys. Rev. Lett.*, 101(25):258001, 2008.
- [185] C. Song, P. Wang, and H. A. Makse. A phase diagram for jammed matter. *Nature*, 453:629–632, 2008.
- [186] R. J. Speedy. Glass transition in hard disc mixtures. *The Journal of Chemical Physics*, 110(9):4559–4565, 1999.
- [187] F. W. Starr, S. Sastry, J. F. Douglas, and S. C. Glotzer. What Do We Learn from the Local Geometry of Glass-Forming Liquids? *Phys. Rev. Lett.*, 89:125501, 2002.
- [188] D. G. Stavenga, S. Stowe, K. Siebke, J. Zeil, and K. Arikawa. Butterfly wing colours: scale beads make white pierid wings brighter. *Proceedings of the Royal Society of London B: Biological Sciences*, 271(1548):1577–1584, 2004. ISSN 0962-8452.
- [189] P. J. Steinhardt, D. R. Nelson, and M. Ronchetti. Bond-orientational order in liquids and glasses. *Phys. Rev. B*, 28:784–805, 1983.
- [190] O. Stenzel, M. Salzer, V. Schmidt, P. W. Cleary, and G. W. Delaney. Quantitative structural analysis of simulated granular packings of non-spherical particles. *Granular Matter*, 16(4):457–468, 2014.
- [191] Y.-J. Sung and R. Farnood. Characterizing anisotropy of the deterministic features in paper structure with wavelet transforms. *J. Ind. Eng. Chem.*, 13(2): 225–230, 2007.
- [192] K. E. Thompson, C. S. Willson, and W. Zhang. Quantitative computer reconstruction of particulate materials from microtomography images. *Powder Technology*, 163(3):169 – 182, 2006. ISSN 0032-5910.
- [193] K. To, P.-Y. Lai, and H. K. Pak. Jamming of granular flow in a two-dimensional hopper. *Phys. Rev. Lett.*, 86:71–74, 2001.
- [194] S. Torquato and Y. Jiao. Dense packings of the platonic and archimedean solids. *Nature*, 460(7257):876–879, 2009.
- [195] S. Torquato and F. H. Stillinger. Local density fluctuations, hyperuniformity, and order metrics. *Phys. Rev. E*, 68:041113, 2003.



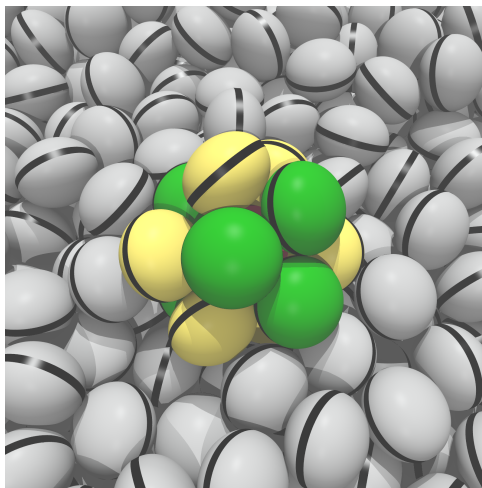
- [196] S. Torquato and F. H. Stillinger. Toward the jamming threshold of sphere packings: Tunneled crystals. *Journal of Applied Physics*, 102(9):093511, 2007.
- [197] S. Torquato and F. H. Stillinger. Jammed hard-particle packings: From kepler to bernal and beyond. *Rev. Mod. Phys.*, 82:2633–2672, 2010.
- [198] S. Torquato, T. M. Truskett, and P. G. Debenedetti. Is random close packing of spheres well defined? *Phys. Rev. Lett.*, 84:2064–2067, 2000.
- [199] M. Tunák and A. Linka. Analysis of planar anisotropy of fibre systems by using 2D Fourier transform. *Fibres Text. East. Eur.*, 15(5–6), 2007.
- [200] M. van Hecke. Jamming of soft particles: geometry, mechanics, scaling and isostaticity. *Journal of Physics: Condensed Matter*, 22(3):033101, 2010.
- [201] T. Varslot, A. Kingston, G. Myers, and A. Sheppard. High-resolution helical cone-beam micro-ct with theoretically-exact reconstruction from experimental data. *Medical Physics*, 38(10):5459–5476, 2011.
- [202] F. X. Villarruel, B. E. Lauderdale, D. M. Mueth, and H. M. Jaeger. Compaction of rods: Relaxation and ordering in vibrated, anisotropic granular material. *Phys. Rev. E*, 61:6914–6921, 2000.
- [203] W. M. Visscher and M. Bolsterli. Random packing of equal and unequal spheres in two and three dimensions. *Nature*, 239:504–507, 1972.
- [204] M. J. Wald, B. Vasilic, P. K. Saha, and F. W. Wehrli. Spatial autocorrelation and mean intercept length analysis of trabecular bone anisotropy applied to in vivo magnetic resonance imaging. *Med. Phys.*, 34(3):1110–1120, 2007.
- [205] P. Wang, C. Song, Y. Jin, K. Wang, and H. A. Makse. Distribution of volumes and coordination numbers in jammed matter: mesoscopic ensemble. *Journal of Statistical Mechanics: Theory and Experiment*, 2010(12):P12005, 2010.
- [206] W. J. Whitehouse. The quantitative morphology of anisotropic trabecular bone. *J. Microsc.*, 101(2):153–168, 1974.
- [207] B. D. Wilts, B. Wijnen, H. L. Leertouwer, U. Steiner, and D. G. Stavenga. Extreme refractive index wing scale beads containing dense pterin pigments cause the bright colors of pierid butterflies. *Advanced Optical Materials*, 5(3):1600879–n/a, 2017. ISSN 2195-1071. 1600879.
- [208] C. Xia, K. Zhu, Y. Cao, H. Sun, B. Kou, and Y. Wang. X-ray tomography study of the random packing structure of ellipsoids. *Soft Matter*, 10(7):990–996, 2014.
- [209] R. Y. Yang, R. P. Zou, and A. B. Yu. Voronoi tessellation of the packing of fine uniform spheres. *Phys. Rev. E*, 65:041302, 2002.

- [210] Z. Zeravcic, N. Xu, A. J. Liu, S. R. Nagel, and W. van Saarloos. Excitations of ellipsoid packings near jamming. *Europhys. Lett.*, 87:26001, 2009.
- [211] S.-C. Zhao, S. Sidle, H.L. Swinney, and M. Schröter. Correlation between Voronoi volumes in disc packings. *EPL*, 97(3):34004, 2012.



[P1]

## Densest local structures of uniaxial ellipsoids

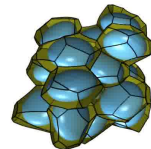


PRX 2016

F. M. Schaller, R. F. B. Weigel, and S. C. Kapfer

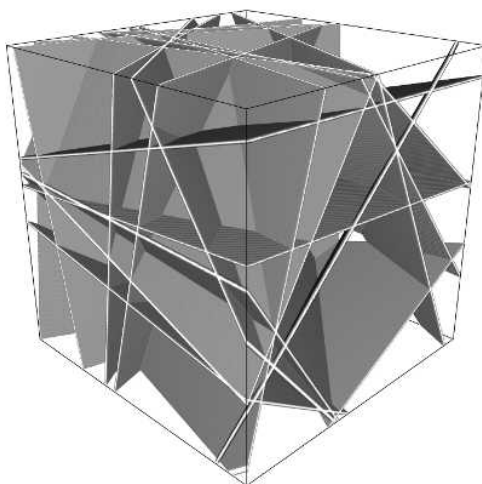
*Phys. Rev. X*, 6:041032, 2016.

Pages 70 - 80 are not available in this version.  
Click [here](#) to view online.



[P2]

## Cell shape analysis of random tessellations based on Minkowski tensors



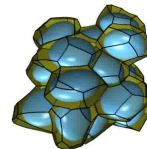
Springer 2016

M. A. Klatt, G. Last, K. Mecke, C. Redenbach, F. M. Schaller, and G. E. Schröder-Turk

*Springer Lecture Notes in Mathematics, Tensor Valuations and their applications in stochastic geometry and imaging, vol 2177, 2016*

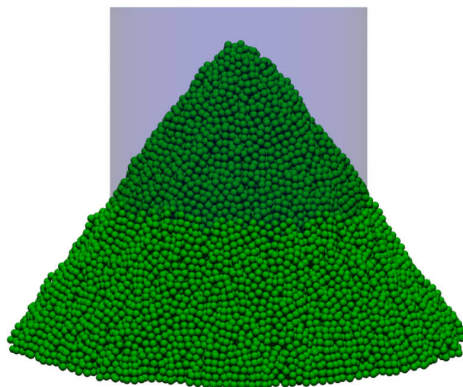


Pages 82 - 120 are not available in this version.  
Click [here](#) to view online.



[P3]

**The microscopic structure of mono-disperse granular heaps and sediments of particles on inclined surfaces**

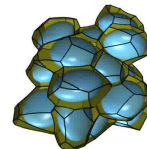


Soft. Mat. 2016

N. Topic, **F. M. Schaller**, G. E. Schröder-Turk, and T. Pöschel

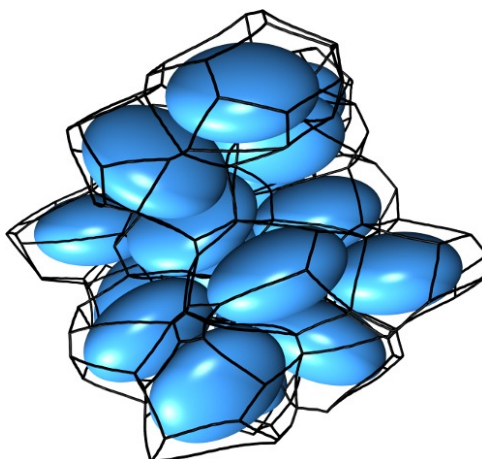
*Soft Matter*, 12:3184–3188, 2016

Pages 122 - 128 are not available in this version.  
Click [here](#) to view online.



[P4]

## Non-universal Voronoi cell shapes in amorphous ellipsoid packs

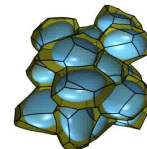


EPL 2015

**F. M. Schaller**, S. C. Kapfer, J. E. Hilton, P. W. Cleary, C. De Michele, K. Mecke,  
T. Schilling, M. Saadatfar, M. Schröter, G. W. Delaney, and G. E. Schröder-Turk

*EPL (Europhysics Letters)*, 111(2):24002, 2015

Pages 130 - 136 are not available in this version.  
Click [here](#) to view online.



[P5]

## Local origin of global contact numbers in frictional ellipsoid packings



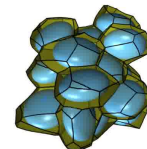
PRL 2015

F. M. Schaller, M. Neudecker, M. Saadatfar,  
G. W. Delaney, G. E. Schröder-Turk, and M. Schröter

*Phys. Rev. Lett.*, 114:158001, 2015

Pages 138 - 152 are not available in this version.  
Click [here](#) to view online.





[P6]

## Set Voronoi diagrams of 3D assemblies of aspherical particles

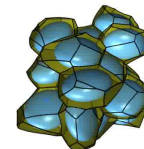


Phil. Mag. 2013

F. M. Schaller, S. C. Kapfer, M. E. Evans, M. J. F. Hoffmann, T. Aste, M. Saadatfar, K. Mecke, G. W. Delaney, and G. E. Schröder-Turk

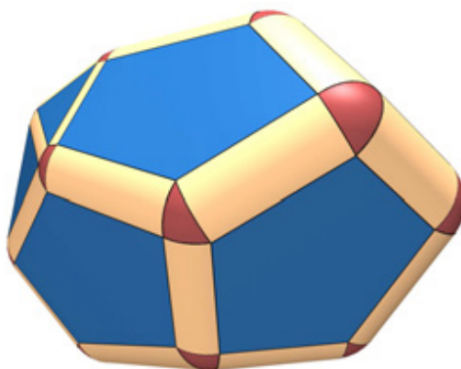
*Philosophical Magazine*, 93(31-11):3993–4017, 2013

Pages 154 - 180 are not available in this version.  
Click [here](#) to view online.



[P7]

## Minkowski tensors of anisotropic spatial structure

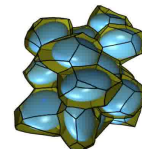


NJP 2013

G. E. Schröder-Turk, W. Mickel, S. C. Kapfer,  
**F. M. Schaller**, B. Breidenbach, D. Hug, and K. Mecke

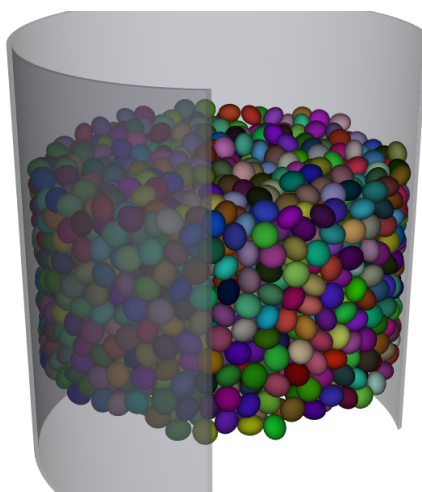
*New Journal of Physics*, 15(8):083028, 2013

Pages 182 - 220 are not available in this version.  
Click [here](#) to view online.



[P8]

## Tomographic analysis of jammed ellipsoid packings

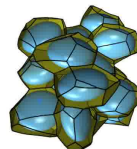


AIP 2013

F. M. Schaller, M. Neudecker, M. Saadatfar, G. Delaney, K. Mecke,  
G. E. Schröder-Turk, and M. Schröter

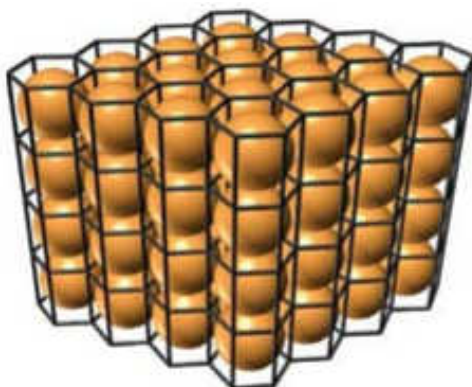
*AIP Conference Proceedings*, 1542(1):377–380, 2013

Pages 222 - 226 are not available in this version.  
Click [here](#) to view online.



[P9]

**Minkowski tensors and local structure metrics:  
Amorphous and crystalline sphere packings**



AIP 2013

G. E. Schröder-Turk, R. Schielein, S. C. Kapfer, **F. M. Schaller**, G. W. Delaney,  
T. Senden, M. Saadatfar, T. Aste, and K. Mecke

*AIP Conference Proceedings*, 1542(1):349–352, 2013



Pages 228 - 232 are not available in this version.  
Click [here](#) to view online.